PEBS

Long-Term Performance of Engineered Barrier Systems

GRS Participation

GRS - 353

Gesellschaft für Anlagen-
und Reaktorsicherheit
(GRS) gGmbH

PEBS

Long-Term Performance of Engineered Barrier Systems

GRS Participation

Klaus Wieczorek
Oliver Czaikowski
Rüdiger Miehe

December 2014

Remark:

This report was prepared under funding reference No. 02E10689 of the German Federal Ministry for Economic Affairs and Energy (BMWi).

The work was conducted by the Gesellschaft für Anlagen- und Reaktorsicherheit (GRS) gGmbH.

The authors are responsible for the content of the report.

GRS - 353
ISBN 978-3-944161-33-4

Keywords

Bentonite, Engineered Barrier, in-situ Testing, Long-Term Simulation, Performance Assessment, Sand/Bentonite Mixture

Preface

The PEBS project ("Long-Term Performance of Barrier Systems") was performed between March 1, 2010, and February 28, 2014 within the Seventh Euratom Framework Programme for Nuclear Research &Training Activities (2007 – 2011) under grant agreement n° FP7-249681.

16 international project partners from six countries contributed to PEBS:

1. Bundesanstalt für Geowissenschaften und Rohstoffe (BGR), Germany (coordinator)
2. Nationale Genossenschaft für die Lagerung radioaktiver Abfälle (NAGRA), Switzerland
3. Svensk Kärnbränslehantering AB (SKB), Sweden
4. Gesellschaft für Anlagen- und Reaktorsicherheit (GRS) mbH, Germany
5. Empresa Nacional de Residuos Radiactivos SA (ENRESA), Spain
6. Asociacion para la Investigation y el Desarollo Industrial de los Recursos Naturales (AITEMIN), Spain
7. Centre Internacional de Mètodes Numèrics en Enginyeria (CIMNE), Spain
8. Universidade da Coruña (UDC), Spain
9. Centro de Investigaciones Energéticas Medioambientales y Tecnológicas (CIEMAT), Spain
10. Agence Nationale pour la Gestion des Déchets Radioactifs (ANDRA), France
11. Universidad Autonoma de Madrid (UAM), Spain
12. Golder Spain (former DM Iberia SA), Spain
13. Solexperts AG, Switzerland
14. TK Consult AG, Switzerland
15. Clay Technology, Sweden
16. Beijing Research Institute for Uranium Geology (BRIUG), China

GRS received additional funding from the Bundesministerium für Wirtschaft und Energie (BMWi) under contract No. 02E10689.

The project description and results are published in a number of deliverables referenced in this report (see appendix). The report represents a summary of the project parts GRS was involved in.

Table of contents

1 Introduction

The evolution of the engineered barrier system (EBS) of geological repositories for radioactive waste has been the subject of many national and international research programmes. The emphasis of the research activities was on the elaboration of a detailed understanding of the complex THMC processes, which are expected to evolve in the early post closure period in the near field. From the perspective of radiological long-term safety, an in-depth understanding of these coupled processes is of great significance, because the evolution of the EBS during the early post-closure phase may have a non-negligible impact on the radiological safety functions at the time when the canisters breach. Unexpected process interactions during the resaturation phase could impair the safety-relevant parameters in the EBS (e. g. swelling pressure, hydraulic conductivity, diffusivity).

In previous projects, remarkable advances have been made to broaden the scientific understanding of THMC coupled processes in the near field around the waste canisters. Less successful, however, was the attempt to use this in-depth process understanding for constraining the conceptual and parametric uncertainties in the context of long-term safety assessment. An integrated approach was considered necessary to set-up the scientific validation procedures in a context which is relevant for the PA purposes.

The PEBS project concentrated on THMC processes associated with the evolution of the nearfield around a heat emitting waste canister in a repository featuring clay-bearing buffer materials. The considered buffer materials were granular bentonite and bentonite/sand mixtures, respectively. The evolution of the disposal system was assessed in the early post closure period with emphasis on the thermal evolution, buffer resaturation and the evolution of swelling pressures in the buffer. According to Fig. 1.1 the model validation focused on the following periods and parameters:

- The early post closure period (early resaturation time), when the buffer is expected to experience the maximum temperature. In this phase the buffer is largely unsaturated and the thermal evolution of the EBS may be controlled by the effective thermal conductivity of the dry buffer material. The main source of uncertainty arises from possible scale effects in the determination of thermal conductivity (upscaling from laboratory to field scale).

- The resaturation period, when competing processes such as water uptake, thermal impact and the swelling of the buffer will interfere and may lead to unexpected transitory effects (e.g. transients of swelling pressure, water saturation, pore pressure). Confirmation has to be gained that the transitory effects will not influence the final equilibrated state of the EBS system.

- The pore pressure recovery period, when the EBS system is close to full water saturation and the key THM-parameters tend to reach equilibrium conditions. Statements on the uncertainties with regard to the safety relevant EBS parameters are required (spatial variability of swelling pressure, hydraulic conductivity and porosity in the buffer and in the Excavated Damaged Zone, EDZ).

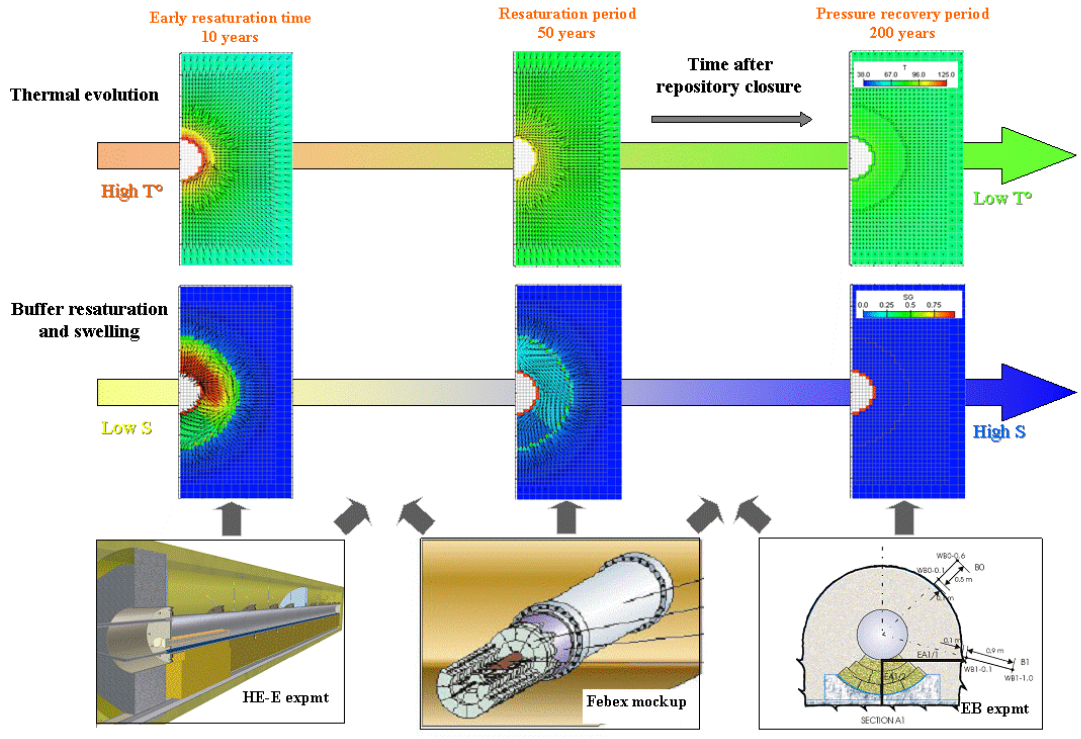

Fig. 1.1 Concept of the validation experiments in the project PEBS

The model validation was executed in the framework of a prediction-evaluation-improvement process. For this purpose, three large-scale experiments were performed, each of them linked to one of the aforementioned evolutionary periods (Fig 1.1):

- The early thermal evolution of the EBS was investigated by a heater experiment (HE-E, Fig. 1.2) planned and constructed in the frame of PEBS at the Mont Terri URL.
- The resaturation phase was addressed through the continuation of the FEBEX mock-up experiment at CIEMAT's laboratories in Madrid.
- The pressure recovery period was investigated by continuation of the long-term monitoring phase of the EB experiment at the Mont Terri URL, followed by careful dismantling and post-test evaluations.

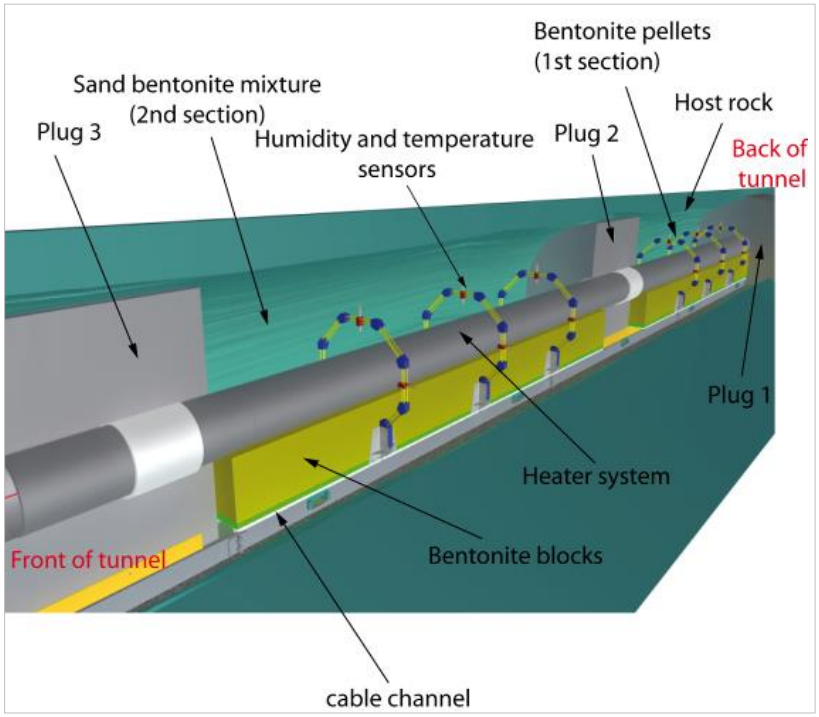

Fig. 1.2 Overview of the HE-E experiment configuration

The large-scale experiments were backed by laboratory investigations on various aspects of material behaviour and parameters. The short-term models calibrated by simulation cycles of the large-scale experiments were used for long-term extrapolation of repository evolution in order to elaborate a more quantitative basis for relating the evolutionary behaviour to the safety functions of the system.

A complete outline of the PEBS project and its contents is given in the description of work (DoW) /DOW 10/.

2 Objectives and work programme

2.1 PEBS objectives

The detailed objectives of the PEBS project, as given in the description of work /DOW 10/, were

- To review recent advances in the current state-of-the-art (methodology, data, knowledge and understanding) affecting the processes in the early evolution of the repository EBS and its treatment in performance assessment
- To discuss how the short-term transients will/may affect the long term performance and the safety functions of the repository
- To evaluate the key thermo-hydro-mechanical and chemical processes and parameters taking place during early evolution of the EBS
- To provide with a reliable good quality experimental HM, THM and THMC data base for the model validation process
- To evaluate the predicted evolution of the EBS using the experimental data as performance indicators and to improve the THM-C models through calibration and further code development
- To use the improved THM-C process models for extrapolation to long-term evolution of the repository EBS taking into account normal and altered scenarios
- To relate the experimental and modeling results and uncertainties to the long-term safety functions of the repository components and to the overall long-term performance of the repository
- To give feedback and guidance for repository design and construction as well as to future R&D

2.2 Work programme

The PEBS project was organized in five scientific work packages, which are described in short in the following paragraphs.

WP1: Analysis of system evolution during early post closure period: Impact on long-term safety functions

The task of WP1 was to describe and discuss the current treatment of the early post-closure phase in PA, to discuss the needs for additional studies and how they can support future assessments, thus giving directions to the other work packages.

WP2: Experimentation on key EBS processes and parameters

All the PEBS experimental work was included in WP2. The work package was structured into three different tasks:

Task 2.1: Experimentation on key HM processes and parameters

This task comprised laboratory infiltration tests with buffer materials and the long-term monitoring and dismantling of the Mont Terri EB experiment.

Task 2.2: Experimentation on key THM processes and parameters

This task comprised laboratory experiments on THM behaviour, including the FEBEX mock-up test performed at the CIEMAT laboratory, long-term THM tests in cells simulating particular disposal concepts, tests on vapour transport in bentonite and studies of stress/strain behaviour, as well as the HE-E is-situ experiment performed at the Mont Terri URL.

Task 2.3: Experimentation on key THMC processes and parameters

The experimental work of this task comprised the THMC mock-up tests (GAME tests) performed at the CIEMAT laboratory and special tests aimed at the study of processes at the canister/bentonite and the bentonite/concrete interfaces.

WP3: Modelling of short-term effects and extrapolation to long-term evolution

Modelling work is concentrated in WP3 of the PEBS. There are five different tasks:

Task 3.1: HM modelling of the Mont Terri Engineered Barrier (EB) Experiment

Modelling of the EB experiment featured new constitutive laws developed in PEBS.

Task 3.2: THM modelling for the planned heater test HE-E

This tasks included design modelling and prediction/evaluation cycles of the HE-E.

Task 3.3: THM modelling of bentonite buffer

This task comprised modelling of various aspects of buffer THM behaviour, with model simulations of the FEBEX mock-up and in-situ tests and of the long-term THM tests performed in CIEMAT's laboratory.

Task 3.4: Modelling of THMC experiments

Advanced multiple-continua THMC models were developed and tested within this task, with the focus on modelling the processes at the canister/bentonite and bentonite/concrete interfaces.

Task 3.5: Extrapolation to repository long-term evolution

Four simulation cases for long-term extrapolation of the repository evolution were defined and the models developed and/or calibrated in WPs 3.1 to 3.4 were used for their simulation.

WP4: Analysis of impact on long-term safety and guidance for repository design and construction

The findings of the WP2 and WP3 experiments and models were reviewed in order to develop a more complete qualitative process-related description of the early evolution phase of the repository (the first several hundred years) and the residual uncertainties in the evolution. Other relevant studies (e.g. the in situ FEBEX experiment and SKB studies) were also considered in this synthesis. The importance of the transient period with regard to the long-term characteristics particularly relevant to system performance and long-term safety was discussed. The significant uncertainties were identified and recommendations for future studies were made.

WPB: China-Mock-up Test on compacted bentonite-buffer

The China-Mock-up was proposed according to a preliminary concept for a HLW repository in China developed in 2009. The China-Mock-up has been performed in the laboratory to evaluate the key THMC processes taking place in the compacted bentonite buffer during the early phase of HLW disposal and to provide a reliable database as input to numerical modelling and further investigations.

All the results obtained within PEBS are documented in a number of public project deliverables. The complete list of deliverables is given in the appendix of this report.

In the following chapters, the work in which GRS was involved is presented, with focus on, but not restricted to the actual GRS contribution. This includes

- Laboratory investigation of the thermal parameters of buffer materials (Chapter 3)
- The HE-E experiment (Chapter 4)
- Model Simulations (Chapter 5)
- Impact on long-term safety considerations (Chapter 6)

3 Laboratory investigations on buffer materials

The laboratory investigations performed by GRS concentrated on the thermal parameters of the three buffer materials employed in the HE-E experiment (see Chapter 4).

- The heater is placed on a foundation of highly compacted bentonite blocks in both sections of the tunnel.
- In one section, the remaining void is backfilled with granular bentonite material. This section is representative for the Swiss disposal concept.
- In the second section, the backfill material is a mixture of 65 % sand and 35 % granular bentonite of the same grain spectrum. The background for choosing this material is explained in Chapter 4.

The buffer materials are specified in detail in the HE-E as-built report, PEBS Deliverable D2.2-3 /TEO 12/.

In order to obtain data on the thermal parameters (thermal conductivity, thermal capacity, and thermal diffusivity) of these materials, respective tests on samples were performed at the GRS laboratory in Braunschweig. For the tests a „Hot Disk Thermal Constants Analyser“ /HDT 07/ was used.

The schedule of the tests was determined by the needs of the modelling groups that performed numerical simulations of the HE-E.

- During the first years of heating, the buffer saturation will remain low, but the buffer temperature will increase rapidly. For interpretative modelling of this test phase, the thermal parameters at as-emplaced saturation and at ambient and elevated temperature are needed.
- At later times, the buffer will begin to re-saturate. For predictive calculations of later experiment stages, the dependence of the thermal parameters on saturation has to be quantified.

The measurements at low saturation and at ambient and elevated temperature were completed for the bentonite blocks and the sand/bentonite mixture and documented in the PEBS Deliverable D2.2-5 (“Measurement of Thermal Parameters of the HE-E Buffer Materials”) end of 2011 /WIE 11/.

Until June 2013, more measurements were performed. Dependence of thermal parameters of the sand/bentonite mixture on saturation was established, although not yet for the whole saturation range. In addition to the measurement of thermal parameters, the retention curve and the permeability of the sand/bentonite were investigated, since no respective data were available, but needed for modelling. This state was documented in Deliverable D2.2-9 (“Thermal characterisation of HE-E buffer”) /WIE 13/.

This chapter summarizes D2.2-9, but includes in addition the results of the measurements on sand/bentonite at high saturation that had not been finished when D2.2-9 was issued. Moreover, results of measurements of the thermal parameters of pure granular bentonite as a function of water content are included.

3.1 Measurement techniques

For all three types of buffer materials – bentonite blocks, bentonite pellets, and granular sand/bentonite mixture – the thermal parameters and the related densities and water contents have been determined. In addition to these measurements, the lack of respective data for the sand/bentonite mixture required measurement of the retention curve and the permeability.

3.1.1 Thermal parameters

For the measurement of thermal parameters a heating sensor in the form of a double spiral consisting of a thin metal sheet insulated by a Kapton body is placed inside the investigated material. An electric current is led through the sensor which increases its temperature in a range between a fraction of one degree and several degrees Celsius. The alteration of the sensor’s electric resistivity is a measure for the thermal parameters of the material. The sensor thus has a combined function of providing the heat source and the dynamic measurement. The principle measurement configuration is shown in Fig. 3.1. Different sensor sizes are available for measurement in different materials (Fig. 3.2).

The analyser outputs the thermal conductivity, thermal capacity, and thermal diffusivity of the sample material. It has to be noted that thermal capacity is given as a volumetric specific heat (in MJ/(m³*K)). In order to obtain the thermal capacity per mass the output value has to be divided by the bulk density of the sample.

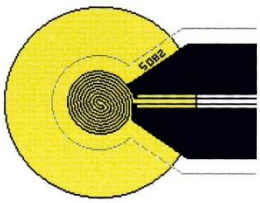	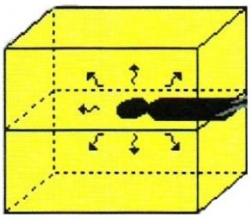	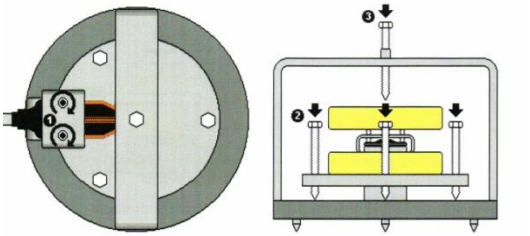
Sensor location in the sample (yellow)	Heating of the sample	Sample holder with installed sample

Fig. 3.1 Principle measurement configuration /HDT 07/

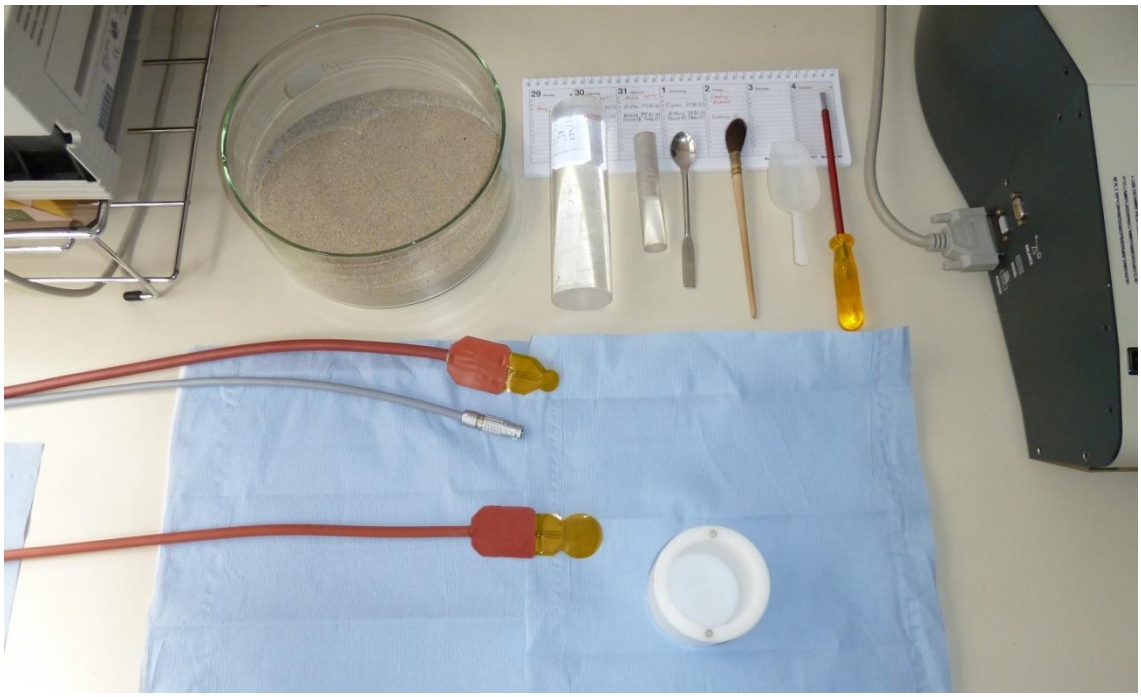

Fig. 3.2 Sensors for the Hotdisk analyser

For performing measurements of the thermal parameters at elevated temperature, the sample/sensor combination can be placed in a drying oven with fittings for the cables. The sample is left in the oven for several hours to ensure the oven temperature has been reached throughout the sample; then the measurement is performed with the sample inside the oven.

The sample volume that is actually affected by the measurement is rather small. Therefore, it is essential to provide a good coupling between the sample and the measuring

probe; otherwise, heat conduction at the contact will be inhibited and the thermal conductivity may be underestimated.

3.1.2 Densities and water content

Besides the thermal parameters, bulk density, grain density and water content were determined. Bulk density was calculated from sample geometry and mass. Grain density was measured using a helium pycnometer. Water content was determined by weighing before and after drying at 105 °C.

3.1.3 Retention curve (granular sand/bentonite mixture)

For determination of the retention curve samples of sand/bentonite mixture were re-saturated in exsiccators containing different salt solutions in order to obtain different relative humidities in the atmosphere. The relative air humidity was measured. From the humidity the suction was calculated. The saturation of each sample was afterwards determined by oven-drying at 105 °C.

3.1.4 Permeability (granular sand/bentonite mixture)

For permeability measurement a sand/bentonite sample with original water content was emplaced in a cylindrical cell. Gas injection tests were performed at five pressure steps. Afterwards, the sample was re-saturated and the permeability of the saturated sample to water was determined by water injection testing.

3.2 Measurements on bentonite blocks

Two types of bentonite blocks are used in the HE-E: The upper blocks have a groove in which the heater is held (see Fig. 3.3). The lower blocks are simply brick-shaped. One block of each type was available for sampling and investigation of the thermal parameters.

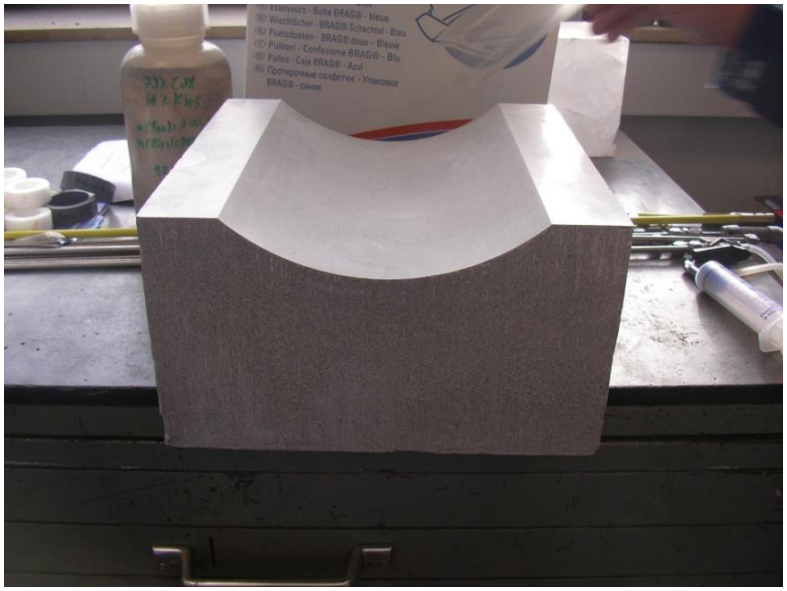

Fig. 3.3 Grooved upper bentonite block

3.2.1 Sample preparation and nomenclature

In order to check whether there are differences between the centre and the near-surface zones of the blocks, samples were taken from both blocks both from the centre and the near-surface. The samples from the block centre were named with the letters STA (for the upper block) or STU (for the lower block) and a number from 1 to 6. The samples 1 through 4 of each block were heated in steps from 20 °C to 105 °C in the state as delivered and the thermal parameters were determined at each step. The sample 5 and 6 were first dried at 105 °C (following DIN 18121) and the temperature dependence of the thermal parameters was measured on the dried samples. In order to obtain the moisture loss due to heating an additional reference sample for determining moisture content was used in each case. The change of bulk density of the sample due to heating was used to recalculate the mass-related specific heat of the samples.

The samples were sawed from the blocks. The sawdust obtained was used for determining the grain density. The dimensions of all samples are 60 mm by 60 mm by 30 mm (Fig. 3.4). For the measurements two single samples (e.g., STU1 and STU2) were put together with the sensor in between. Thus, the considered sample pairs had a size of 60 mm by 60 mm by 60 mm.

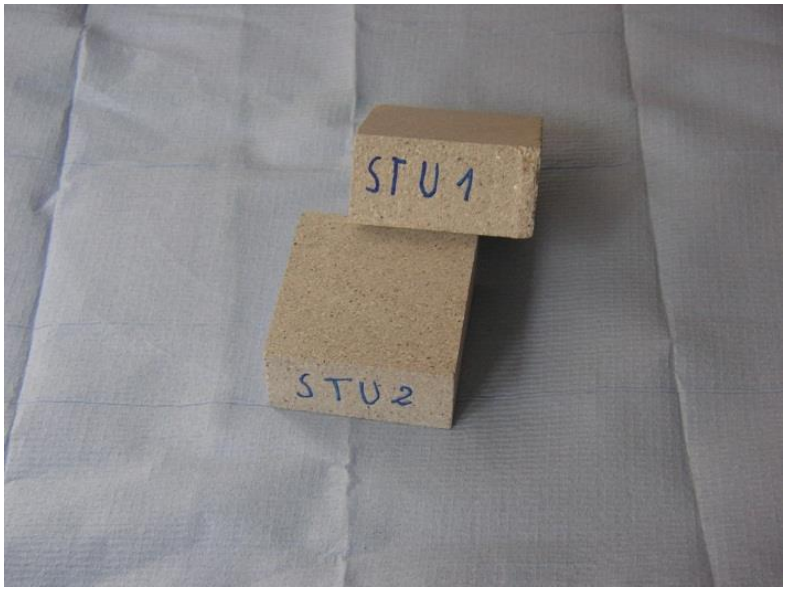

Fig. 3.4 Sample pair STU1/STU2

3.2.2 Determination of thermal parameters

For the measurement the sensor is placed between the two single samples of one pair. Sensor coupling to the sample is ensured by use of a clamping device (Fig. 3.5). The tests are performed while the compound sample (sample pair with sensor) is placed in a drying oven with fittings for the cables.

Fig. 3.5 Sample pair in the drying oven (the clamping device is used to assure coupling of sensor to the bentonite)

At each of the temperature steps of 20 °C, 40 °C, 60 °C, 80 °C und 105 °C a measurement is performed. A waiting time between the measurements is needed to ensure that a constant temperature has been reached in the sample. This time was set to approximately 7 h per step.

3.2.3 Results for bentonite blocks

3.2.3.1 Bulk density and grain density

The density values show a variation depending on block and sampling position. Close to the block surface, the samples from both blocks show density values of 2350 kg/m³ to 2450 kg/m³ (bulk density) and 2100 kg/m³ to 2190 kg/m³ (dry density), respectively. In the centre of the blocks, 2060kg/m³ bulk density (1840 kg/m³ dry density) were measured on the samples from the lower block, the values for the upper block of 2030 kg/m³ to 2070 kg/m³ bulk density (1830 kg/m³ to 1850 kg/m³ dry density) were comparable. These results compare well with measurements of ETH Zürich which are published in the HE-E as-built report /TEO 12/. ETH found a macroscopic density of 2080 kg/m³. After sampling from the blocks at ETH, however, somewhat smaller densities were found. This was explained by ETH by relaxation and drying between production and lab analysis. Indeed, the water content measured by ETH was lower than the values measured by GRS (see Section 3.2.3.3).

Grain density was measured to be 2695.8 kg/m³ for the dry material, which compares well to ETH measurements of 2699 kg/m³.

3.2.3.2 Water content

The water content of the different samples was very homogeneous: On the block surface, always 11.88 % were measured. Inside both blocks, values of 11.7 % to 11.83 % were obtained.

The water content measured by ETH ranged between 9.3 % and 11.6 %, with an average of 10.34 % /TEO 12/. This is somewhat lower and was explained by ETH by some drying between sample production and analysis (see also previous section). The water content of the sawdust samples for grain density determination at GRS was lower

(5.1 % to 6.2 %), too. This is a consequence of the sawing procedure which led to drying.

3.2.3.3 Thermal parameters

In the Tables 3.1, 3.2, and 3.3 the measurement results for thermal conductivity, thermal diffusivity, and specific heat for the different temperature steps are given, together with bulk density and (remaining) water content. Tables 3.1 and 3.2 show the results for the upper and low block (as delivered), respectively. Note that the water content of the samples is reducing with each temperature step. Table 3.3 summarizes the respective results for samples from both blocks which were dried before the measurements.

Tab. 3.1 Parameters of the upper block, as delivered

Sample	Density ρ	Thermal Conductivity λ	Thermal Diffusivity κ	Specific Heat c	Temperature T	Remaining Water Cont. w
	kg/m^3	W/(m*K)	mm^2/s	MJ/(kg*K)	°C	%
STA1 / STA2	2052	1.114	0.422	$1.29*10^{-3}$	20°C	11.51
STA1 / STA2	2014	1.036	0.280	$1.84*10^{-3}$	40°C	9.44
STA1 / STA2	1946	1.050	0.280	$1.93*10^{-3}$	60°C	6.00
STA1 / STA2	1921	0.921	0.200	$2.40*10^{-3}$	80°C	4.69
STA1 / STA2	1888	0.908	0.189	$2.54*10^{-3}$	105°C	2.52
STA3 / STA4	2030	1.086	0.412	$1.30*10^{-3}$	20°C	11.42
STA3 / STA4	1991	1.057	0.366	$1.45*10^{-3}$	40°C	9.43
STA3 / STA4	1930	1.076	0.344	$1.62*10^{-3}$	60°C	5.97
STA3 / STA4	1906	1.129	0.378	$1.57*10^{-3}$	80°C	4.67
STA3 / STA4	1866	0.942	0.271	$1.86*10^{-3}$	105°C	2.42

Tab. 3.2 Parameters of the lower block, as delivered

Sample	Density ρ	Thermal Conductivity λ	Thermal Diffusivity κ	Specific Heat c	Temperature T	Remaining Water Cont. w
	kg/m^3	W/(m*K)	mm^2/s	MJ/(kg*K)	°C	%
STU1 / STU2	2064	1.326	0.612	$1.05*10^{-3}$	20°C	11.77
STU1 / STU2	2029	1.033	0.334	$1.52*10^{-3}$	40°C	9.69
STU1 / STU2	1959	1.069	0.358	$1.53*10^{-3}$	60°C	6.09
STU1 / STU2	1933	1.044	0.335	$1.61*10^{-3}$	80°C	4.72
STU1 / STU2	1892	1.024	0.369	$1.47*10^{-3}$	105°C	2.47
STU3 / STU4	2044	1.091	0.300	$1.78*10^{-3}$	20°C	11.65
STU3 / STU4	2023	0.981	0.238	$2.04*10^{-3}$	40°C	9.68
STU3 / STU4	1958	1.001	0.249	$2.05*10^{-3}$	60°C	5.06
STU3 / STU4	1933	0.990	0.242	$2.11*10^{-3}$	80°C	4.67
STU3 / STU4	1891	0.965	0.247	$2.07*10^{-3}$	105°C	2.39

The measurement results on thermal conductivity and specific heat with the different samples are compiled in the Figures 3.6 – 3.8.

Thermal conductivity (Fig. 3.6) of the as-delivered samples shows a slight decrease with temperature which can be attributed to the water loss during heating of the sample (see Tab. 3.1 and 3.2). For the previously dried samples this behaviour is not observed. It can be deduced that the thermal conductivity of the solid phase is independent of temperature in the considered temperature range. Variations of the thermal conductivity in the as-delivered samples are thus exclusively related to replacement of the water phase in the pores by air (air having a lower thermal conductivity than water).

Tab. 3.3 Parameters of the upper and lower block samples after drying

Sample	Density ρ	Thermal Conductivity λ	Thermal Diffusivity κ	Specific Heat c	Temperature T	Remaining Water Cont. w
	kg/m^3	W/(m*K)	mm^2/s	MJ/(kg*K)	°C	%
STU5 / STU6	2093	0.812	0.431	$9.00*10^{-4}$	20°C	0.1
STU5 / STU6	1838	0.820	0.410	$1.09*10^{-3}$	40°C	0.41
STU5 / STU6	1833	0.845	0.398	$1.16*10^{-3}$	60°C	0.21
STU5 / STU6	1830	0.885	0.415	$1.17E*10^{-3}$	80°C	0.02
STU5 / STU6	1826	0.791	0.284	$1.53*10^{-3}$	105°C	0.1
STA5 / STA6	2037	0.777	0.539	$7.07*10^{-4}$	20°C	0.14
STA5 / STA6	1847	0.763	0.470	$8.78*10^{-4}$	40°C	1.14
STA5 / STA6	1845	0.812	0.472	$9.33*10^{-4}$	60°C	1.02
STA5 / STA6	1836	0.771	0.378	$1.11*10^{-3}$	80°C	0.51
STA5 / STA6	1828	0.810	0.404	$1.10*10^{-3}$	105°C	0.07

The thermal conductivity of the as-delivered samples converges towards the dry sample value as temperature is increased. Nevertheless, the thermal conductivity values do not reach the low value measured in dry samples as the remaining water content of the as-delivered samples is still higher than that of the dried samples. This is illustrated in Fig. 3.7 where the results on thermal conductivity are plotted as a function of water content instead of temperature.

It can be expected that the thermal conductivity will increase further with higher water contents. Respective measurements would have to be performed to deduce a respective function. Significant temperature dependence, on the other hand, has not been found.

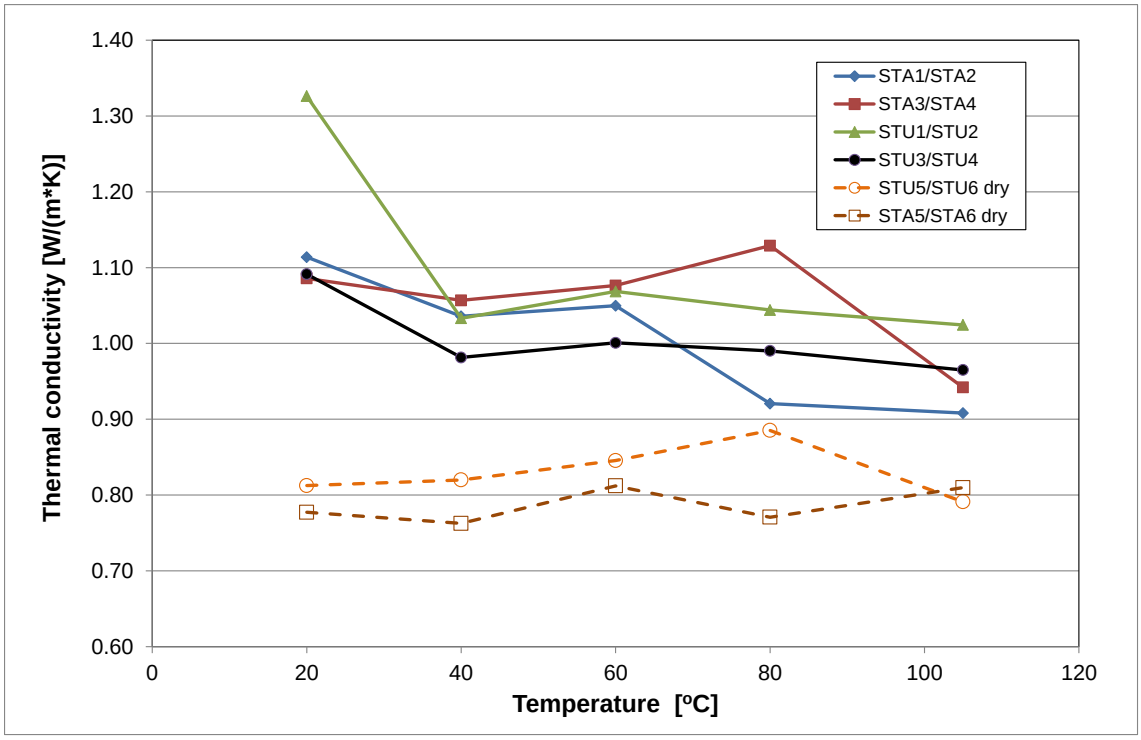

Fig. 3.6 Thermal conductivity of the different samples from the bentonite blocks as a function of temperature

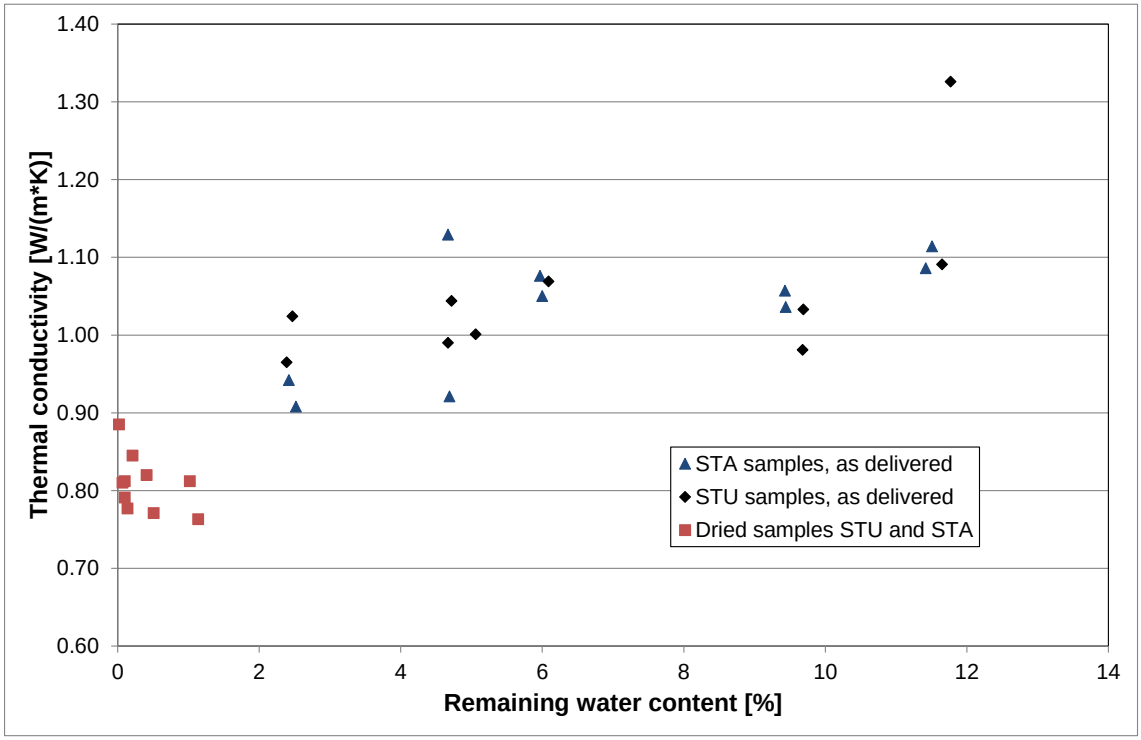

Fig. 3.7 Thermal conductivity of the different samples from the bentonite blocks as a function of water content

For the as-delivered water content, a temperature-independent value of about 1.1 W/(m*K) seems to be a good approximation that could be used as starting value for predictive calculations. During the first years of heating, no significant increase in saturation is expected. For simulating longer time spans when saturation increases, however, a saturation-dependent function for thermal conductivity will be needed.

The specific heat (Fig. 3.8) of all samples increases with temperature. It shows rather large variations between the as-delivered samples. The measured values for the dried samples are considerably lower, showing that water content seems to have a considerable influence on the specific heat. While the temperature effect on the results is visible, the variations between the individual as-delivered samples are much higher. Therefore, it seems reasonable to neglect the temperature dependence and assume a constant specific heat for constant water content. A value of $1.8 \cdot 10^{-3}$ MJ/(kg*K) seems appropriate for as-delivered water content with the temperature range covered in the HE-E. With increasing saturation, it can again be expected that specific heat will change, just as thermal conductivity does. Consequently, the dependence of specific heat on water content will have to be quantified.

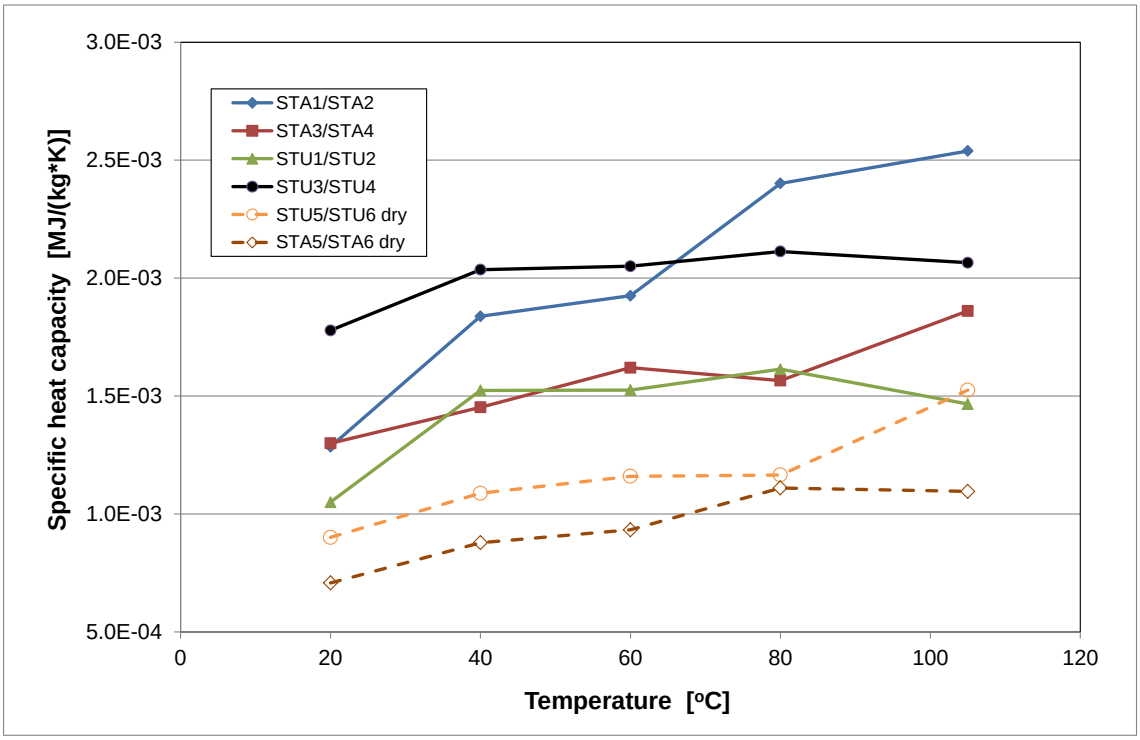

Fig. 3.8 Specific heat of the different samples from the bentonite blocks as a function of temperature

3.3 Measurements on granular sand/bentonite mixture

The measurements were performed on samples consisting of a mixture of sand (65 wt.%) and granular sodium bentonite GELCLAY WH2 (35 wt.%) with an identical grain spectrum of 0.5 – 1.8 mm, the material used in one section of the HE-E in-situ experiment (see Chapter 4). For this granular material a special sample container had to be developed. The sample container, however, made it impossible to determine water content of the sample at each temperature step. Therefore, an individual sample of the as-delivered material was prepared for each temperature step between 20 °C and 105 °C. After the measurement of the thermal parameters, the water content was measured for each sample. Since evaporation is hindered by the sample container, it showed that all samples had approximately the same water content (in contrast to the bentonite blocks which had open surfaces for evaporation).

3.3.1 Sample preparation for measurement of thermal parameters

The sample container which had to be made for the measurements is shown in Fig. 3.9. The container was first filled with a sand/bentonite (SB) layer of 30 mm height which was compacted to a density of 1500 kg/m^3, the density that was measured for the SB buffer emplaced in the HE-E (Fig. 3.9).

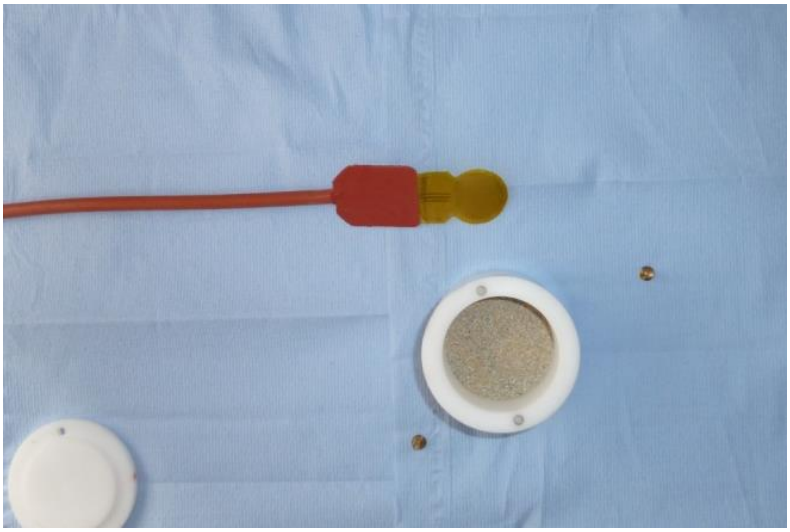

Fig. 3.9 Sample container with SB layer, in red: measurement sensor

Then, the sensor was inserted by a slot in the container side, so that it lay on top of the SB layer (Fig. 3.10).

Fig. 3.10 Sensor and SB layer inside the sample container

Afterwards, a second layer of SB material was filled into the container and compacted (Figures 3.11 and 3.12).

Fig. 3.11 Emplacement of second SB layer into the sample container

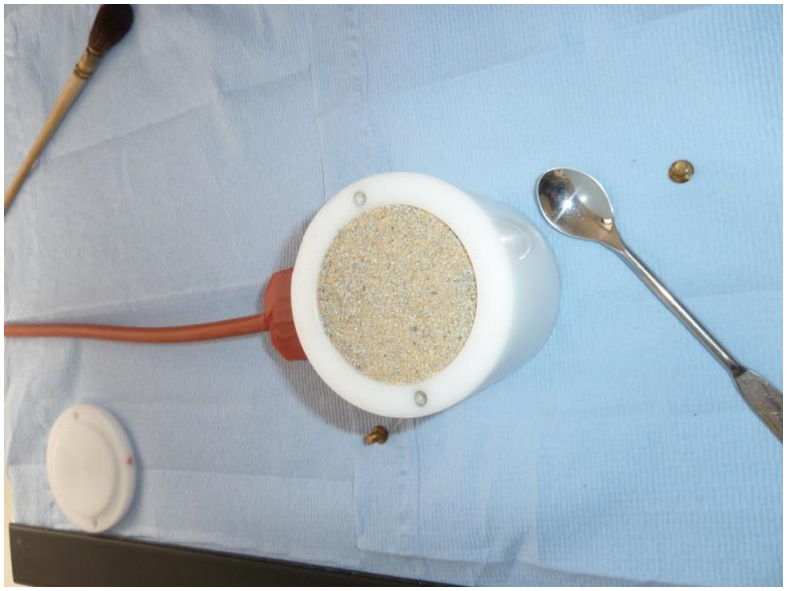

Fig. 3.12 Filled sample container before closing

Finally, the filled sample container was closed with a lid and placed in the oven, which is equipped with lead-throughs for the connection cable (Fig. 3.13).

Fig. 3.13 Prepared sample in the oven

3.3.2 Determination of thermal parameters

Each of the samples with as-delivered water content was placed in the oven for six hours at the target temperature (20 °C, 40 °C, 60 °C, 80 °C und 105 °C); then the

thermal parameters were measured. Afterwards, the sample was dried for the determination of water content.

For comparison, measurements were performed on samples of dried material as well. The dry samples were measured at the same temperature steps, but the same samples were used for the different steps, since no change in water content needed to be considered. The time for each step was one day. The samples were not removed from the container between the steps.

3.3.2.1 Bulk density and grain density

The bulk density of the samples from as-delivered material was quite homogeneous with values between 1517 kg/m^3 and 1548 kg/m^3 (see Tab. 3.4). The density of the dried samples did not vary significantly. For the calculation of the specific heat a mean value of 1503 kg/m^3 could be used (Tab. 3.5).

The grain density was determined on the dried material; the resulting value was 2546 kg/m^3.

Tab. 3.4 Parameters of the granular sand/bentonite at as-delivered water content

Sample	Density ρ	Thermal Conductivity λ	Thermal Diffusivity κ	Specific Heat c	Temperature T	Remaining Water Cont. w
	kg/m^3	W/(m*K)	mm^2/s	MJ/(kg*K)	°C	%
sand/bentonite granulate (65/35)	1517	0.300	0.247	7.99*10^{-4}	20°C	3.51
sand/bentonite granulate (65/35)	1537	0.368	0.269	8.89*10^{-4}	40°C	3.36
sand/bentonite granulate (65/35)	1548	0.404	0.284	9.20*10^{-4}	60°C	3.54
sand/bentonite granulate (65/35)	1543	0.418	0.276	9.84*10^{-4}	80°C	3.48
sand/bentonite granulate (65/35)	1518	0.437	0.204	1.44*10^{-3}	105°C	3.4

Tab. 3.5 Parameters of the dried granular sand/bentonite buffer material

Sample	Density ρ	Thermal Conductivity λ	Thermal Diffusivity κ	Specific Heat c	Temperature T	Remaining Water Cont. w
	kg/m^3	W/(m*K)	mm^2/s	MJ/(kg*K)	°C	%
sand/bentonite granulate dry	1503	0.297	0.2553	$7.74*10^{-4}$	20°C	dry
sand/bentonite granulate dry	1503	0.3015	0.2587	$7.75*10^{-4}$	40°C	dry
sand/bentonite granulate dry	1503	0.3061	0.2484	$8.20*10^{-4}$	60°C	dry
sand/bentonite granulate dry	1503	0.3168	0.2449	$8.61*10^{-4}$	80°C	dry
sand/bentonite granulate dry	1503	0.3253	0.2399	$9.02*10^{-4}$	105°C	dry

3.3.2.2 Water content

The water content of the individual samples did not show a great variation (Tab. 3.4) after the measurement at elevated temperature. The mean value was at 3.5 % and compares well with the original material. Obviously, evaporation from the sampling container was insignificant.

For the dried sample a slight increase to 0.06 % of water was observed after the measurement, which was a consequence of the sample taking up air humidity after removal from the oven.

3.3.2.3 Thermal parameters at varying temperature

The thermal conductivity of the samples with as-delivered water content is steadily rising with temperature (Tab. 3.4 and Fig. 3.14). Thermal conductivity of water rises with temperature, but the increase of the thermal conductivity measured in the samples cannot be attributed to that because of the small water content of the samples. In addition, the same trend, although less pronounced, can be seen for the dried samples (Tab. 3.5 and Fig. 3.14).

An explanation may be that the increased temperature in the confined sample leads to thermal stresses and a somewhat softer behaviour of the material (especially if some water is present). This may result in an improved coupling between the granular material and the sensor. Such a behaviour was not found for the bentonite blocks, because of their higher thermal conductivity (as a consequence of higher density and water content), better coupling from the beginning, and because of the fact that the blocks' thermal expansion is not restricted by a container. Because of the rather small sample dimensions and, in comparison, large contact surface coupling seems to be a major problem for this type of measurement, especially for granular material.

Specific heat is shown in Fig. 3.15. Specific heat is again slightly increasing with temperature. The reason for the extreme value of the as-delivered sample at 105 °C is unclear. Otherwise, a value of $9*10^{-4}$ MJ/(kg*K) seems appropriate for model calculations at as-delivered water content.

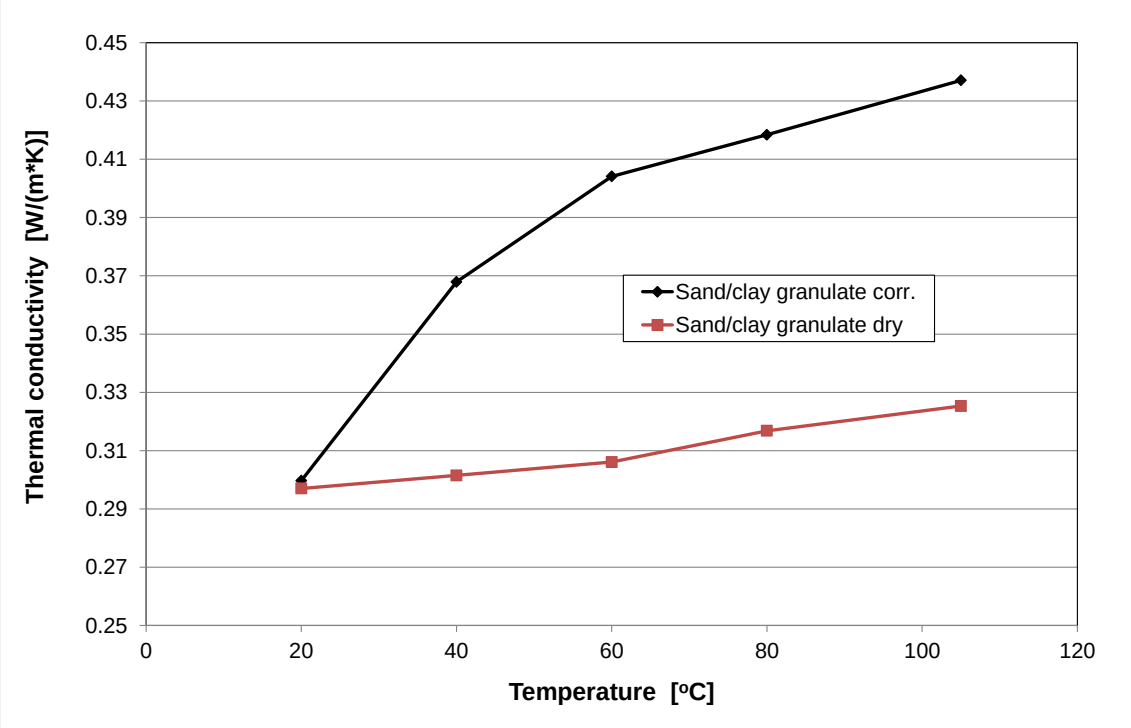

Fig. 3.14 Thermal conductivity of the dry (red) and as-delivered (black) SB samples as a function of temperature

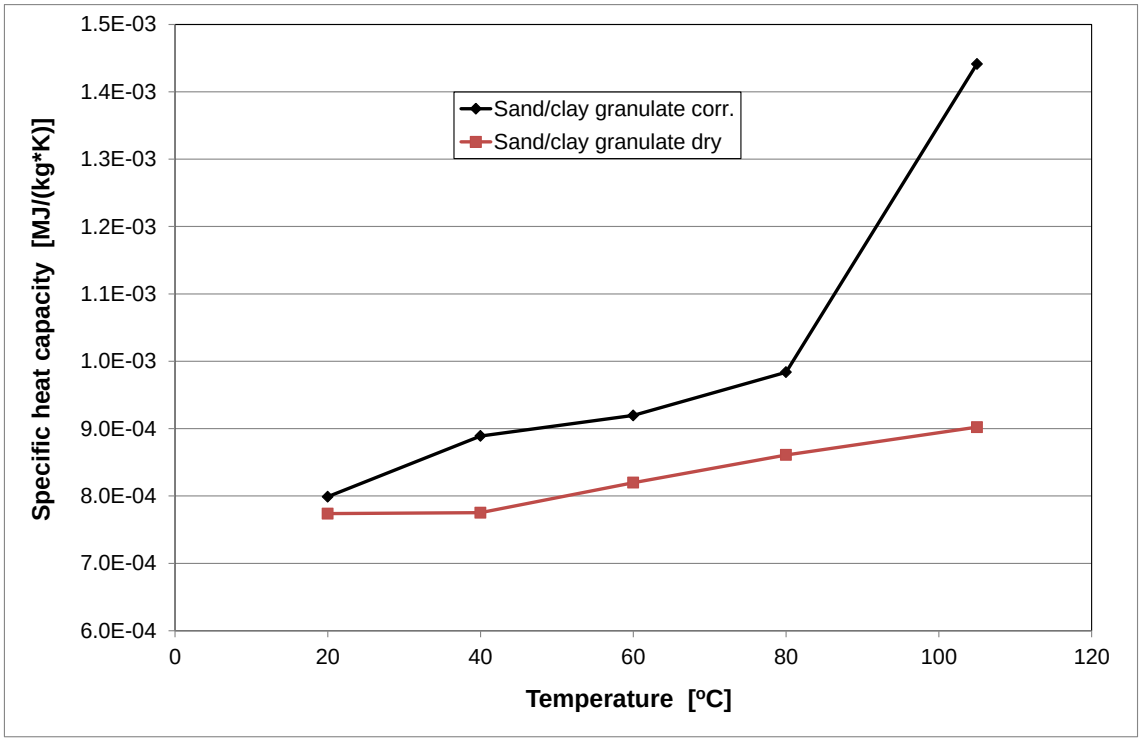

Fig. 3.15 Specific heat of the dry (red) and as-delivered (black) SB samples as a function of temperature

3.3.2.4 Thermal conductivity as a function of water content

Since the actual temperature influence on the thermal parameters does not seem very significant, thermal conductivity as a function of water content was only measured at ambient temperature. In a first series of experiments, sand/bentonite samples with different water contents were prepared by placing them in exsiccators containing different salt solutions where they were stored until constant weight was reached (see next section for a more detailed description of the procedure).

The water content of 9.07 % reached at 100 % humidity in the exsiccator was, however, far from the value required for full saturation of the sample. From dry density and grain density of the sand/bentonite a porosity around 41 % can be calculated. A water content in the range of 27 % would be required for full saturation. The reason for this low water content is the low suction of the material which reaches a zero-value already around 28 % saturation (see next section). As a consequence, samples had to be prepared differently for investigating thermal parameters of the sand/bentonite at higher saturation. Instead of resaturating them under a moist atmosphere, the water was added directly to the granular material, which was then compacted to the required density.

The thermal parameters of all samples were measured using the Hotdisk system, in the same way as described before. After each measurement the actual water content of the sample was determined. The results are summarized in Tab. 3.6. The first six lines of Tab. 3.6 represent results obtained on samples prepared in the exsiccator, while the last three lines are results obtained from directly saturated samples. Thermal conductivity as a function of water content is also shown in Fig. 3.16. At full saturation a rather high value of about 1.5 W/(m*K) is reached. The graph of the specific heat as a function of water content shows great variability with unexpectedly low values at high saturation. Variations in the sample density (Tab. 3.6) are not sufficient to explain this behaviour. No reasonable explanation for this result can be given.

Tab. 3.6 Parameters of granular sand/bentonite mixture at variable water content

Relative Humidity	Density ρ	Thermal Conductivity λ	Thermal Diffusivity κ	Specific Heat c	Temperature T	Water Content w
	kg/m^3	W/(m*K)	mm^2/s	MJ/(kg*K)	°C	%
12%	1508	0.305	0.278	$7.28*10^{-4}$	25	1.14
31%	1541	0.362	0.280	$8.42*10^{-4}$	25	2.70
54%	1545	0.370	0.288	$8.32*10^{-4}$	25	3.75
70%	1528	0.364	0.247	$9.77*10^{-4}$	25	4.63
90%	1539	0.411	0.314	$9.25*10^{-4}$	25	5.27
100%	1477	0.433	0.306	$9.5*10^{-4}$	25	9.07
-	1503	0.492	0.292	1.12*10-3	24	9.18
-	1499	0.804	0.606	8.86*10-4	24	13.29
-	1505	1.577	1.167	9.03*10-4	24	25.25

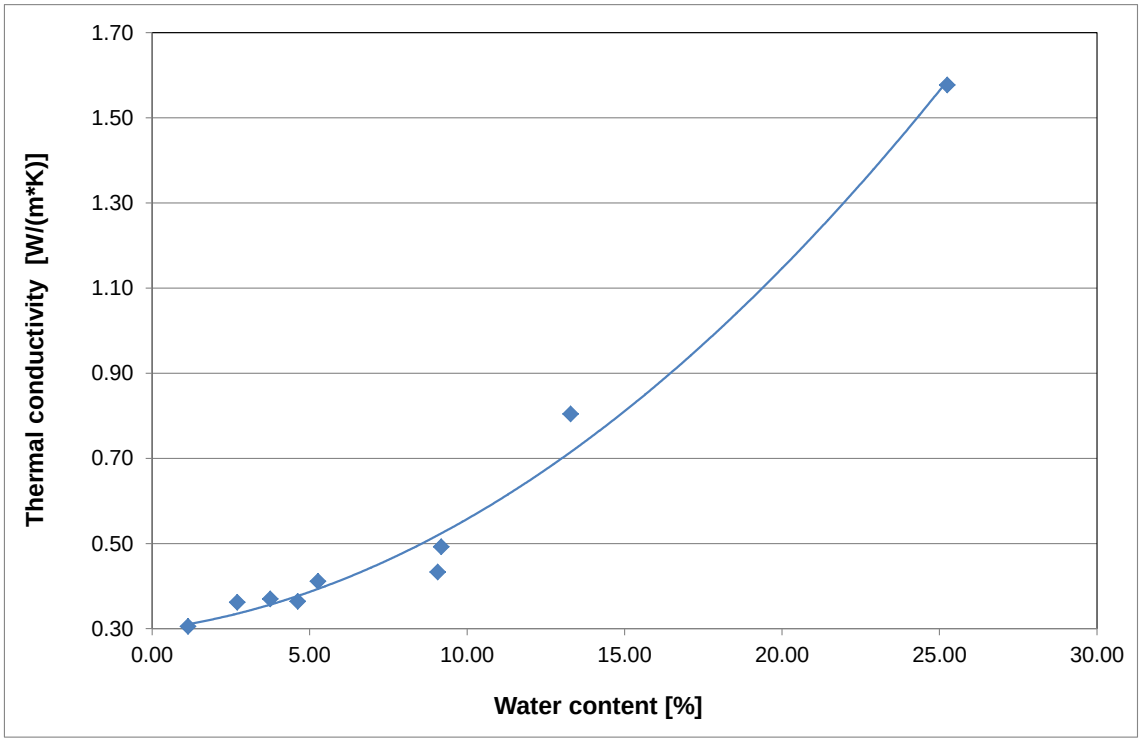

Fig. 3.16 Thermal conductivity of granular sand/bentonite as a function of water content

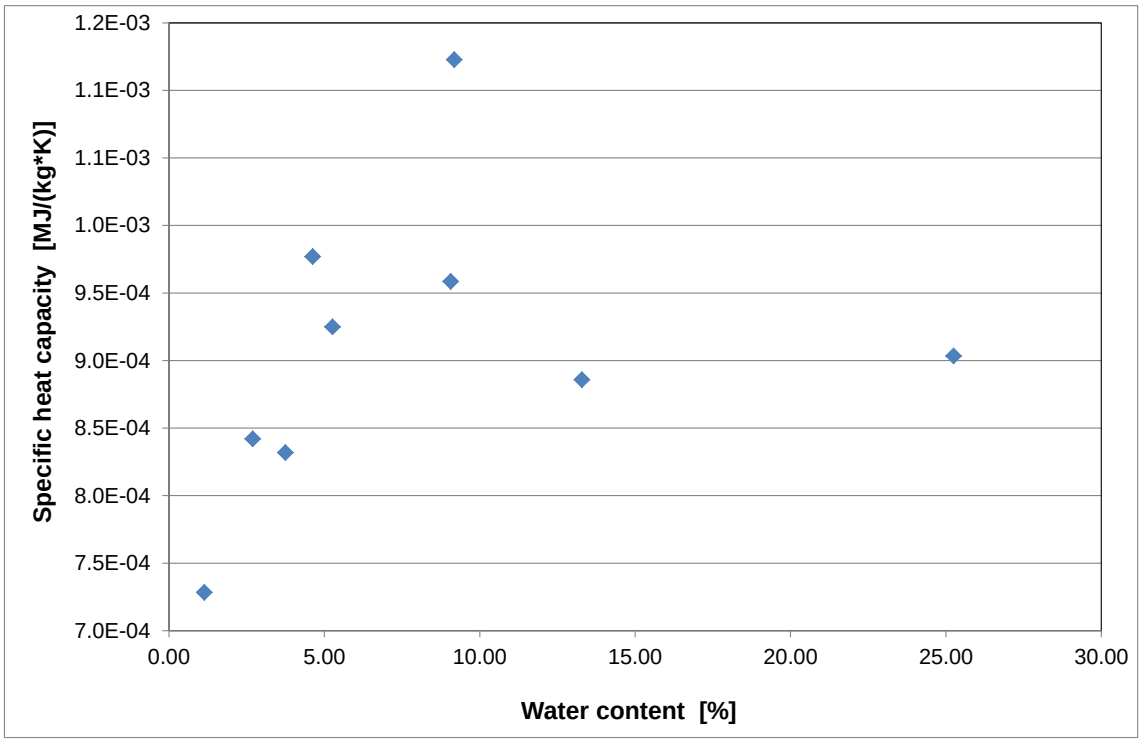

Fig. 3.17 Specific heat of granular sand/bentonite as a function of water content

3.3.3 Sample preparation and measurement of retention curve

For determination of the retention curve samples of sand/bentonite mixture were re-saturated in exsiccators (Fig. 3.18) containing different salt solutions in order to obtain different relative humidities in the atmosphere. Ten different solutions were used to obtain relative humidities between 6 % and 100 %. At each humidity value two samples were measured. The sample material was placed in open PVC cells with pierced bottom plates (Fig. 3.19) in order to get good contact between the humid air and the sample. To avoid sample material falling through the bottom holes, a filter paper was placed in the cell before emplacing the sand/bentonite. The cell dimensions are 48 mm diameter and 20 mm height.

Fig. 3.18 Exsiccators with sensors for temperature and humidity measurement

The sample material was emplaced and flattened so that the surface was flush with the cell rim (Fig. 3.20). Emplacement density was chosen in a way that, considering the initial water content of the samples of 3.5 %, a dry density of 1.4 g/cm^3 – 1.45 g/cm^3 was reached.

The samples were left in the exsiccators until constant air humidity was reached; the minimum time for equilibration was seven days. Afterwards, the samples were removed from the exsiccators and the actual water content was determined by oven- drying at 105 °C following DIN 18121.

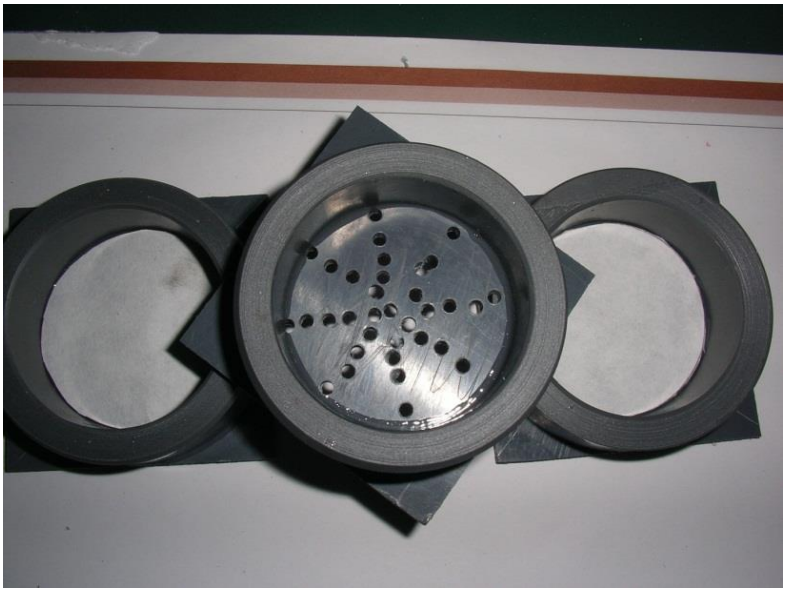

Fig. 3.19 PVC cell before emplacement of the sand/bentonite sample

Fig. 3.20 Measurement cell filled with sand/bentonite sample

From the water content the dry density was calculated. For calculation of the porosity the grain density of 2.546 g/cm^3, measured with a gas pycnometer, was used. Porosity is calculated as

$$\Phi = 1 - \frac{\rho_d}{\rho_s} \tag{3.1}$$

Φ	Porosity of the mixture [-]
ρ_d	Dry density of the mixture [kg/m^3]
ρ_s	Grain density of the mixture [kg/m^3]

For plotting suction as a function of saturation the saturation is calculated as

$$S = \frac{\rho_d \cdot w}{\rho_w \cdot \Phi} \tag{3.2}$$

S	Degree of water saturation [-]
w	Water content [-]
ρ_d	Dry density of the mixture [kg/m3]
Φ	Porosity of the mixture [-]

From the psychrometric law /FRE 93/ the suction is obtained from

$$s = \frac{R \cdot T \cdot \rho_w}{\omega_v} \cdot \ln(RH) \tag{3.3}$$

s	Soil suction [kPa]
R	Universal gas constant (8.31432 J/(mol K))
T	Absolute temperature ($T = 273.16 + t$) [K]
t	Temperature [°C]
ρ_w	Density of water (998 kg/m3 at 20 °C)
ω_v	Molecular mass of water vapour (8.016 kg/kmol)
RH	Relative air humidity, [-]

In Tab. 3.7 the results of the measurements are summarized. Figure 3.21 shows the corresponding suction/saturation diagram.

The sand/bentonite mixture shows very low suction once a saturation above 15 % is reached. In fact, suction apparently drops to zero at a saturation of only 28 %. This is a consequence of the rather low bentonite content and the high porosity. When the bentonite in the mixture is already saturated, there is still free pore space left in the material. This behaviour is also documented by the permeability properties of the material, as shown in the next section.

Tab. 3.7 Results of the retention curve measurements of granular sand/bentonite

Dry Density ρd	Porosity Φ	Water Content w	Relative Air Humidity RH	Saturation S	Suction s
g/cm^3	-	-	-	-	MPa
1.437	0.436	0.0045	0.08	0.015	341.03
1.440	0.434	0.0048	0.08	0.016	341.03
1.382	0.457	0.0082	0.12	0.025	286.28
1.389	0.454	0.0082	0.12	0.025	286.28
1.411	0.446	0.0213	0.22	0.068	204.44
1.425	0.440	0.0193	0.22	0.063	204.44
1.421	0.442	0.0243	0.32	0.078	153.85
1.427	0.439	0.0265	0.32	0.086	153.85
1.438	0.435	0.0404	0.55	0.134	80.72
1.439	0.435	0.0406	0.55	0.135	80.72
1.431	0.438	0.0427	0.7	0.140	48.16
1.436	0.436	0.0400	0.7	0.132	48.16
1.446	0.432	0.0466	0.74	0.156	40.66
1.455	0.429	0.0463	0.74	0.157	40.66
1.468	0.423	0.0512	0.85	0.178	21.94
1.476	0.420	0.0554	0.85	0.195	21.94
1.470	0.423	0.0582	0.9	0.203	14.23
1.447	0.432	0.0518	0.9	0.174	14.23
1.445	0.433	0.0847	1	0.283	0
1.436	0.436	0.0849	1	0.280	0

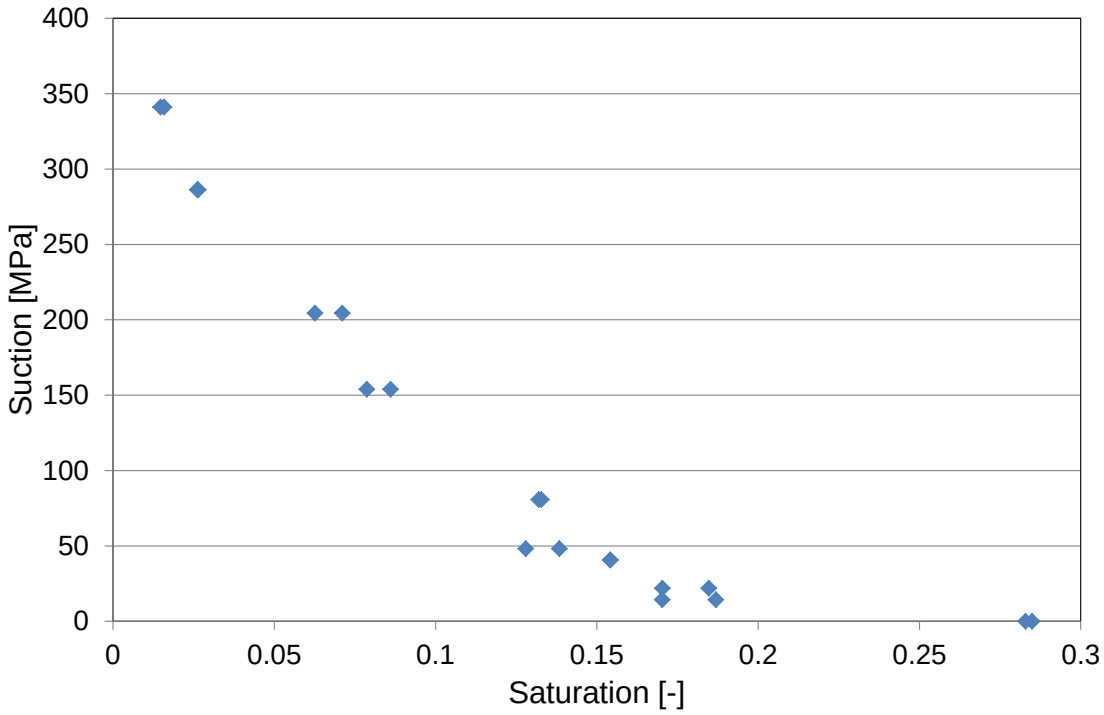

Fig. 3.21 Retention curve of granular sand/bentonite mixture

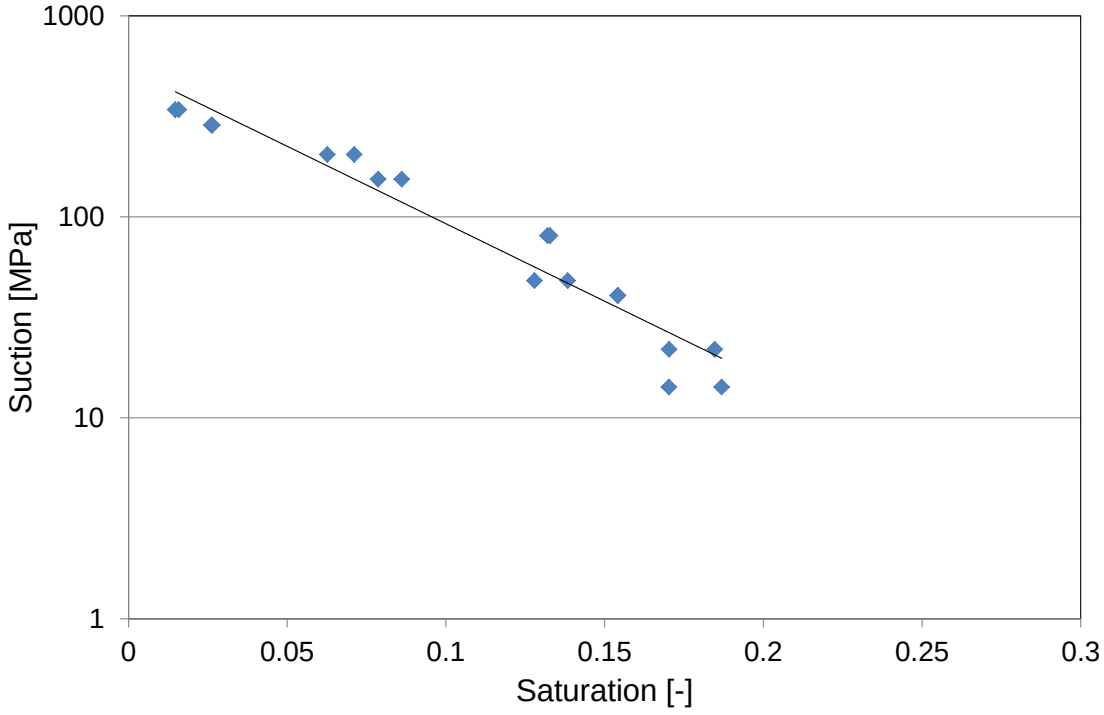

Fig. 3.22 Retention curve of granular sand/bentonite mixture, logarithmic scale

The suction of zero at 28 % saturation may be due to inaccuracy of the relative humidity measurement. In Fig. 3.22, the retention curve is plotted in a logarithmic scale, leaving out the value at 28 % porosity. The results seem to follow a straight line; the corresponding suction at 28 % porosity would be around 3 MPa and the humidity about 98 %.

3.3.4 Permeability of granular sand/bentonite

The granular sand/bentonite material was placed in a cylindrical cell (Fig. 3.23). Emplacement density was 1504 kg/m^3 and the corresponding porosity 42.7 %. Permeability to gas was determined by nitrogen injection at five pressure steps between 0.111 MPa and 0.151 MPa (absolute pressure); the gas flow was measured using a burette. The permeability derived using Darcy's law was nearly identical for all pressure steps, with a value of $2.1 \cdot 10^{-12}$ m^2.

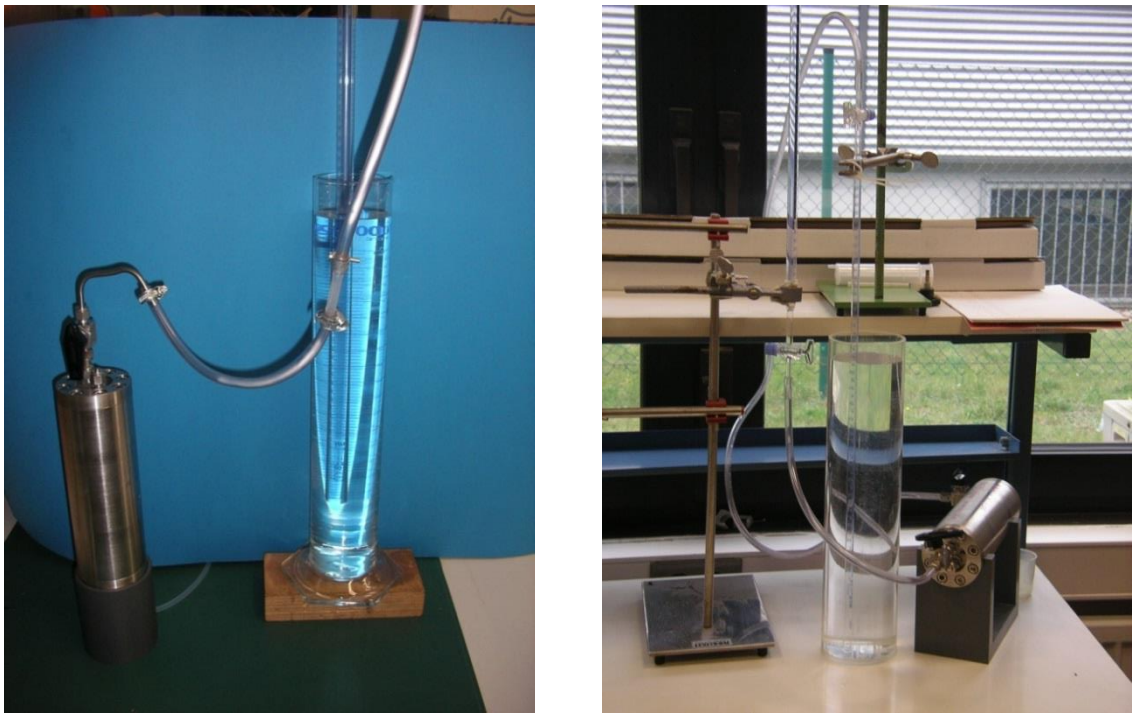

Fig. 3.23 System for measurement of sand/bentonite permeability to gas (left) and water (right)

For measurement of the permeability to water the cell was placed horizontally (Fig. 3.23) and the sample was re-saturated with Pearson water very slowly at very low overpressure in mbar-range. The idea of the slow injection was to avoid flushing out of

small particles. The following permeability measurement was performed at three differential pressures around 0.01 MPa. The resulting mean permeability was $1.2 \cdot 10^{-13}$ m^2.

After finishing the experiment the sample was pressed out of the cell and dissected for water content measurement (Fig. 3.24). On the injection side the water content amounted to 29.9 %, decreasing slighly to 27.3 % on the outlet side. The mean water content was 28.3 %, meaning the material was completely saturated.

Fig. 3.24 Removal of saturated sand/bentonite from the cell

3.4 Measurements on granular bentonite

The third material emplaced in the HE-E is the granular bentonite material of NAGRA's reference concept. Preliminary measurements with the pure granular bentonite material were already performed in 2010. It has, however, to be noted that the sample density was higher than the actual density of the material emplaced in the HE-E. The material was emplaced in layers in Plexiglas containers. The sensor was located in the sample mid-plane, similar to the measurements with the SB material (Fig. 3.25). The material was investigated at as-delivered water content and after drying at 105 °C. The measurement results are compiled in Tab. 3.8.

In autumn 2011, a new measurement series was performed with the same buffer material, but with the new sample containers.

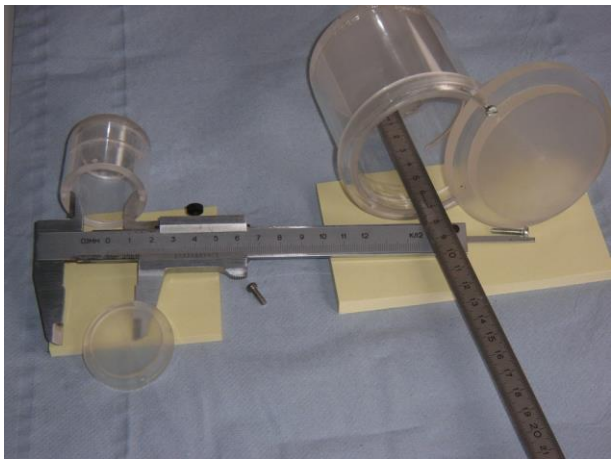

Sample containers

Sample inside the container

Fig. 3.25 Sample containers for the preliminary measurements on bentonite pellets

Tab. 3.8 Thermal parameters of granular bentonite buffer material, preliminary tests

Sample	Density ρ	Thermal Conductivity λ	Thermal Diffusivity κ	Specific Heat c	Temperature T	Water Content w
	kg/m^3	W/(m*K)	mm^2/s	MJ/(kg*K)	°C	%
As-delivered material	1752	0.447	0.327	$7.82*10^{-4}$	20°C	6.33
Dry material	1641	0.386	0.302	$7.79*10^{-4}$	20°C	dry

3.4.1 Sample preparation

In the laboratory of ETH Zürich the minimum (1470 – 1490 kg/m³) and maximum (1680 – 1700 kg/m³) emplacement densities for the granular bentonite material were determined /TEO 12/. For the measurement of the thermal parameters at the GRS lab it was tried to prepare samples with a bulk density below 1500 kg/m³. The preparation procedure was the same as for the sand/bentonite material (see Section 3.3.1).

It proved, however, impossible to prepare samples of this density with a sufficient coupling between the bentonite and the measuring probe. In contrast to the SB material, the pure granular bentonite has a much higher variation in grain size, which is the reason for this problem. Therefore, samples with a bulk density around 1700 kg/m³ had to

be used for investigating the dependence of the thermal parameters on temperature. Later, these problems were partially overcome. Measurements of the thermal parameters at varying water content of the material could be performed on samples with bulk densities of 1600 kg/m³.

3.4.2 Determination of thermal parameters

3.4.2.1 Thermal parameters at varying temperature

The measurements were performed in the same way as with the sand/bentonite material. From the as-delivered granular bentonite an individual sample was prepared for each temperature step, while with the dried material the same sample could be used for all temperature steps, as discussed already in Section 3.3. The measurement results are shown in the Tables 3.9 and 3.10.

Tab. 3.9 Thermal parameters of the granular bentonite buffer material at as-delivered water content

Sample	Density ρ	Thermal Conductivity λ	Thermal Diffusivity κ	Specific Heat c	Temperature T	Water Content w
	kg/m^3	W/(m*K)	mm^2/s	MJ/(kg*K)	°C	%
granular bentonite buffer material	1667	0.338	0.366	5.54E-04	25	5.91
granular bentonite buffer material	1720	0.401	0.332	7.03E-04	40	5.62
granular bentonite buffer material	1687	0.415	0.316	7.78E-04	60	5.75
granular bentonite buffer material	1691	0.408	0.317	7.62E-04	80	5.42
granular bentonite buffer material	1726	0.435	0.315	8.01E-04	105	4.52

Tab. 3.10 Thermal parameters of the dried granular bentonite buffer material

Sample	Density ρ	Thermal Conductivity λ	Thermal Diffusivity κ	Specific Heat c	Temperature T	Water Content w
	kg/m^3	W/(m*K)	mm^2/s	MJ/(kg*K)	°C	%
granular bentonite buffer material; dry	1702	0.389	0.267	8.56E-04	25°C	dry
granular bentonite buffer material; dry	1702	0.403	0.278	8.52E-04	40°C	dry
granular bentonite buffer material; dry	1702	0.416	0.270	9.05E-04	60°C	dry
granular bentonite buffer material; dry	1702	0.427	0.266	9.46E-04	80°C	dry
granular bentonite buffer material; dry	1702	0.429	0.248	1.02E-03	105°C	dry

The density of the samples ranged around 1700 kg/m³. The water content of the as-delivered material ranged between 4.5 % and nearly 6 %, with a downward trend at higher temperature. It seems that, in contrast to the measurements with sand/bentonite, there was some evaporation during heating. The water content of 5.91 % at ambient temperature is in good agreement with ETH measurements /TEO 12/ which resulted in 5.9 % - 6.0 %.

The thermal conductivity as a function of temperature is shown in Fig. 3.26. The curves for the dried and as-delivered material are very close, for two temperatures, the as-delivered material has an even lower thermal conductivity than the dried material. This is a clear hint that there are still major coupling problems. In the temperature range which is interesting for the HE-E, the thermal conductivity of the granular bentonite is in the same range (0.4–0.43 W/(m*K) as for the granular sand/bentonite with a considerably lower density.

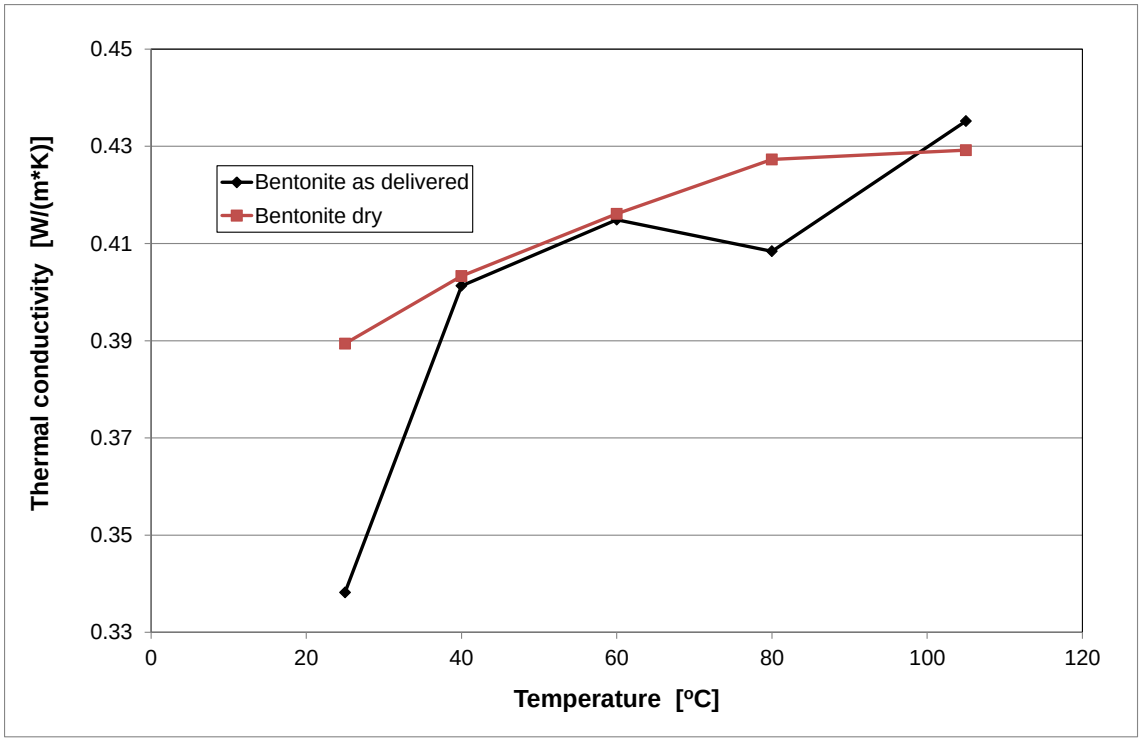

Fig. 3.26 Thermal conductivity of the dry (red) and as-delivered (black) bentonite samples as a function of temperature

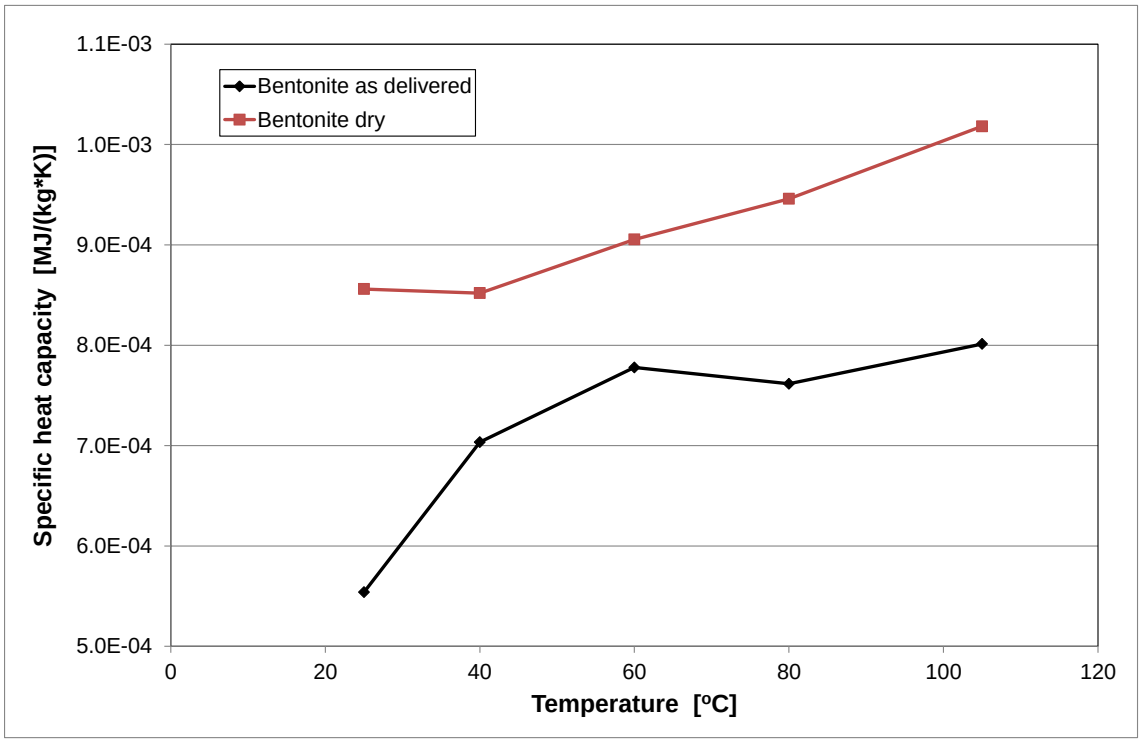

Fig. 3.27 Specific heat of the dry (red) and as-delivered (black) bentonite samples as a function of temperature

Specific heat (Fig. 3.27) is higher for the dried sample than for the as-delivered one, which can again only be explained by coupling problems, considering the fact that two of the as-delivered samples had an even higher density than the dry one. The specific heat of the as-delivered material of about $7*10^{-4}$ MJ/(kg*K) - $8*10^{-4}$ MJ/(kg*K) therefore is rather questionable, although it agrees with the earlier measurements.

3.4.2.2 Thermal parameters at varying water content

Measurements of the thermal parameters of granular bentonite as a function of water content were performed on samples with densities of about 1600 kg/m³. The water content of the samples was controlled by storing them in exsiccators with suitable salt solutions, as described in Section 3.3.3. Five different humidities were employed, and for each humidity step three samples were prepared and measured. The results are shown in Tab. 3.11.

Tab. 3.11 Parameters of granular bentonite at variable water content

Relative Humidity	Density ρ	Thermal Conductivity λ	Thermal Diffusivity κ	Specific Heat c	Temperature T	Water Content w
	kg/m^3	W/(m*K)	mm^2/s	MJ/(kg*K)	°C	%
12% (1)	1598.2	0.4261	0.3015	8.84E-04	25	3.8
12% (2)	no value	no value	no value	no value	25	3.8
12% (3)	1603.3	0.3701	0.4135	5.58E-04	25	3.8
54% (1)	1599.9	0.4381	0.2615	1.05E-03	25	8.93
54% (2)	1599.7	0.3994	0.2638	9.46E-04	25	8.93
54% (3)	1604.1	0.4109	0.3654	7.01E-04		8.93
75% (1)	1597.1	0.5014	0.2731	1.15E-03	25	12.24
75% (2)	1599.7	0.46	0.275	1.05E-03	25	12.24
75% (3)	1595.7	0.5193	0.3673	8.86E-04	25	12.24
85% (1)	1599	0.4651	0.298	9.76E-04	25	12.6
85% (2)	1599.5	0.4588	0.2785	1.03E-03		12.6
85% (3)	no value	no value	no value	no value	25	12.6
100% (1)	1587.8	0.7008	0.2739	1.61E-03	25	24.32
100% (2)	1596	0.7184	0.2686	1.68E-03	25	24.32
100% (3)	1595.7	0.7385	0.2618	1.77E-03	25	24.32

Figure 3.28 shows the thermal conductivity of the granular bentonite material as a function of water content. The thermal conductivity at high saturation is considerably lower than for the sand bentonite mixture.

The specific heat is plotted in Fig. 3.28. In this case, it shows a much more consistent behaviour than for the sand/bentonite mixture, with a more or less linear trend to higher values at higher water content.

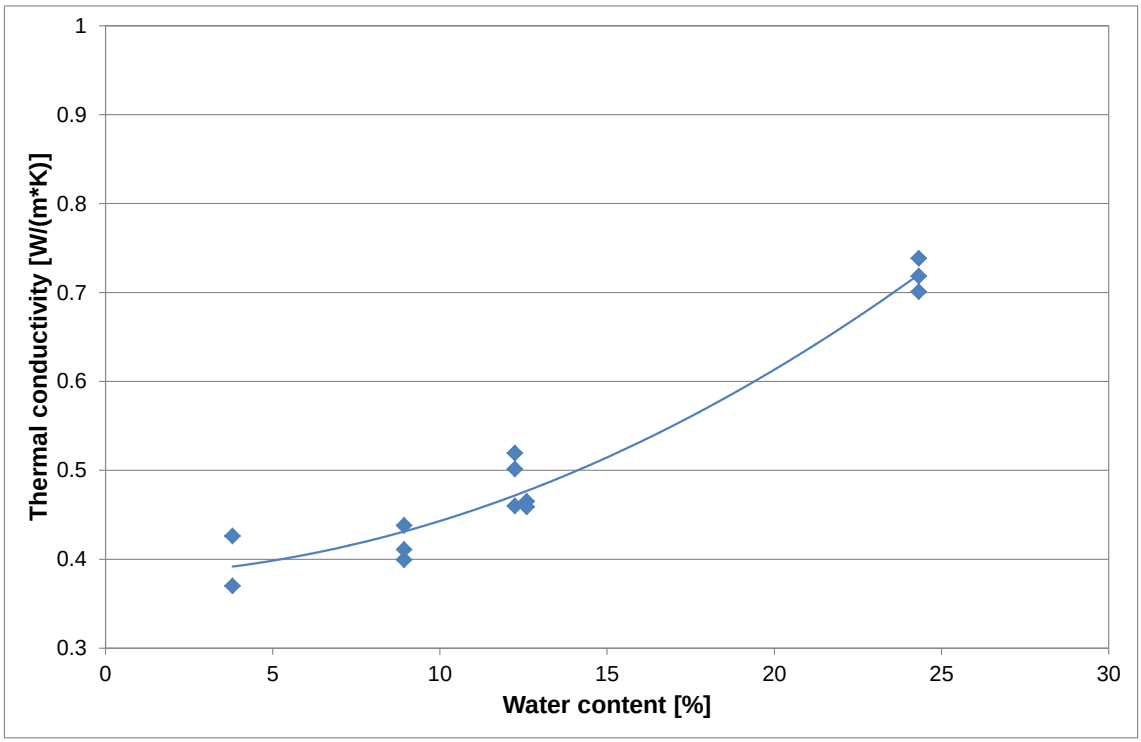

Fig. 3.28 Thermal conductivity of granular bentonite as a function of water content

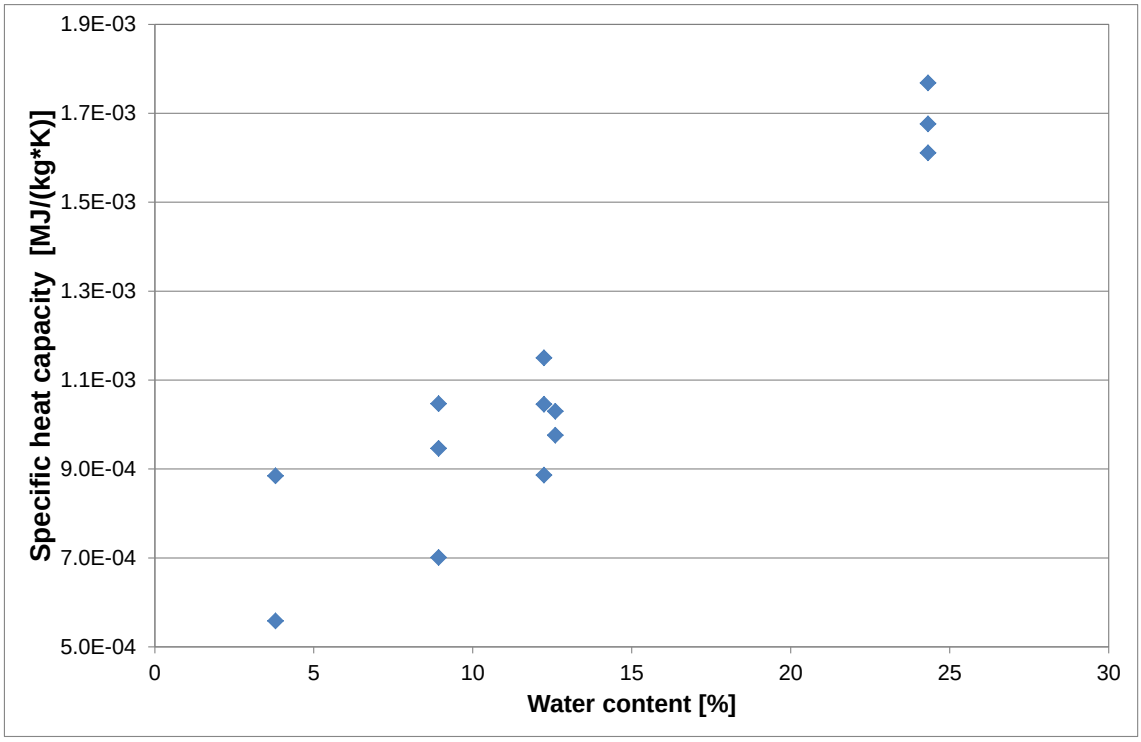

Fig. 3.29 Specific heat of granular bentonite as a function of water content

3.5 Conclusions from laboratory testing

The thermal parameters of the three buffer materials employed in the Mont Terri HE-E experiment were determined in the laboratory.

The parameters of the bentonite blocks were in the expected range, measured densities and water contents are comparable with parallel measurements of ETH.

For the granular materials, coupling of the measuring probe to the sample material proved to be an issue, especially for the granular bentonite exhibiting a wide grain spectrum. For this material, acceptable measurement results could only be obtained for the upper end of the relevant density range. The values themselves are consistent, although the thermal conductivity of 0.7 W/(m*K) at full saturation seems somewhat low.

The sand/bentonite mixture exhibited good thermal conductivity up to 1.5 W/(m*K) at full saturation. The scatter of measurement data for the specific heat may hint to coupling problems again.

In addition to the thermal parameters, measurements of the retention curve and the permeability were performed for the sand/bentonite mixture, since no respective data were available. The material has not been used before, it was chosen because it showed no segregation in emplacement tests (see Chapter 4). Because of constraints in handling, the material had to be installed in the HE-E without any compaction. The resulting high porosity led to insignificant swelling pressure and high permeability at full saturation, as was measured in the laboratory. Suction is very low already at 20 % saturation. While the results are valuable for modelling the HE-E, they also show that this material, in the actual configuration, is hardly suitable as buffer material. For use in a repository, the material would have to be changed, either by changing bentonite content and/or grain spectrum or by compaction, in order to arrive at significant swelling pressure and sufficiently low permeability.

4 The HE-E experiment at Mont Terri

The HE-E experiment was planned in the frame of PEBS as a new experiment in Mont Terri, concentrating on the effects of the early non-isothermal resaturation period after emplacement and its impact on the THM behaviour. The objectives /GAU 14/ were

- To provide the experimental data base required for the calibration and validation of existing THM models of the early resaturation phase.
- To upscale thermal conductivity of the partially saturated EBS from laboratory to field scale for bentonite and sand/bentonite mixture.

All information on the HE-E is given in the following PEBS deliverables:

- Design and predictive modelling of the HE-E test (Deliverable D3.2-1) /CZA 11/
- Report on the construction of the HE-E experiment (Deliverable D2.2-3) /TEO 12/
- The HE-E Experiment: Lay-out, Interpretation and THM Modelling (the HE-E final report, Deliverable D2.2-11 and D3.2-2) /GAU 14/

An overview of the HE-E design, construction and realization is given in the following sections.

4.1 Experiment design

The HE-E experiment was constructed in the former VE test section of the raise-bored micro-tunnel of the Mont Terri Rock Laboratory excavated in 1999 in the shaly facies of the Opalinus Clay, using the horizontal raise-boring technique. Until 2006, the VE experiment /MAY 07/ was performed in the micro-tunnel. Advantage could be taken of the extensive instrumentation of the VE section. Only a few additions were needed to complete rock instrumentation for the HE-E.

The HE-E experiment (Figs. 1.2 and 4.2) consists of two independently heated sections, each 4 metres long. The heaters are placed in a steel liner supported by MX80 bentonite blocks (dry density 1.8 g/cm³, water content 11 %, see Section 3.2.3). The two sections are fully symmetric apart from the granular filling material. While Section 1 is filled with a granular 65/35 sand/bentonite mixture, Section 2 is filled with pure MX80 bentonite pellets. This allows comparing the thermo-hydraulic behaviour of the two

EBS materials under almost identical conditions. The MX80 materials (blocks and pellets) are similar to those materials considered for the repository EBS in Switzerland. Sand/bentonite mixtures are under consideration as an alternative EBS material in Germany. Therefore, the two experiment sections are often referred to in the reports as NAGRA section and GRS section, respectively.

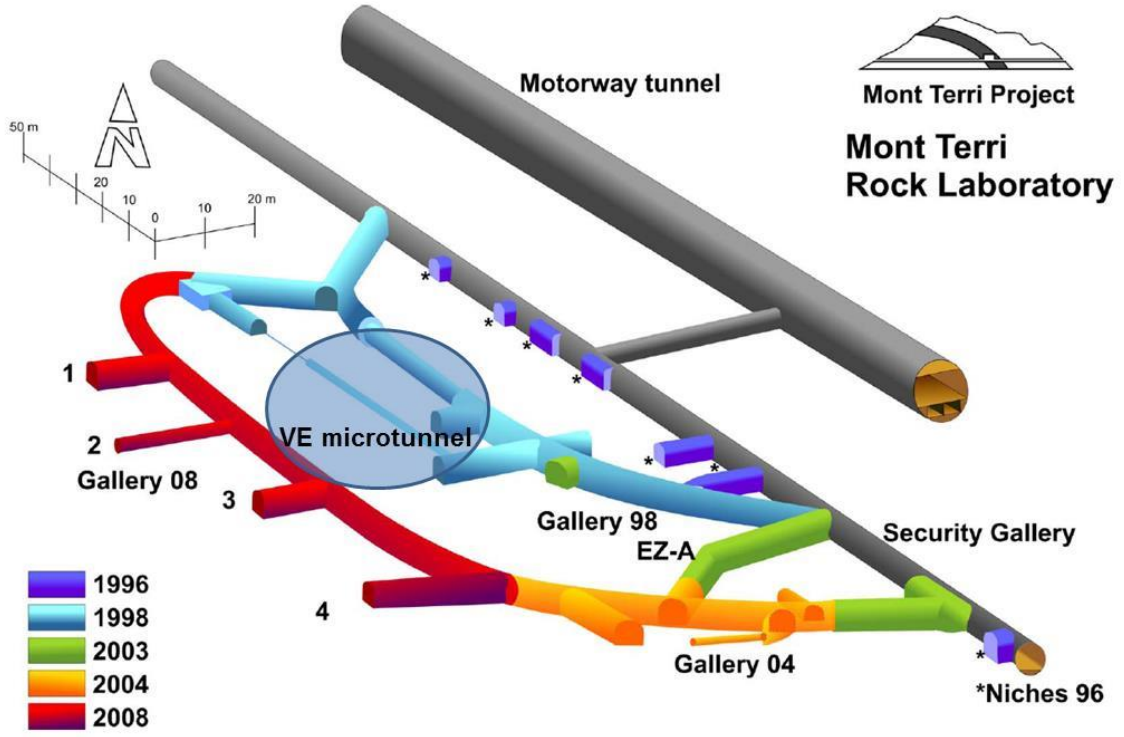

Fig. 4.1 VE microtunnel – location of the HE-E experiment in the Mont Terri URL

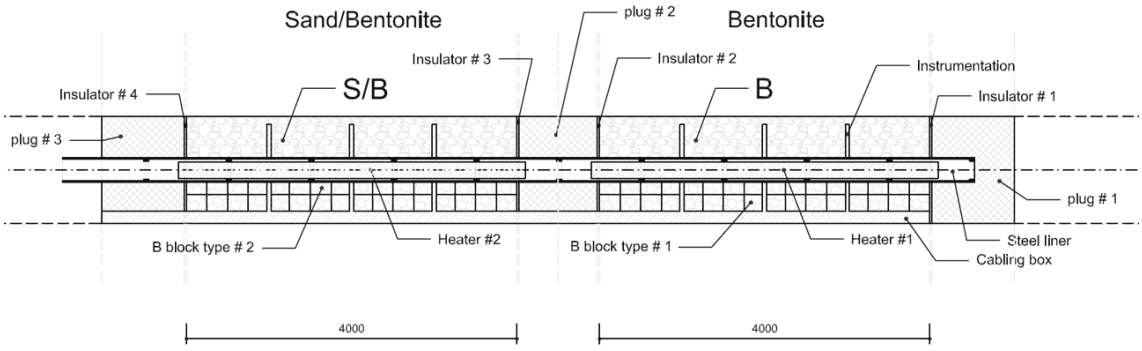

Fig. 4.2 HE-E experiment layout showing the section in the back of the tunnel filled with bentonite pellets and the section in the front of the tunnel filled with sand/bentonite

4.2 Construction and instrumentation

The dimensions of the microtunnel (1.3 m diameter) made it necessary that all experiment components be pre-assembled outside the tunnel. For each of the two sections, the heater liner, the bentonite blocks on which it rested, and the corresponding buffer instrumentation were assembled in one module and then pushed on rails into the microtunnel (Fig. 4.3).

Fig. 4.3 HE-E experiment module (heater liner, bentonite blocks and buffer sensors) before (left) and after (right) installation in the microtunnel

Afterwards, the granular buffer materials were installed using an auger system. The two sections were separated from each other and from the open microtunnel by plugs of thermal insulation (rockwool) and a vapour barrier (aluminium foil) between walls of cement bricks and mortar /GAU 14/.

4.2.1 Heaters

Two 4 meter long electrical heaters (providing each a maximum power of 2400 W) were installed in the central steel liner (Fig. 4.3). Heaters were designed to be operated by either power or temperature control, and they function independently for the two sections. 24 thermocouples (12 for each section), placed on 6 radial planes at the inner part of the 8 mm thick heater liner allow for monitoring of the heater surface temperature in four radial directions. Heat transmission between the sections and through the front and back plug of the test section is limited by the thermal insulation of the plugs.

4.2.2 Buffer materials

Bentonite blocks of sodium bentonite (MX-80) from Wyoming are used for the support of the heaters in both the bentonite and sand/bentonite sections of the experiment. They were fabricated by Alpha Ceramics (Aachen, Germany). Data on the bentonite blocks are given in Section 3.2.3 of this report and in /TEO 12/ and /GAU 14/.

The granular bentonite is the same as the one used for the ESDRED project, mixture type E (sodium bentonite MX-80 from Wyoming). Main properties include a water content of 5.4 %, a bulk density of 1,595 kg/m³ and a dry density of 1,513 kg/m³. A total of 6,665 kg granular bentonite was emplaced in the bentonite section with a mini-auger /GAU 14/.

The sand/bentonite mixture emplaced was a new material. A 65/35 sand/bentonite mixture had been investigated in the frame of the Mont Terri SB experiment /ROT 12/. This material, however, could not be used for the HE-E, because it needs manual emplacement and compaction. Due to the dimensions of the microtunnel, a manual emplacement was not possible. Attempts of creating a pelletized material from sand and bentonite with a relevant water content were undertaken to overcome this problem, but proved unsuccessful. Therefore, a granular mixture of sand and bentonite with identical grain spectrum was chosen.

The sand/bentonite mixture used was provided by MPC, Limay/France. The components are 65 % of quartz sand with a grain spectrum of 0.5 – 1.8 mm and 35 % of sodium bentonite GELCLAY WH2 (granular material of the same composition as MX-80) of the same grain spectrum which was obtained by crushing and sieving from the qualified raw material. Water content is 13 % for the bentonite and 0.05 % for the sand, giving a total water content of the mixture in the range of 4 %.

Due to the PEBS time schedule, a preceding characterization of the material was not possible. In the course of the laboratory investigations (Section 3.3) performed after installation, it was found that swelling pressure and permeability of this material were not as expected. For use as buffer material, a modification of the sand/bentonite mixture would be required.

A total mass of 6043 kg of granular sand/bentonite was emplaced in the HE-E.

4.2.3 Buffer instrumentation

A total of 18 humidity/temperature sensors were emplaced at the tunnel wall and an additional 60 humidity/temperature sensors were emplaced within the sand/bentonite or bentonite section. The position of the sensors is shown in Figs. 4.4 and 4.5. The sensors closest to the heater (first layer) have a distance of 250 mm to the centre of the tube or 100 mm to the surface of the liner. The second layer of sensors has a distance of 400 mm to the centre or 250 mm to the liner surface. The third layer of sensors is attached to the wall; the distance to the centre varies with the roughness of the wall /GAU 14/.

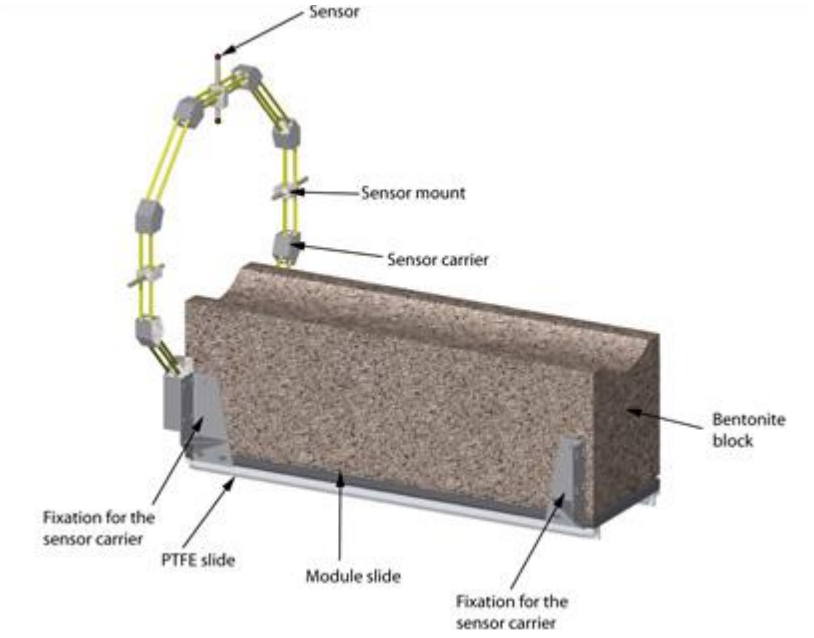

Fig. 4.4 Bentonite block with sensor carrier and temperature/humidity sensors /GAU 14/

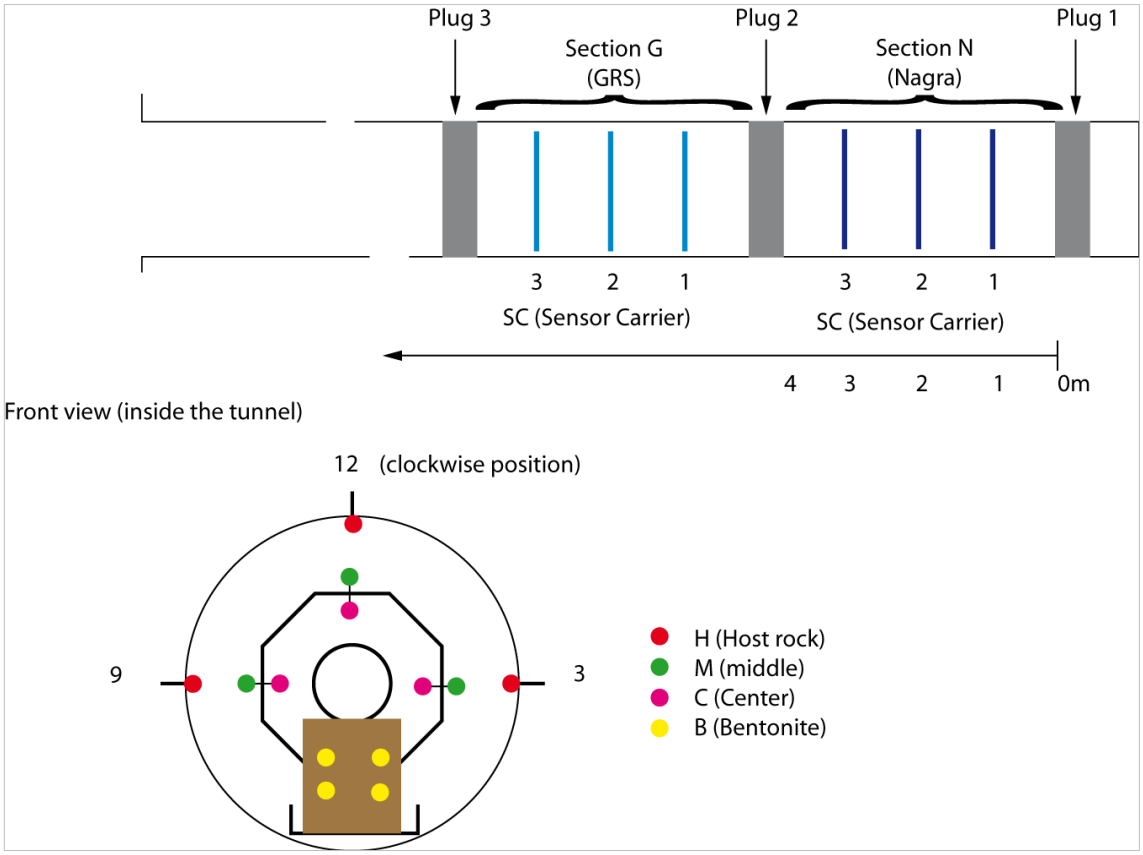

Fig. 4.5 Position of sensors in the buffer and on the microtunnel wall /GAU 14/

4.2.4 Rock instrumentation

Most of the rock instrumentation around the microtunnel was installed during the set-up of the VE experiment. Minipiezometers, capacitive humidity/temperature sensors, extensometers, and psychrometers had been installed in 8 cross-sections in boreholes drilled from the microtunnel (Fig. 4.6). During planning of the HE-E, however, it was decided that additional pore pressure sensors might be needed close to the microtunnel wall. Therefore, GRS installed another 10 minipiezometers and temperature sensors in two of the cross sections (Figs. 4.7 and 4.8). After installation, permeability tests were performed by water injection into the minipiezometers. These resulted in permeability values between 10^{-17} m² and 10^{-20} m², the interpretation, however, was problematic because the rock close to the microtunnel was in suction.

Details of the complete instrumentation in the 8 measurement cross sections are given in /TEO 12/.

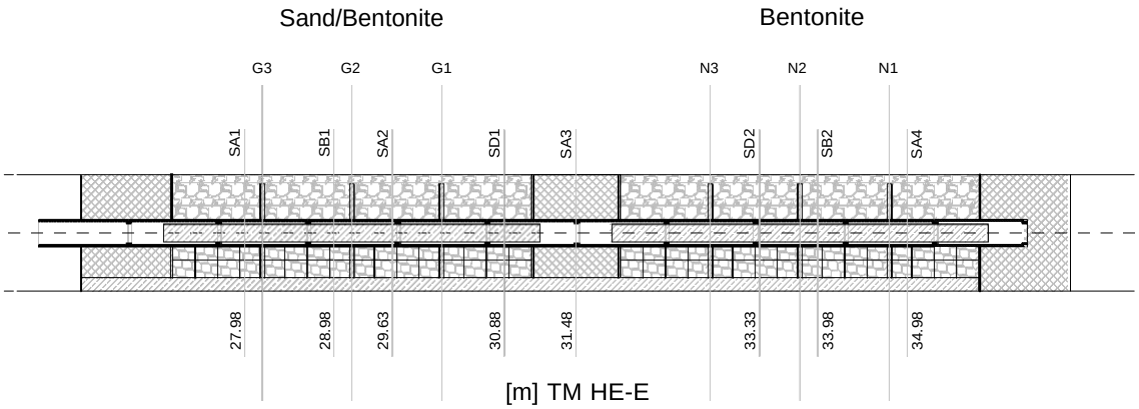

Fig. 4.6 Longitudinal section of the HE-E showing the instrumentation cross sections /GAU 14/

Fig. 4.7 Installation of GRS minipiezometers in the microtunnel

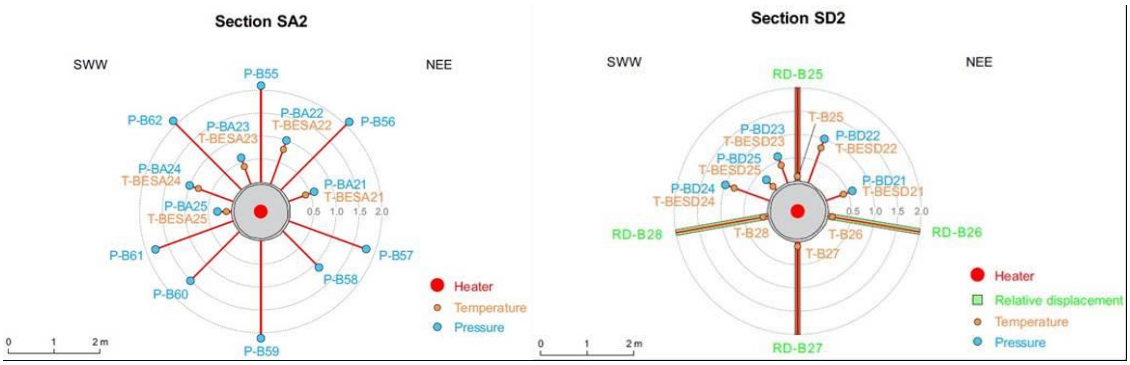

Fig. 4.8 Location of GRS minipiezometers (P-BA.., P-BD..) and temperature sensors (T-BESA.., T-BESD..) in the cross sections SA2 and SD2

In addition to the direct monitoring, BGR installed a seismic array consisting of five piezoelectric transducers which serve as emitters and ten transducers which serve as receivers in three 1 m deep boreholes in a section of the micro tunnel. The seismic

transmission experiment aims at characterising changes in the Opalinus Clay and EBS properties caused by the heating.

At larger distances from the microtunnel, only two multipacker probes installed from the Gallerey 98 were available from the VE instrumentation. Design modelling /CZA 11/ of the HE-E, however, had shown that pore pressure increase could be expected at larger distances (in the range of several metres) from the microtunnel. Therefore, it was decided to install another two multipacker probes. The additional boreholes were drilled by GRS in the direction of the micro tunnel from Gallery 98 and equipped with quadruple packer systems in May 2011. Figure 4.9 shows the location of the new boreholes together with the previously existing boreholes BE-1 and BE-91 in a plan view.

The new boreholes both have a diameter of 80 mm and a length of 10 m. They are located in the vertical planes coinciding with the centre of each HE-E heater. Each borehole is equipped with a quadruple packer probe. The locations of the test intervals in relation to the microtunnel are shown in Fig. 4.10.

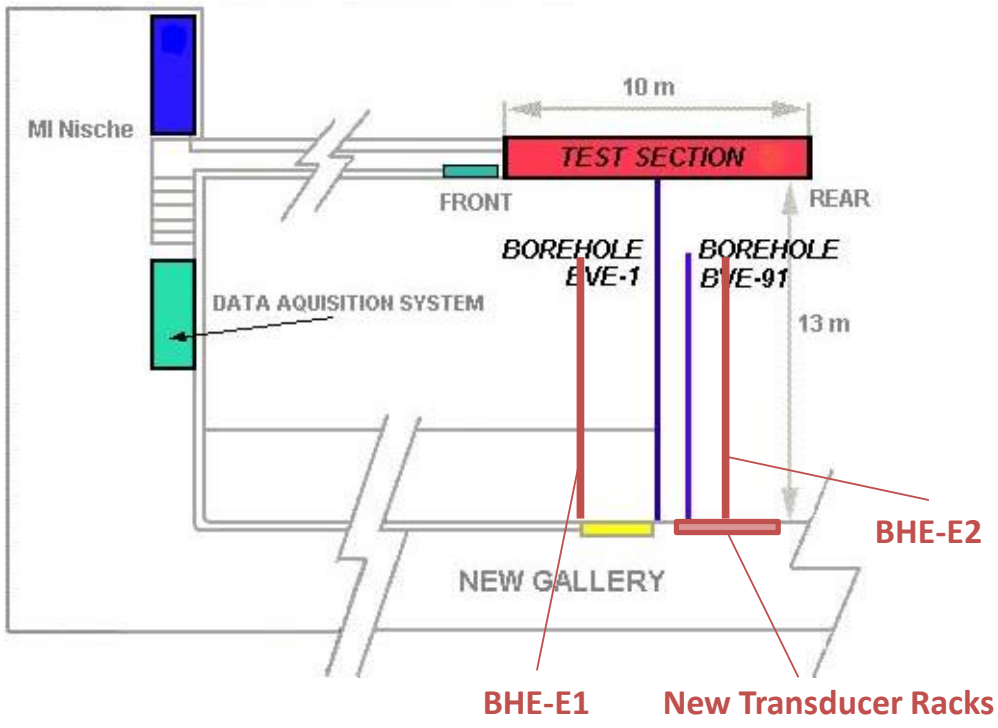

Fig. 4.9 Plan view showing the locations of the old VE boreholes BVE-1 and BVE-91 and of the additional packer boreholes BHE-E1 and BHE-E2

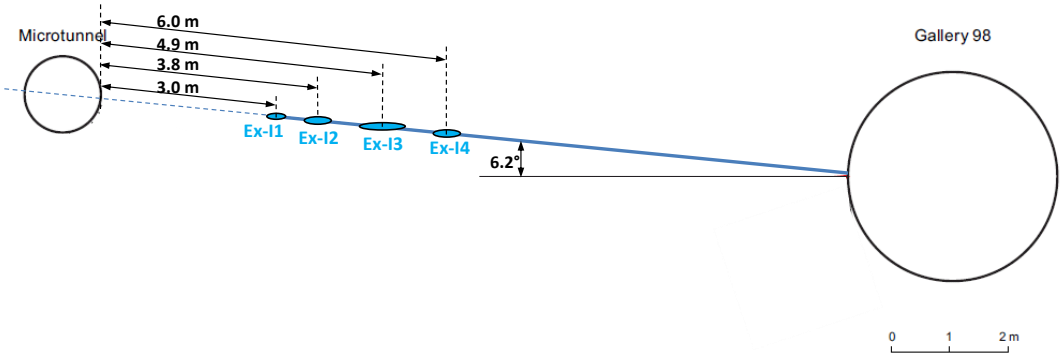

Fig. 4.10 Location of boreholes BHE-E1 and BHE-E2 and distances of the test intervals to the microtunnel

4.3 Experiment conduction and monitoring

After completion of construction and instrumentation, the heaters were started on June 30, 2011. The following heating strategy was applied:

- Initial power controlled heating to calibrate the temperature control algorithm (150 – 200 W applied during a few days)
- Temperature controlled linear increase until a temperature of 80 – 90 °C is reached at the surface of the liner, approximately three months after start-up of heating
- Temperature controlled linear increase until a temperature of 140 °C is reached at the surface of the liner, approximately three months after start-up of heating
- temperature control at the heater surface to maintain 140 °C for the remaining two years of the experiment

In the following sections, selected measured data from the heater, the buffer, and the rock are presented. The information is an excerpt from the HE-E final report, PEBS Deliverable D2.2-11/D3.2-2 /GAU 14/.

The graphs cover data obtained until end of 2013. The experiment has been providing valuable and reliable data. Since the early resaturation phase is continuing and important data are still produced, the HE-E was, not stopped with the end of the PEBS project. A consortium of NAGRA, ENRESA, BGR and GRS decided to continue the HE-E. At GRS, HE-E is now part of a new Mont Terri project.

4.3.1 Heater power and temperature

As planned, external temperature at the casing reached 80 °C on day 95 day of the heating phase for the sand/bentonite heater (Heater HE-E SB) and on day 93 for the bentonite heater (Heater HE-E B). The maximal temperature of 140 °C was reached on day 368 and 390, respectively. Since then the heaters have been run at constant temperature. A few electricity supply incidents caused disruption of the heating on April 14, 2011 (for 12 hours), August 30, 2012 (for 14 hours), January 22, 2013 (for 3 days), and February 8, 2013 (for 12 hours). Since then the heaters have been functioning without disruption.

The total heating power supplied to the two heaters and the heater temperatures in the middle of the two heated sections after February 2012 are shown in Fig. 4.11. The power needed to maintain the constant temperature of 140 °C is slightly different in the two sections of the experiment, as a consequence of the difference in thermal conduction of the various buffer materials.

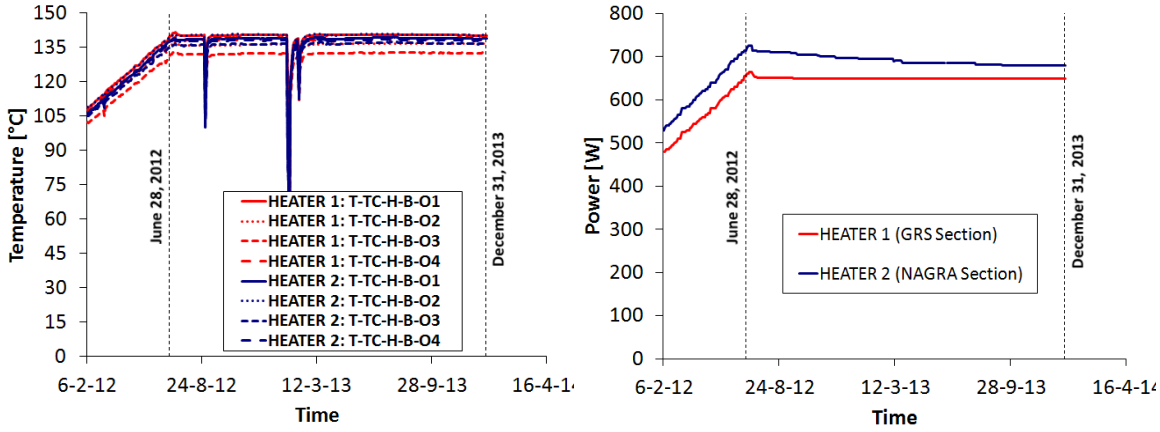

Fig. 4.11 Evolution of temperature (left) and heating power (right) in the heaters for the two heated sections (from February 2012 to December 2013)

Measurements from the sensors installed in the EBS (Figs. 4.12 and 4.13) indicate temperature increase during the first year of heating followed by a non-significant change in temperature after that period of time, showing that steady-state is reached relatively fast in the EBS. In both heated sections the maximum temperature at the sensors closest to the heater surface is about 100 °C after one year of heating. A slight difference in temperature depending on the direction taken (3, 9 or 12 o'clock in the granular material) can be noted (Fig. 4.12).

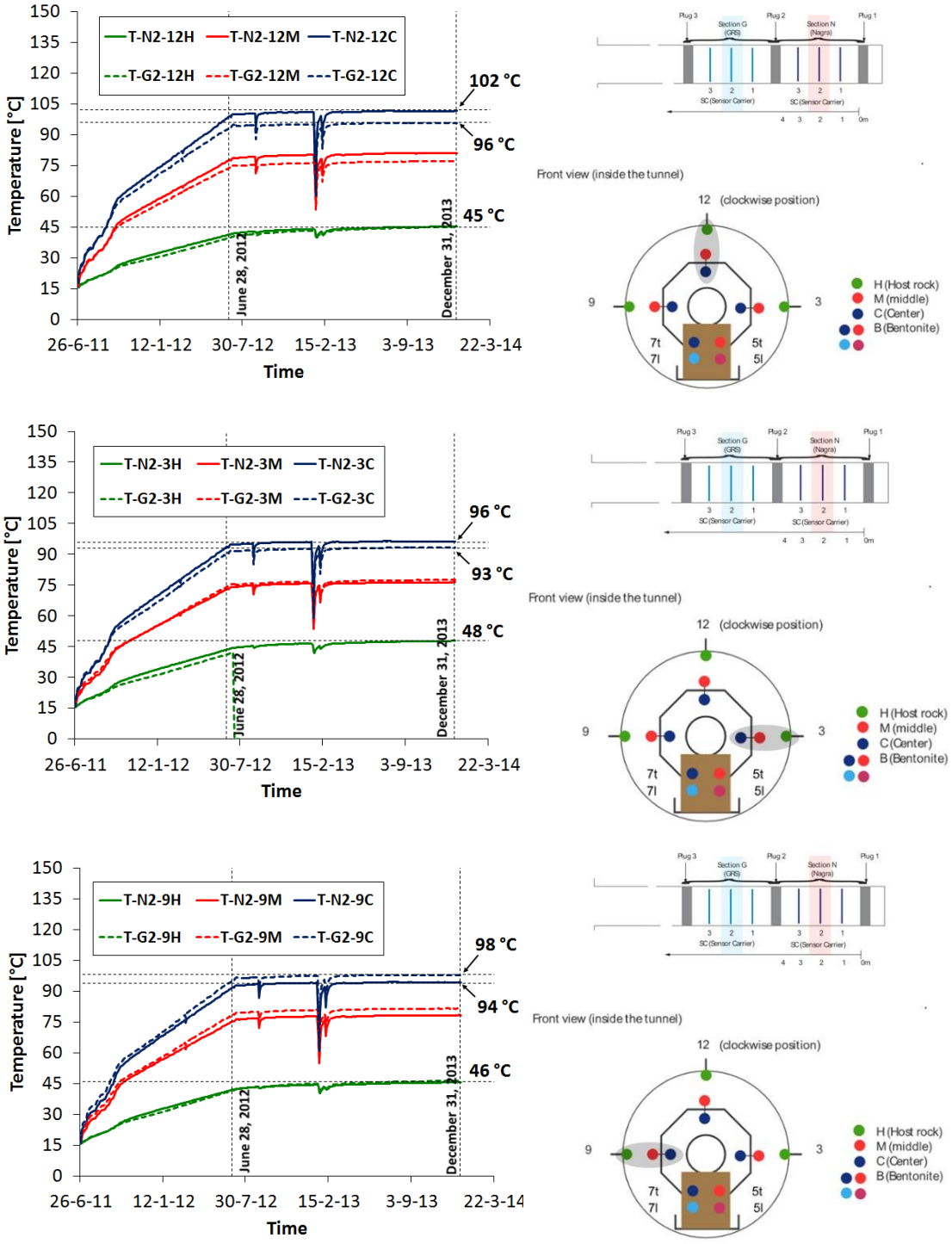

Fig. 4.12 Evolution of temperature in the middle of the bentonite section (full lines) and in the middle of the sand/bentonite section (dashed lines) at three main directions: 12 o'clock (up), 3 o'clock (centre) and 9 o'clock (down)

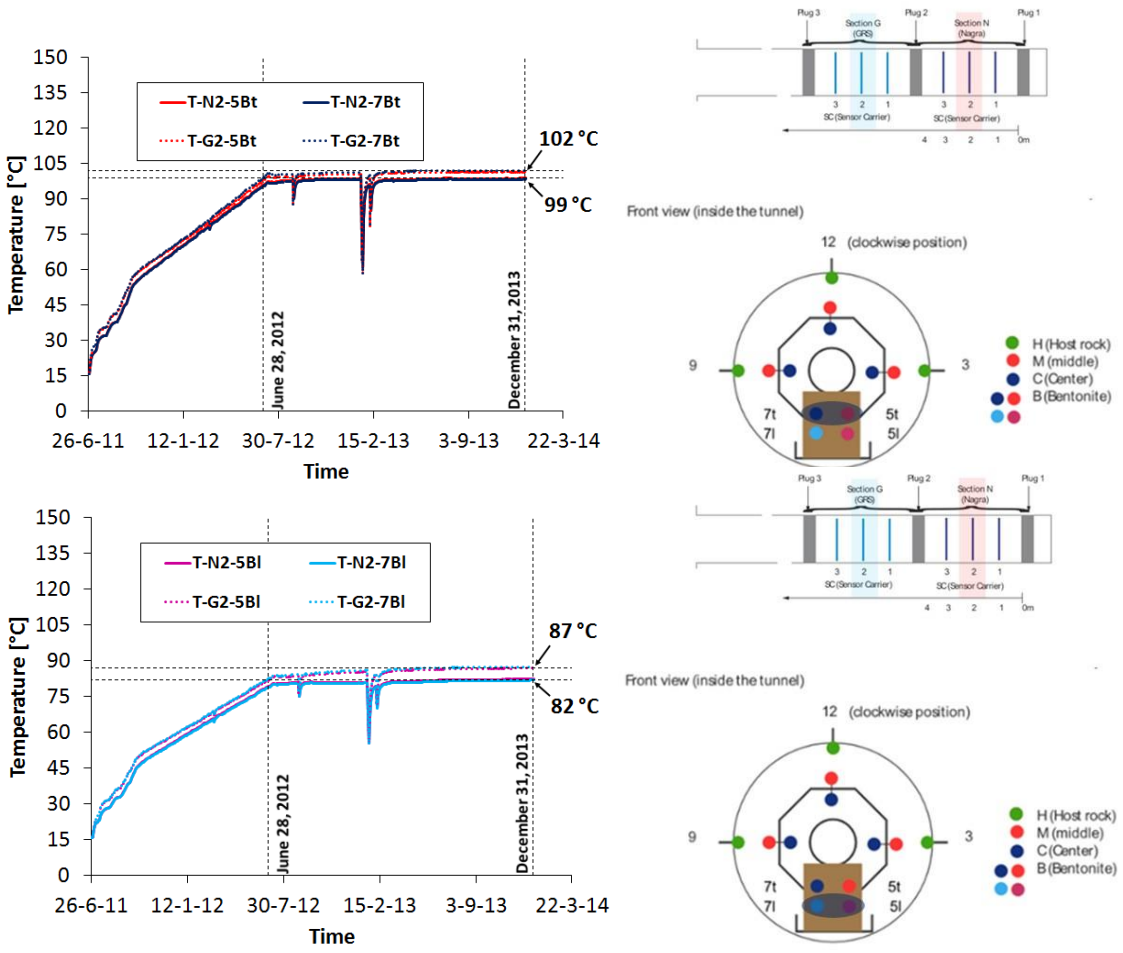

Fig. 4.13 Evolution of temperature in the middle of the bentonite section (full lines) and in the middle of the sand/bentonite section (dotted lines) in the upper layer (up) and the lower layer of sensors (down) inside the compacted blocks

In the compacted blocks this temperature dependence on the sensor position (5 or 7 o'clock) is not significant (see Fig. 4.13) due to the greater homogeneity of relevant parameters (dry density, water content, porosity) inside the bentonite blocks. Close to the buffer/rock interface, temperature is around 45 °C after 2.5 years of heating (end of December 2013) and keeps increasing at a slow rate (Fig. 4.12).

In Fig. 4.14 the evolution of temperature in the Opalinus clay for two instrumented sections is shown. Most of the temperature increase occurs during the first year of heating. Some of the temperature sensors which had already been installed for the VE experiment yield unreliable data (e. g., T-B25 in Fig. 4.14).

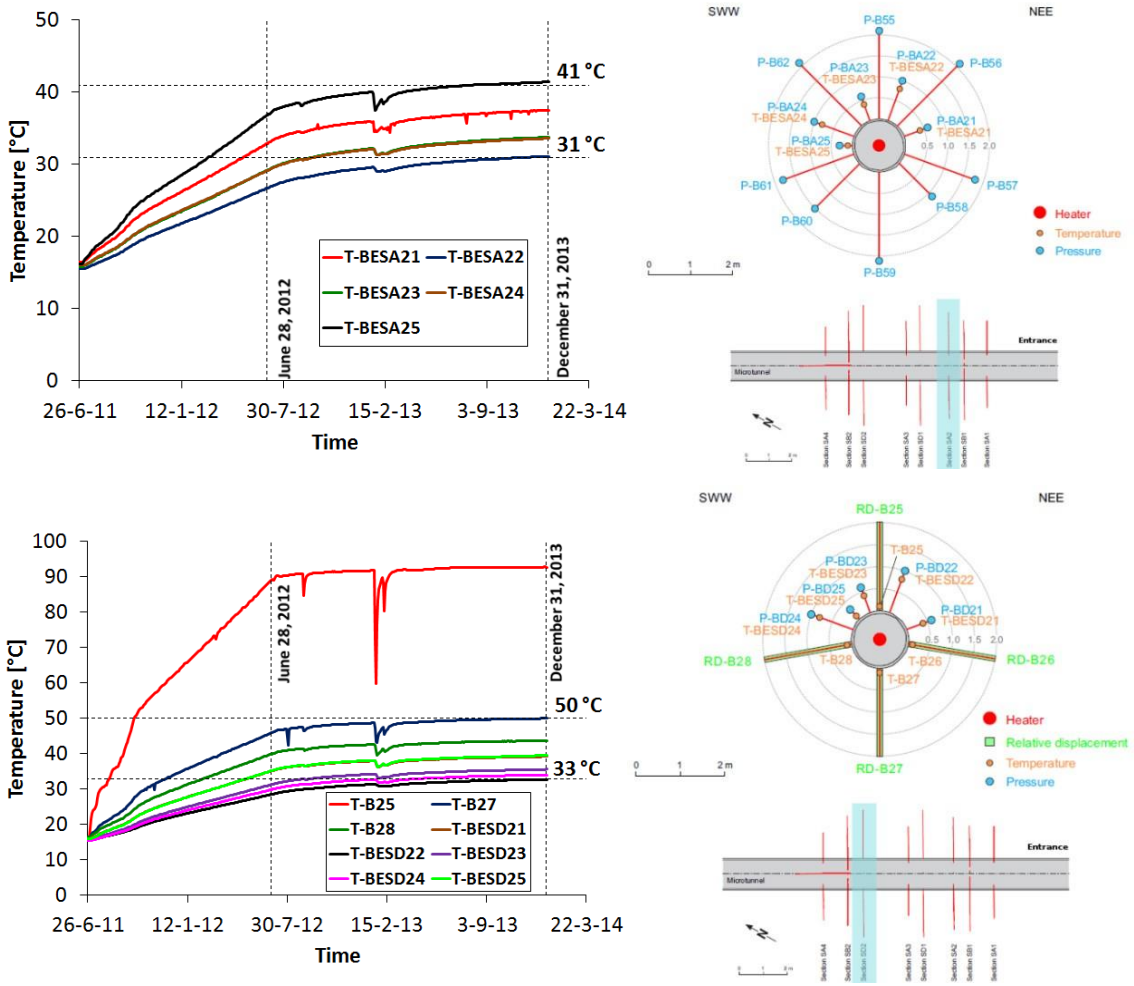

Fig. 4.14 Evolution of temperature in the Opalinus clay for the instrumented cross sections SA2 (sand/bentonite section, up) and SD2 (bentonite section, down)

4.3.2 Relative humidity

Relative humidity measurements inside the EBS (Figs. 4.15 and 4.16) show a similar behaviour in both heated sections: a fast increase in the relative humidity close to the rock, with almost all sensors at that location showing a relative humidity of 100 % before the end of the second year of heating and a strong reduction in the relative humidity for those sensors located near the heaters. These data show the coupled thermal-hydro-mechanical behaviour of the EBS due to the combined effect of heating and hydration, since it is expected that the increase of temperature in the inner region of the barriers induces water evaporation and vapour diffusion towards the cooler zones (close to the buffer/rock interface). This phenomenon combined with the water flux from

the rock to the EBS due to the high hydraulic gradient between these materials explains the high hydration rate observed near the buffer-rock interface.

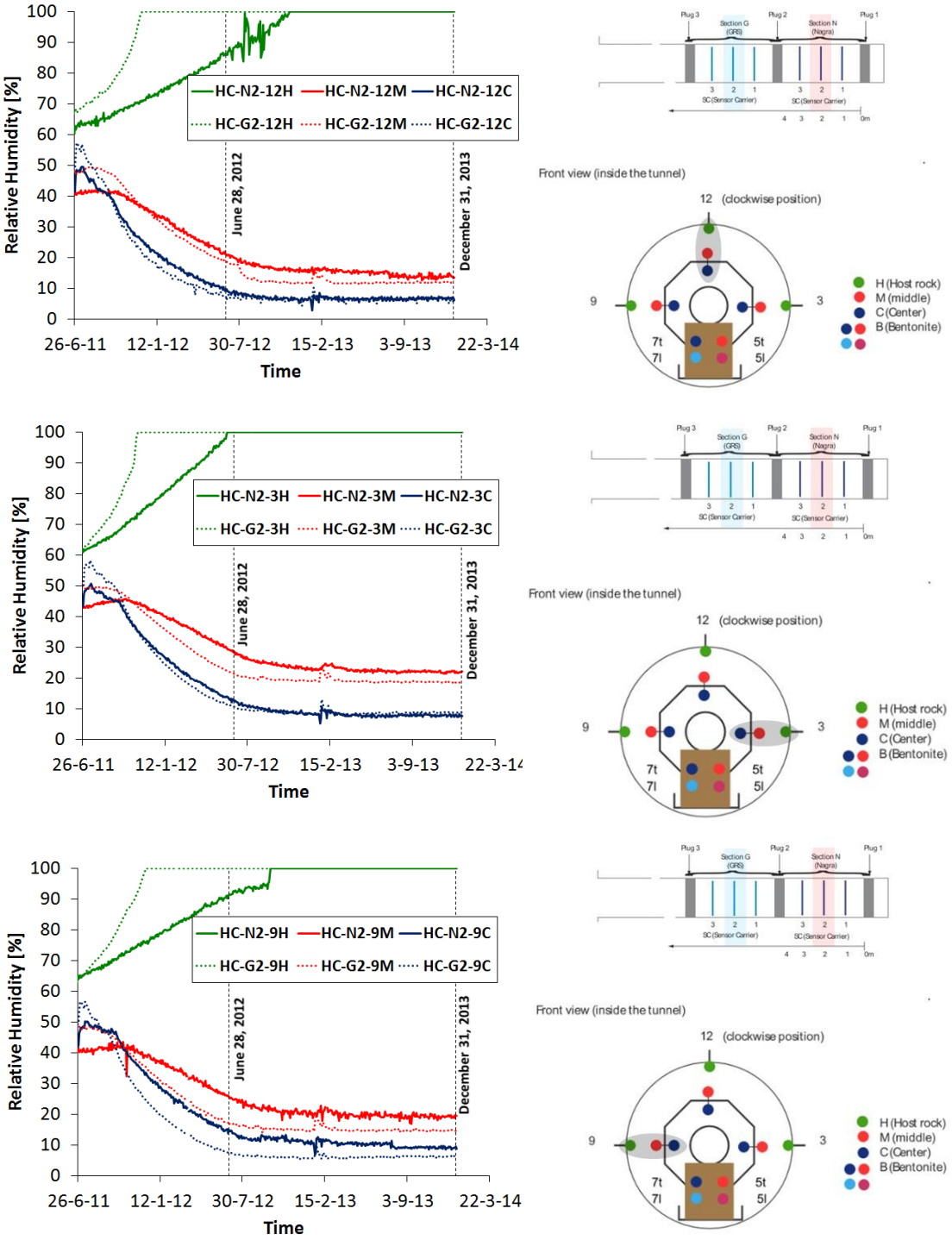

Fig. 4.15 Evolution of relative humidity in the middle of the bentonite section (full lines) and in the middle of the sand/bentonite section (dashed lines) at three main directions: 12 o'clock (up), 3 o'clock (centre) and 9 o'clock (down)

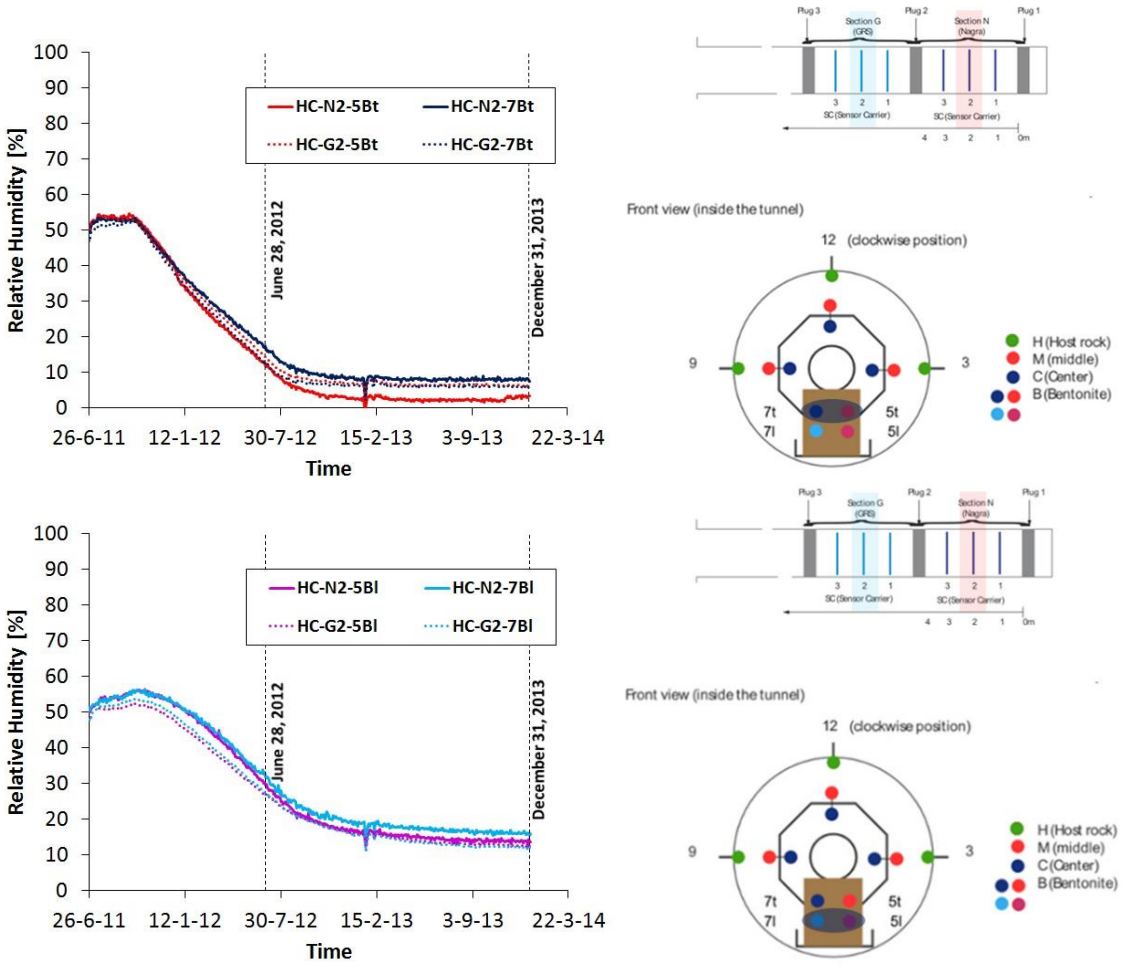

Fig. 4.16 Evolution of relative humidity in the middle of the bentonite section (full lines) and in the middle of the sand/bentonite section (dotted lines) in the upper layer (up) and the lower layer of sensors (down) inside the compacted blocks

The hydration rate for the sand/bentonite section close to the rock is higher than for the bentonite section. This can possibly be explained by the high water permeability of the sand/bentonite mixture (see Section 3.3.4). Data provided by the sensors located close to the heaters, on the other hand, indicate that both buffers are very dry (at that location) after 2.5 years of the experiment, with relative humidity in the range of 7 – 11 %. Taking into account the psychrometric law that relates the relative humidity to the total suction together with the water retention curves of the bentonite buffer materials, the degree of saturation in the first instrumented layer can be estimated inside each bentonite-based material. For the granular buffers, the average degree of saturation close to the heater is around 8 – 11 %; while it varies between 26 % and 33 % for the upper RH sensors in the blocks (in both heated sections). In the granular buffers the sensors at a distance of 25 cm from the heater also show a desaturation of the material due to

heating (Fig. 4.15). This tendency is also recorded in all the sensors of the second instrumented (lower) layer in the bentonite blocks, for the two sections of the HE-E experiment (see Fig. 4.16). Values are varying between 10 % and 14 % for the sand/bentonite mixture and the bentonite pellets and around 33 % for the bentonite blocks at the end of December 2013.

4.3.3 Pore water pressure

Data from the pore water pressure sensors close the micro tunnel (Fig. 4.17 for an example) suggest that the zone under suction after 2.5 years of heating extends up to a distance about 1.5 – 2.0 m from the microtunnel wall. Most of the sensors located at a smaller distance indicated no significant response during this time. Pore pressure increased up to peak values ranging between 300 kPa and 1000 kPa for those sensors that react during operation of the HE-E experiment.

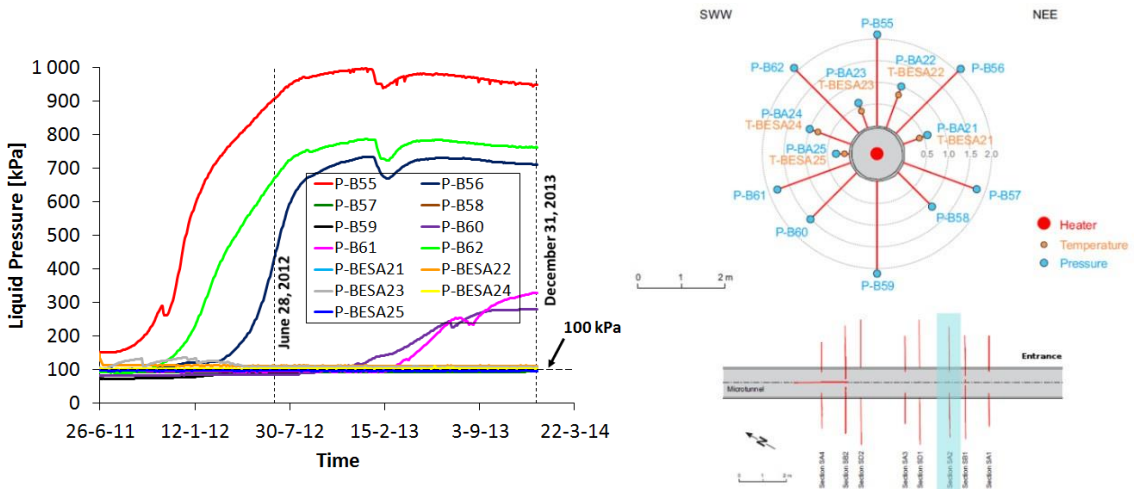

Fig. 4.17 Evolution of pore water pressure in the Opalinus Clay in the vicinity of the sand/bentonite section for the instrumented cross section SA2

The evolution of pore pressure at larger distances from the microtunnel is shown in Fig. 4.18 for boreholes BHE-E1 and BHE-E2. Distance from the microtunnel wall to the sensors in these boreholes ranges from 3 m to 6 m. The sensors exhibited a pore pressure reduction in the early stages of heating followed by a gradual increase up to a peak in the range of 600 – 900 kPa, after about19 months of heating.

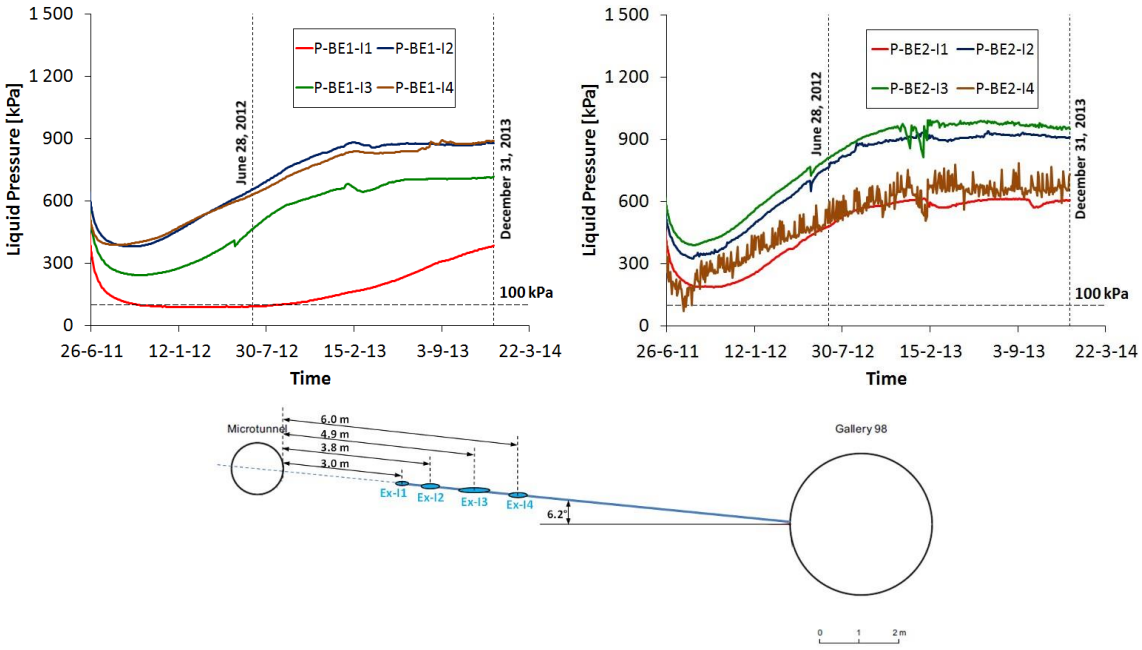

Fig. 4.18 Evolution of pore water pressure in the Opalinus Clay for the sensors in borehole BHE-E1 (left) and BHE-E2 (right)

5 Model simulations

5.1 Interpretative modelling

Modelling performed in order to design and interpret the PEBS experiments was organized in four tasks (compare Section 2.2). GRS was involved in the modelling of the HE-E (Task 3.2) and also coordinated the complete modelling work package. The next two sections of this report present GRS' HE-E modelling and a summary of the interpretative modelling results of all PEBS partners, respectively.

5.1.1 GRS modelling of HE-E

The idea of GRS' simulations was to use simple standard models installed in CODE_BRIGHT to try to model the HE-E THM behaviour. The following discussion can also be found in /GAU 14/.

5.1.1.1 Model description and parameters

GRS' simulations used CODE_BRIGHT, a fully coupled Thermal-Hydraulic-Mechanical (THM) finite element code for porous media. The theoretical framework is formed of three main parts:

- balance equations,
- equilibrium restrictions and
- constitutive equations.

Balance equations are solved for solid, liquid, and gas phases, as well as for energy and momentum. The liquid phase may contain water and dissolved air, and the gas phase may be a mixture of dry air and water vapour. Thermal equilibrium between phases is assumed. A general and detailed description is given by Olivella et al. /OLI 96/ and in the code manual /UPC 02/.

Equilibrium restrictions are given for the concentration of water vapour in gas via the psychrometric law and for the concentration of dissolved air in water via Henry's law.

The constitutive equations establish the link between the independent variables and the dependent variables. They are assigned the material parameters compiled in Tab. 5.1.

Heat propagation is described by Fourier's law. Variation of thermal conductivity with saturation is considered by linear interpolation between the dry and saturated values.

For the hydraulic problem it is assumed that the liquid and gas flows follow Darcy's law, with the actual effective permeability to each phase being given by the product of intrinsic and relative permeability. The dependence of intrinsic permeability k on porosity ϕ is given by

$$k = \mathbf{k}_0 \cdot \frac{\phi^3}{(1-\phi)^2} \cdot \frac{(1-\phi_0)^2}{\phi_0^3} \tag{5.1}$$

with initial values k_0 and ϕ_0. The relative permeabilities of the liquid and gaseous phases are dependent on the degree of liquid saturation according to

$$S_e = \frac{S_l - S_{lr}}{S_{ls} - S_{lr}} \text{ and } k_{rl} = A \cdot S_e^{\lambda} \ , \ k_{rg} = 1 - k_{rl} \tag{5.2}$$

where S_l, S_{lr}, S_{ls}, S_e are the actual, residual, maximum and effective saturation of liquid, respectively, and A and λ are parameters. It is necessary to define the retention curve of the materials relating the degree of saturation to suction. Generally, the formulation of van Genuchten with material parameters β, P_0 and σ_0 is selected.

$$S_e = \left[1 + \left(\frac{P_g - P_l}{P}\right)^{1/(1-\beta)}\right]^{-\beta} \text{ where } P_g - P_l \geq 0 \text{ and } P = P_0 \cdot \frac{\sigma}{\sigma_0} \tag{5.3}$$

The molecular diffusion of vapour is governed by Fick's law, a constant dispersion coefficient corresponding to the molecular diffusion of vapour in air is assumed.

$$D_m^w = \tau D \left(\frac{(273.15 + T)^n}{P_g}\right) \tag{5.4}$$

Where P_g is given in MPa. For the tortuosity τ a value of 1.0, for n a value of 2.3 and for D a value of 5.9E-6 m²/s were adopted. Regarding mechanical behaviour, all materials were modelled as poroelastic. Damage was not considered. Time-dependent deformation is only possible as a consequence of pore pressure variation.

Tab. 5.1 Material parameters used for the simulations

Parameter	Unit	Symbol	OPA	Bentonite pellets	Bentonite blocks	Granular sand-bentonite
Physical parameters						
Solid grain density	kg/m^3	ρ_S	2700	2700	2700	2546
Start porosity	-	ϕ_0	0.137	0.45	0.33	0.43
Hydraulic parameters						
Intrinsic permeability	m^2	K_{iso}		3.5E-20	2.5E-21	1.0E-19
Anisotropic permeability	m^2	$K_{//}$ $K_{\perp}$	2.0E-20 6.0E-21	-	-	-
Liquid rel. permeability	-	λ	3	3	3	3
Liquid rel. permeability	-	A	1	1	1	1
Vapour diffusion coefficient	m^2/s	D	5.9E-06	5.9E-06	5.9E-06	5.9E-06
Tortuosity	-	τ	1	1	1	1
Exponent	-	n	2.3	2.3	2.3	2.3
Retention curve	MPa	P_0	12	10.0	21.9	10.0
Retention curve	N/m	σ_0	0.072	0.072	0.072	0.072
Retention curve	-	γ	0.3	0.31	0.3	0.55
Retention curve	-	S_{rl}-S_{rs}	0.01-1.0	0.01-1.0	0.01-1.0	0.0-1.0
Thermal parameters						
Saturated thermal conductivity	W·m/K	λ_{sat}	1.7	1.3	1.3	1.3
Unsaturated thermal conductivity	W·m/K	λ_{dry}	1.3	0.3	0.8	0.3
Specific heat of solid grain	J/kg·K	C	995	893	1058	775
Mechanical parameters						
Young`s modulus	MPa	E	3000	40	40	40
Poisson ratio	-	ν	0.29	0.35	0.35	0.35
Viscosity	MPa·s	η	2.1E-12	2.1E-12	2.1E-12	2.1E-12
Coupling parameters						
Biot coefficient	-	b	0.6	1.0	1.0	1.0
Swelling coefficient	1/MPa	γ_s	1.0E-4	1.0E-4	1.0E-4	1.0E-4
Linear thermal expansion of the solid grain	1/K	α	1.5E-06	2.5E-05	2.5E-05	2.5E-05
Linear thermal expansion of the skeleton	1/K	α_s	1.5E-06	2.5E-05	2.5E-05	2.5E-05

The material parameters given in Tab. 5.1 generally follow the HE-E as-built modellers' dataset worked out in the frame of the project. For the granular sand/bentonite buffer, however, little data were available. Thermal conductivity and saturated permeability were measured (see Section 3.3), while relative permeabilities, thermal expansion coefficients and mechanical parameters were estimated the same as for bentonite pellets. For the retention curve, measurements were available (Section 3.3). It was found that fitting the data using the van Genuchten formulation was not very satisfying. Therefore, a square law with P0=0.7 MPa was considered alternatively for the granular sand-bentonite buffer:

$$S_e = \left[1 + \frac{P_g - P_l}{P_0}\right]^{-1/2} \tag{5.5}$$

The measured data and the approximations are shown in Fig. 5.1. Since the square law gives an acceptable fit in the interesting saturation bandwidth, it was used for the reference model.

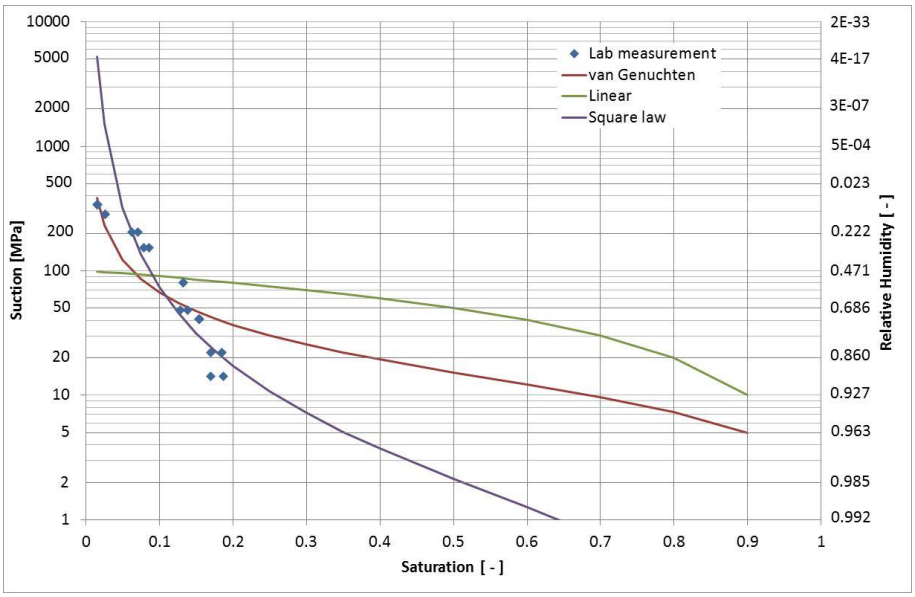

Fig. 5.1 Laboratory measurements and approximations of the retention curve for granular sand-bentonite buffer (the linear approximation was not used)

Both THM and TH calculations were performed for comparison. The geometrical model is a plane-strain vertical section through the micro-tunnel and the parallel Gallery 98. The same model was used for simulating two sections: the heater midplanes of the NAGRA section with bentonite pellet buffer and the GRS section with granular sand-

bentonite mixture. **Fehler! Verweisquelle konnte nicht gefunden werden.**igure 5.2 hows the model together with the boundary conditions.

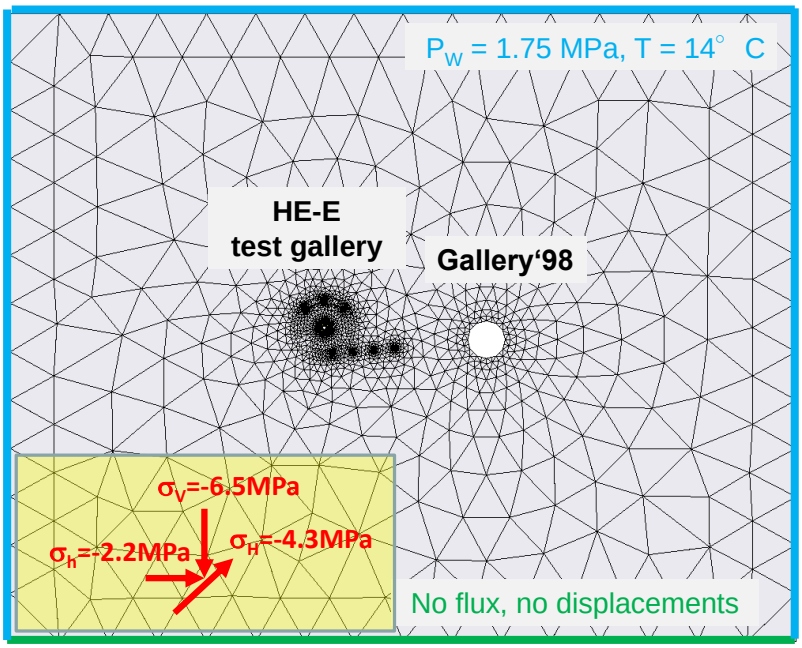

Fig. 5.2 Plane strain model with boundary conditions for the HE-E simulation

The initial state is given by a rock temperature of 14 °C, a stress state as given in Fig. 5.2, and an assumed pore pressure of 1.75 MPa. The pore pressure distribution, however, was significantly disturbed by the ventilation experiment (VE) performed in the microtunnel prior to the HE-E and also by the ventilated Gallery 98. Therefore, the history of the test region had to be taken into account. This was done in a simplified way, by fixing a high suction value of -5 MPa on the microtunnel wall to simulate the ventilation prior to the VE and by setting suction to atmospheric pressure for the time of the VE and the installation of the HE-E. On the contour of Gallery 98, atmospheric pressure was fixed all the time. With installation of the HE-E, the suction on the contour is set according to the initial suction in the buffer material which is given by the initial saturation. One month after installation heating is started. An overview of the boundary conditions at the gallery contours is shown in Fig. 5.3.

For simulation of the heating a temperature boundary condition was applied on the heater surface. The temperature curve used is shown in Fig. 5.4, together with the actually measured temperatures.

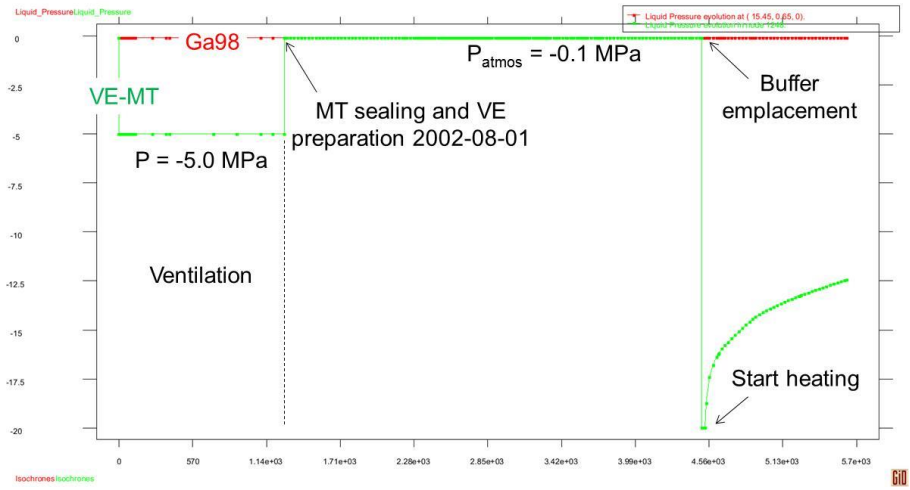

Fig. 5.3 Boundary conditions at the contours of the microtunnel (VE-MT) and the Gallery 98 (Ga98)

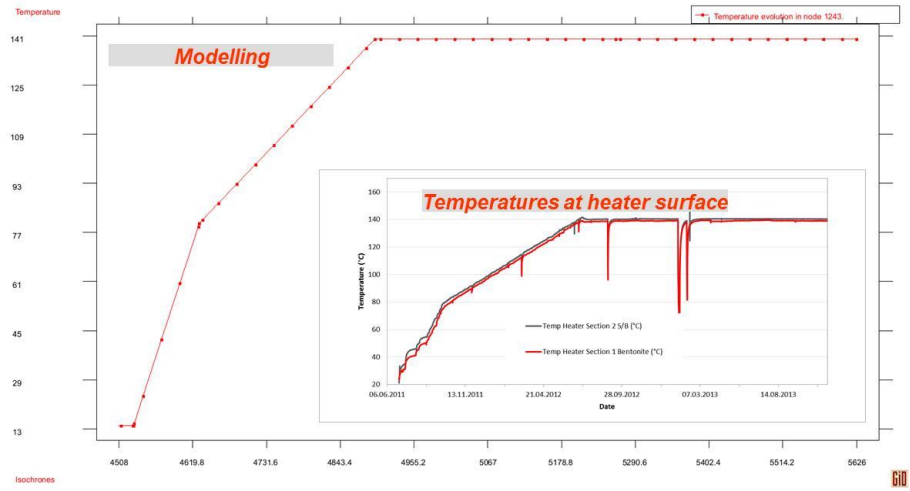

Fig. 5.4 Temperature curve used as boundary condition for the simulation, with measured heater surface temperatures for comparison

5.1.1.2 Calculation results for the sand/bentonite section

The coupled THM calculation results for the temperature in the buffer of the sand/bentonite section using the reference data set (with square law retention curve) are shown in Fig. 5.5 (granular buffer above the heater) and Fig. 5.6 (bentonite blocks), together with the actually measured data.

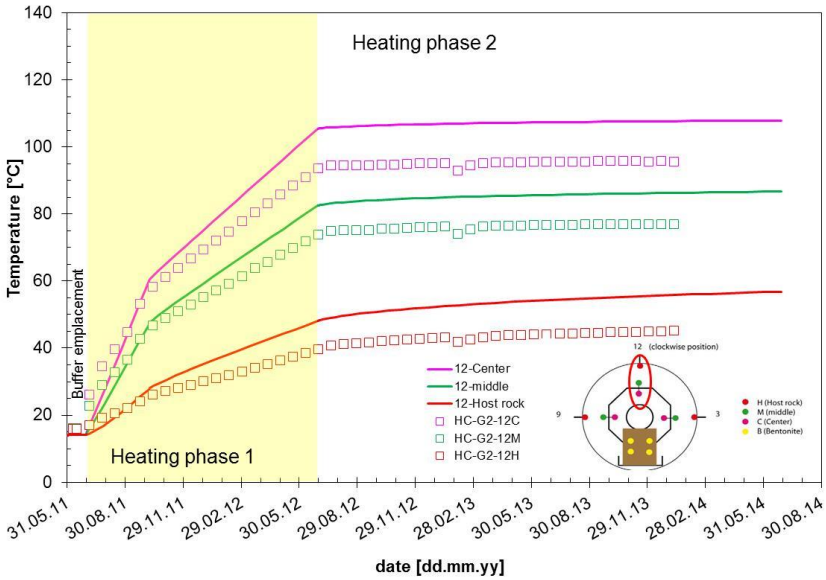

Fig. 5.5 Temperature evolution at the measuring points in the heater midplane in the granular sand/bentonite buffer (lines = calculation, open squares = temperature measurement) – reference model

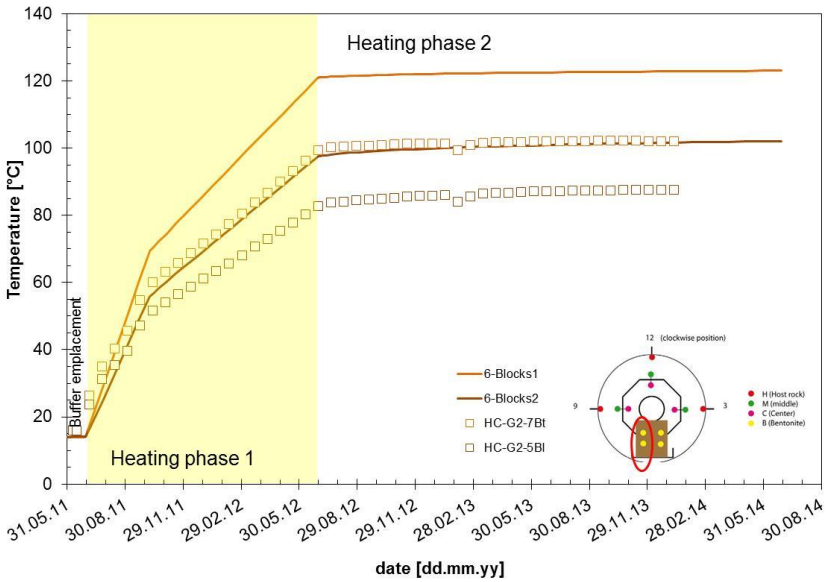

Fig. 5.6 Temperature evolution at the measuring points in the heater midplane in the bentonite blocks (lines = calculation, open squares = temperature measurement) – reference model

The calculated temperatures are generally higher than the measured ones, an expected effect stemming from the difference in geometry. In the plane strain model the heat flow in the axial direction is not considered, therefore the radial heat flow is overestimated.

Figure 5.7 and Fig. 5.8 show the evolution of relative humidity in the granular buffer and the bentonite blocks, respectively. While there are some discrepancies in the time evolution, the general trends are met. The simple elastic model for the granular buffer and the material parameters seem adequate for modelling its behaviour in this case.

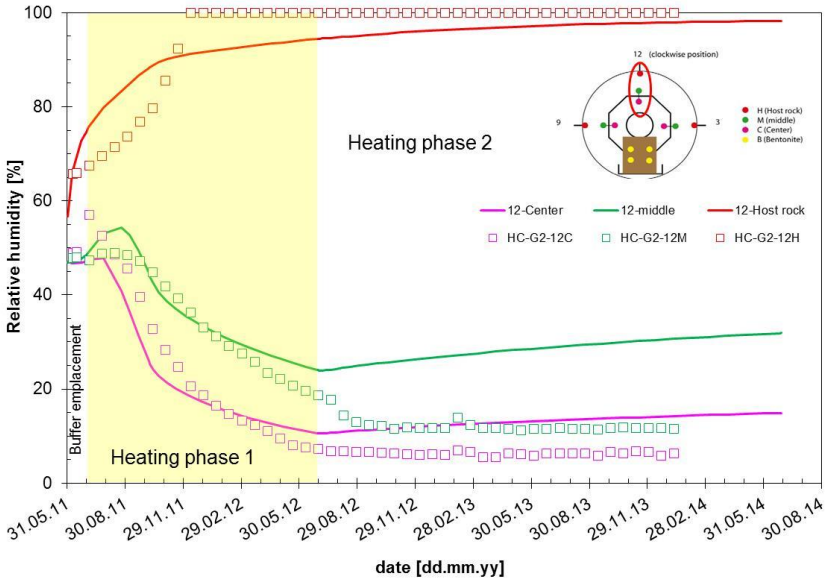

Fig. 5.7 Evolution of relative humidity at the measuring points in the heater mid-plane in the granular sand/bentonite buffer (lines = calculation, open squares = temperature measurement) – reference model

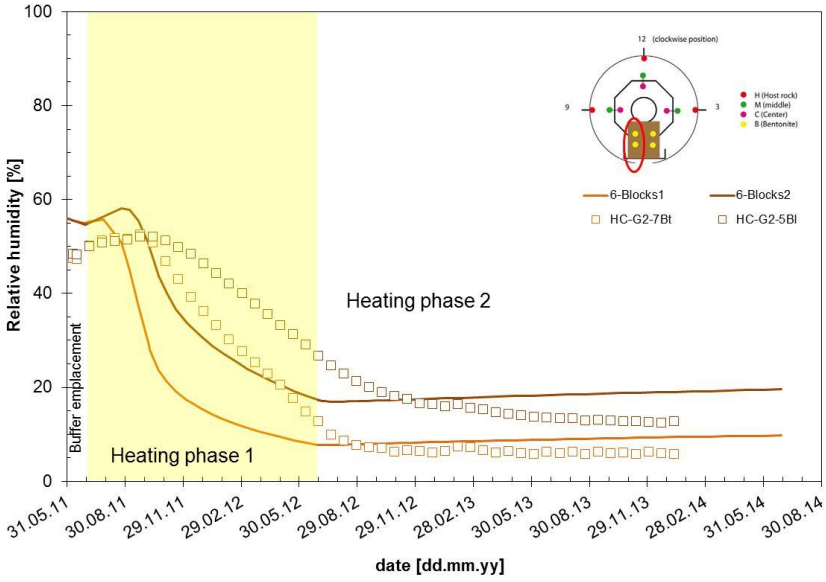

Fig. 5.8 Evolution of relative humidity at the measuring points in the heater mid-plane in the bentonite blocks (lines = calculation, open squares = temperature measurement) – reference model

An alternative case considered the van Genuchten fit instead of the square law (see Fig. 5.1) in order to investigate the influence of the retention curve. Figure 5.9 and Fig. 5.10 show the results for temperature and relative humidity, together with the measured data and – in grey – the results of the square law calculation for comparison.

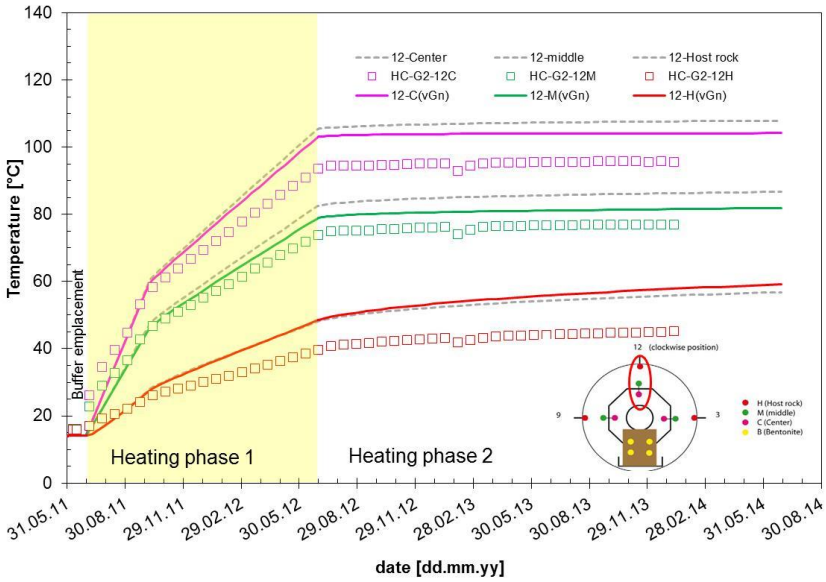

Fig. 5.9 Temperature evolution in the heater midplane in the granular sand/bentonite buffer (lines = calculation, open squares = temperature measurement) – van Genuchten approximation of the retention curve (curves from Fig. 6.3-9 in grey)

With the van Genuchten retention curve, a faster saturation of the buffer in the second heating phase close to the heater is modelled which is not found in the measured data (Fig. 5.10). As a consequence of the faster saturation, the thermal conductivity of the buffer rises, and the temperatures are somewhat lower than for the square law (Fig. 5.9). While the discrepancy for the temperatures is a known geometrical effect that is not relevant with respect to the quality of material properties, the difference in the humidities clearly shows that the better fit of the retention curve data by the square law directly improves the calculation results.

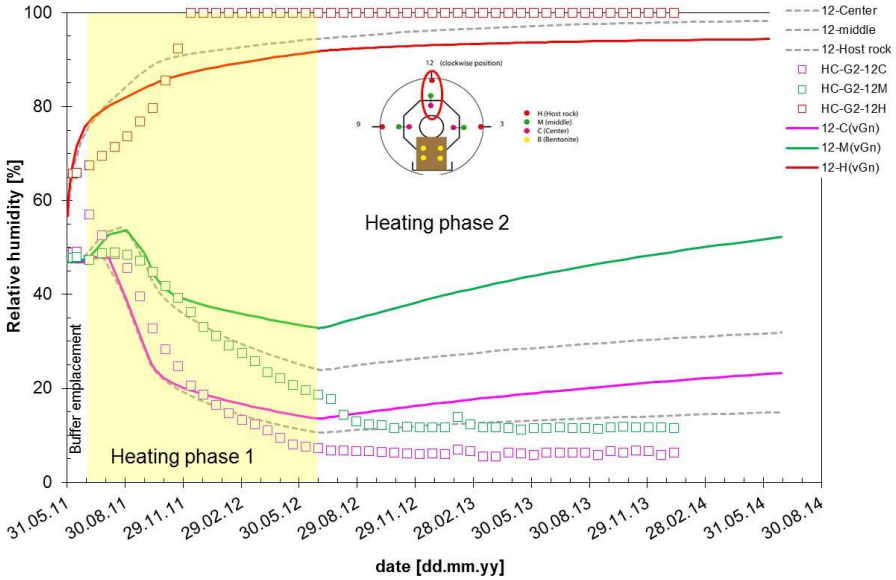

Fig. 5.10 Evolution of relative humidity in the heater midplane in the granular sand/bentonite buffer (lines = calculation, open squares = temperature measurement) – van Genuchten approximation of the retention curve (curves from Fig. 6.3-10 in grey)

As a consequence of heating, pore pressure in the rock around the microtunnel rises. Measurements in the borehole BHE-E1 equipped with a multipacker system are shown in Fig. 5.11 together with calculation results of the reference model. While a slight rise of pore pressure is calculated in the very early heating phase, the pressure starts decreasing soon. The reason for this is not quite clear. In any case, the simple elastic model used for the rock does not seem adequate for simulation of the rock behaviour.

In contrast to the pore pressure evolution for the coupled THM simulation of the reference case, Fig. 5.12 shows the respective results for a TH simulation without mechanical coupling which was performed for comparison. In this model, the pore pressure rises fast – in fact, the characteristic of the measured pressure curves is similar, but the calculated pressures are too high by a factor of five. This is a consequence of neglecting the thermal expansion of the rock's grain skeleton in the TH simulation.

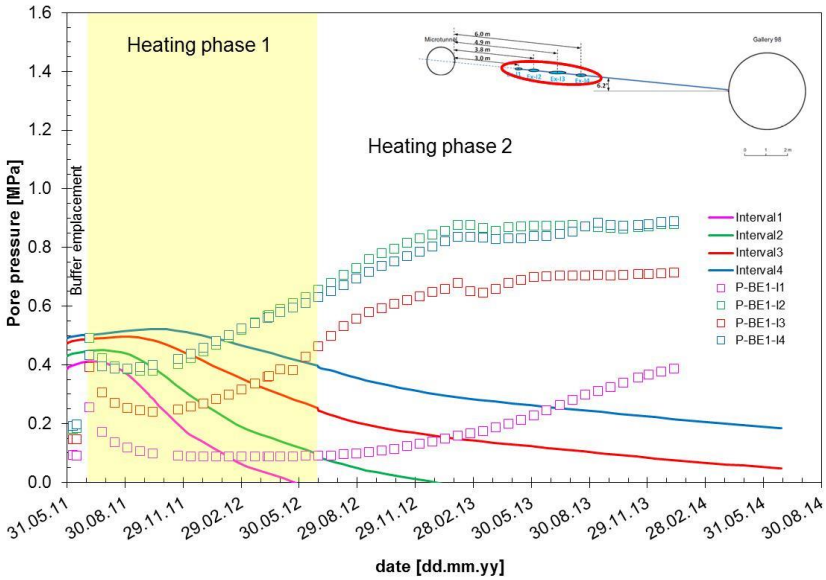

Fig. 5.11 Pore pressure evolution in the rock at the measuring points of the multi-packer system BHE-E1 (lines = calculation, open squares = pressure measurements) – reference model

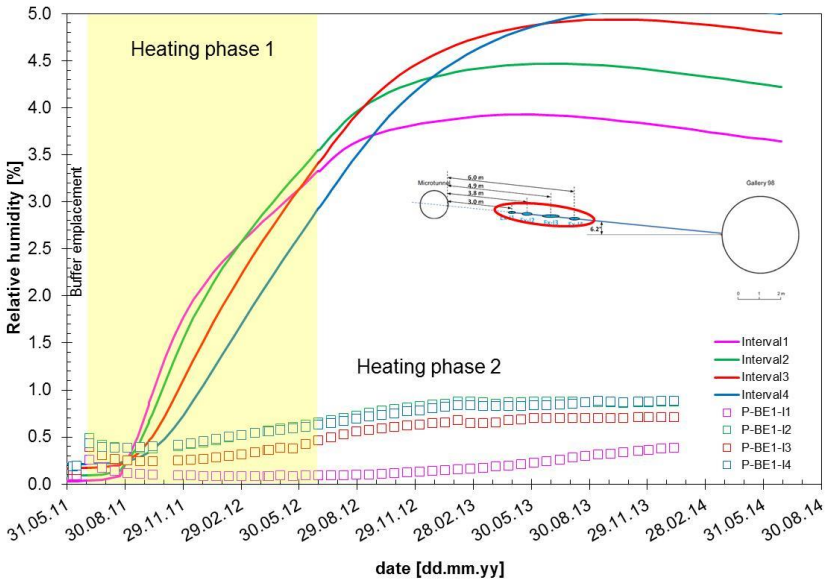

Fig. 5.12 Pore pressure evolution in the rock at the measuring points of the multi-packer system BHE-E1 (lines = calculation, open squares = pressure measurements) – TH simulation without mechanical coupling

5.1.1.3 Bentonite pellet section

Coupled THM using the reference data set were also performed for the bentonite pellet section. Regarding the temperature, similar results were obtained as for the sand-

bentonite section. It was, however, found that a simple elastic model was not sufficient to model saturation behaviour; the relative humidities calculated were far from realistic. For the bentonite pellets, a more elaborated model (at least the Barcelona Basic Model, BBM), is required. For that reason, no results of the bentonite pellet section are shown here.

5.1.1.4 Conclusion

The plane-strain THM simulations of the HE-E using simple standard models for the different buffer materials were successful for the sand/bentonite section in the sense that temperature and relative humidity evolution in the buffer could be captured in an adequate way. For the bentonite pellet section, it was concluded from this section that the BBM or more elaborated models are necessary for modelling the buffer.

For the retention curve of the granular sand-bentonite buffer it was found that fitting the data using the van Genuchten formulation was not very satisfying. Since the square law gives an acceptable fit in the interesting saturation bandwidth, it was used for the reference model. The humidity results clearly show that the better fit of the retention curve data by the square law directly improves the simulation.

Regarding the clay rock, an elastic model using the approach as described here does not seem sufficient to simulate the THM behaviour in a satisfactory manner in the case of the HE-E. Again, a more capable model is needed.

5.1.2 Summary of interpretative modelling in the frame of PEBS

Four modelling tasks were considered in the frame of the interpretative simulations performed in PEBS.

- Task 3.1 – “HM modelling of the Mont Terri Engineered Barrier (EB) Experiment”, aimed at providing a satisfactory scientific representation and a sound basis for interpretation of the EB hydration phase and of the dismantling data, by using new or improved constitutive laws adjusted to the experimental data.
- Task 3.2 – “THM modelling for the planned heater test HE-E”, focused on design modelling as well as predictive and interpretative modelling of the HE-E heater test

and the validation of constitutive models developed in earlier projects, such as NF-PRO.

- Task 3.3 – “THM modelling of bentonite buffer”, has the objective to study various aspects of buffer behaviour in different experiments and disposal concepts. This involves numerical studies on buffer evolution in the Swedish concept, the set-up and use of an inverse modelling framework for the analysis of the FEBEX in-situ test, and a continuing interpretation of the long-term FEBEX mock-up test as well as analyses for the long-term THM tests performed in cells in the CIEMAT laboratory.
- Task 3.4 – “Modelling of THM-C experiments on bentonite buffer”, had the objective to develop advanced multiple-continua THC(m) models for clay barriers and test them with lab and in-situ tests performed in the frame of PEBS and NF-PRO. The emphasis is on the numerical interpretation of container-bentonite interactions and concrete-bentonite interactions.

This modelling work is discussed in detail in the corresponding deliverables of the PEBS project. The summary of the activities and results given here can also be found in the PEBS Final Scientific Report, /SCH 14/, Deliverable D5.16 of the project.

5.1.2.1 Task 3.1 – HM modelling of the Mont Terri Engineered Barrier (EB) experiment

Modelling of the EB experiment addressed both the buffer behaviour during the hydration phase and the state of the buffer at the end of the test, as established during the dismantling operation. The coupled hydraulic-mechanical analyses were performed using the computer code CODE_BRIGHT with a plane-strain geometry. The mechanical behaviour of the compacted bentonite blocks was described by a thermo-elastoplastic model, commonly known as the Barcelona Basic Model (BBM). The main advancement in this task was the development and application of a double porosity model for the bentonite pellets. The macrostructural behaviour is described by equations for unsaturated non-expansive soils (like the BBM). For the microstructural behaviour, saturation and reversible deformation are assumed to be independent of macrostructural effects. Coupling between the two structural levels takes into account irreversible macrostructural strains when elastic microstructural strains take place; that means elastic microstructural strain (swelling or shrinking) leads to irreversible macrostructural strain. The

functions describing the coupling between the structural levels are dependent on the "degree of openness" of the macrostructure relative to the applied stress. The parameters required for the double-structure model were calibrated from the numerical modelling of wetting-drying tests at constant vertical load and wetting tests at constant volume. The complete model description can be found in Deliverable D3.1-1/D3.1-2.

The new model was successfully used to simulate the granular buffer evolution. An alternative approach additionally taking into account a variable density for the liquid phase had also been considered, but was not required in the end.

The progress of hydration, as observed in the evolution of relative humidity (in the buffer and in the rock) and pore pressure (in the rock) is generally satisfactorily reproduced by the numerical model. Larger discrepancies concern the time evolution of relative humidity in the buffer, which is a likely consequence of the complexity of the artificial hydration system as well as a lack of control in some of the early hydration stages.

Dismantling revealed that the barrier was at or very close to full saturation throughout, and that a significant degree of homogenization was been achieved, although some heterogeneities persisted. Again, the numerical model achieved a very good representation of the state of the buffer at dismantling. A practically fully saturated barrier was predicted and the degree of homogenization is also well reproduced. Even the pattern of heterogeneities in the cross section of the barrier is well reproduced.

It has been considered likely that part of the heterogeneity observed upon dismantling may be caused by an initially heterogeneous barrier due to emplacement difficulties and possible segregation of the granular bentonite. It should be noted, however, that the numerical analyses assumed an initially homogeneous granular bentonite. Therefore, the modelling suggests that at least some of the observed heterogeneity at the dismantling stage is a direct consequence of the layout and geometry of the test.

5.1.2.2 Task 3.2 – THM modelling for the heater test HE-E

Three teams participated in the modelling of the HE-E experiment in the framework of PEBS. The Nagra team used TOUGH2 with a thermo-hydraulic (TH) approach and a three-dimensional model. GRS used CODE_BRIGHT with a thermo-hydraulic-mechanical (THM) approach and a two-dimensional plane-strain model. CIMNE also used CODE_BRIGHT with the full THM approach and a two-dimensional axisymmetric

model; for some considerations, also a plane-strain model was used. The history of the HE-E tunnel, which had formerly been used for the Mont Terri Ventilation Test, involving a complicated series of drying/wetting cycles of the surrounding rock, was accounted for by suitable simplifications leading to a reasonable initial pore pressure.

In a first step, scoping calculations were performed with preliminary material data prior to the installation of the HE-E. The objective was to give a first idea of the response to heating that could be expected and to find out whether the planned instrumentation was suitable to measure this response. While there were considerable deviations in the results of the three teams, they agreed that an early pore pressure increase was to be expected not in the close vicinity of the HE-E tunnel, but a few metres away. Consequently, the instrumentation was supplemented accordingly. Details on the scoping calculations are found in Deliverable D3.2-1.

While performing the first predictive simulations of the HE-E, a modellers' database was developed, compiling all the material data needed for the simulations. This involved existing data on the THM behaviour of the buffer materials and the rock as well as laboratory testing results obtained in PEBS Work Package 2, especially regarding the bentonite pellets and the granular sand-bentonite mixture.

With the completed database interpretative calculations were performed and compared to the actual measurement results, in terms of temperature, relative humidity in the buffer, and pore pressure in the rock. The models and assumptions used in thee simulations are described in detail in the combined Deliverable D2.2-11/D3.2-2 "The HE-E Experiment: Lay-out, Interpretation and THM Modelling".

Nagra's thermal-hydraulic 3D simulations resulted in a good representation of the temperature field. A sensitivity study on the effect of the relation between thermal conductivity and saturation of the buffer showed that a significant impact is restricted to the vicinity of the heater. Regarding the evolution of relative humidity as a measure of saturation of the buffer, there was some deviation between the measured data and simulation results. Desaturation in both sections of the granular buffer was restricted to the close vicinity of the heater, and no desaturation of the bentonite blocks was observed in the simulation, as opposed to the relative humidity measurements. In order to reproduce pore pressure evolution in the rock, the thermal expansion of the grains in comparison to the thermal expansion of the pore water was investigated numerically. With an additional adaption of the pore compressibility as a compensation for transverse an-

isotropy which cannot be considered in TOUGH2, a reasonable representation of pore pressure evolution could be obtained.

GRS used CODE_BRIGHT with plane-strain geometry, full THM coupling, and simple elastic models for rock and buffer in order to explore their performance in simulating the HE-E (see previous section). As a consequence of the plane geometry, temperature was overestimated in the buffer, since the axial heat flow component is neglected. For the relative humidity evolution in the sand-bentonite buffer, a satisfying representation was obtained with a square-law retention curve which represents the measurement results in the relevant saturation range better than the alternatively considered van Genuchten curve. In the bentonite pellet buffer, the elastic model proved to be inadequate. The pore water pressure evolution in the rock was underestimated in these simulations.

Most of CIMNE's simulations were carried out using an axial symmetric model which is not capable of catching the difference between the bentonite blocks and the granular buffer materials, but avoids the thermal overestimation introduced by a plane model. Consequently, satisfying modelling results of the temperature field were obtained. Using an elastoplastic model (Barcelona Basic Model) for the buffer and retention curves of a modified van Genuchten type which represented well the laboratory and additional back-analysis results, the simulation of relative humidity in both buffer types was also reasonable. Still, some uncertainties regarding the retention curves of the granular buffer materials remain. The initial state of pore pressure in the rock could not be simulated adequately with the axial symmetric model; a n additional plane-strain model produced a better match. On the other hand, the axial symmetric model gave better results in terms of the impact of heating on pressure evolution.

As an overall conclusion of the HE-E simulations one can state that turning the attention to different aspects of modelling, as the different teams did, led to good results regarding these aspects. The shortcomings could be attributed to accepted simplifications in considered processes, geometry or constitutive models. In particular, the buffer behaviour can be simulated in an adequate way, although uncertainties concerning the retention curves of the granular buffer materials and the dependence of their thermal conductivities and permeabilities on the degree of saturation remain.

5.1.2.3 Task 3.3 – THM modelling of bentonite buffer

Task 3.3 was dedicated to the investigation of various aspects of buffer THM behaviour. A special emphasis was on the use of approaches exceeding standard views and applications.

Clay Technology studied eleven modelling tasks involving the bentonite buffer for the Swedish disposal concept. An overview of these tasks is given in Deliverable D3.3-2, including information about the objective, models used, some main results, and uncertainties. The tasks with higher relevance regarding the PEBS framework were described in more detail, namely: Analysis of time scale of buffer hydration, analysis of moisture redistribution in dry rock scenario, and buffer homogenization. The respective simulations using CODE_BRIGHT and ABAQUS were performed early in the project and made use of the data available at that time.

The results of the Clay Technology team studying THM behaviour of the bentonite buffer in the Swedish disposal concept are described in Deliverable D3.3-2. One major finding was that the saturation time for the buffer is mainly affected by changes in the retention curve. Buffer permeability was less important for given hydraulic conditions in the rock. Thermodynamics as well as experiments suggest that retention is stress dependent. Therefore, the evolution of the actual stress state should be represented in the retention curve. Stress dependence is not included explicitly in the normally used van Genuchten formulation, but should implicitly be accounted for. Furthermore, it can be concluded from Clay Technology's studies, that existing models like the Barcelona Basic Model are not sufficient to simulate buffer homogenization behaviour in a system representing the Swedish concept, where the void between ring-shaped or cylindrical bentonite blocks and the emplacement borehole wall is backfilled with bentonite pellets. A thermodynamically/chemically based model might be of benefit (see Section 5.2.2).

TK Consult and Nagra studied whether TH inverse approaches can be applied for interpreting long-term THM experiments, neglecting mechanical processes as induced e.g. by bentonite swelling, but profiting from the computational efficiency introduced by the reduction of complexity. In order to ensure predictive reliability, the study derived the involved parameters from inverse modelling of the full-scale FEBEX in-situ test which provides pressure, temperature, and saturation data from a heating experiment for a period of 15 years. A series of models had to be maintained, each representing one phase of the experimental setup, which includes, (1) excavation and installation,

(2) isothermal hydration, (3) first heating phase, (4) cooling down of first heater, (5) dismantling of first heater, and (6) second heating phase. The initial conditions being transferred in each case from the previous phase, the six models differed in geometry and boundary conditions but were driven by the same set of model parameters. Details are given in the PEBS Deliverable D3.3-1. The joint inversion of the whole set of measurement data resulted in parameter estimates of permeability, porosity, relative permeability and capillary pressure functions for both, host rock and bentonite buffer. In addition, the inverse model provided uncertainty estimates of the resulting parameters in form of standard deviations which can be applied in following modelling steps in order to assess the uncertainty of long-term predictions.

For TK Consult's inverse modelling of the FEBEX in-situ experiment (see Deliverable D3.3-1), comparisons of model simulations with the observations show different degrees of agreement. While the pressure fit obtained in the granite boreholes is suffering from the unconsidered heterogeneity and potential measurement errors the agreement of relative humidity in the buffer and temperature in both, buffer and rock is remarkable, taking into account the simplicity of the axisymmetric model. Moreover, the estimated thermal and two-phase parameter values fit well into the range of available laboratory measurements. Other parameter estimates (e.g. the low porosity of the bentonite) include the influence of neglected/simplified processes and, thus, refer to the TH modelling approach, solely.

CIMNE simulated two long-term infiltration cell tests (an isothermal cell test and a thermal gradient cell test) and the FEBEX mock-up test using CODE_BRIGHT with a full THM formulation. Earlier analyses had shown that there were some discrepancies between modelling results and observations, especially regarding the rate of water uptake of compacted bentonite. In the framework of PEBS, enhanced constitutive laws were taken into account in order to explain the deviations. Four types of analyses were carried out:

- Reference analyses, using the conventional THM formulation (BBM);
- Analyses assuming non-Darcy flow due to the existence of a threshold gradient in the liquid flow law;
- Analyses incorporating thermo-osmosis;
- Analyses incorporating the evolution of micro-fabric by means of a double structure constitutive law.

The three enhanced models (taking into account threshold gradient, thermo-osmosis or microfabric evolution) used by CIMNE for the simulation of the long-term infiltration tests and the FEBEX mock-up are all able to model reasonably accurately the hydration of the mock-up test at early and later stages (Deliverable D3.3-3). Although the PEBS project was not designed to establish experimentally the potential existence and effects of those three phenomena, the results of THM modelling of the FEBEX mock-up test (16 years of observations) gives some useful information on the effects likely to be associated with each one of the individual hypotheses considered. Numerical modelling has shown that each of these possibilities is capable of providing results in reasonable good agreement with observations. However, numerical analysis, on its own, is unable to identify with certainty which is the phenomenon (or combination of phenomena) underlying the observed slowing down of hydration. However, there are noticeable differences between the predictions of the different hypotheses for the longer-term situation. Therefore, availability of long-term observations of the mock-up test may help in identifying the relevant phenomena at the later stages of hydration.

5.1.2.4 Task 3.4 – Modelling of THMC experiments on bentonite buffer

Starting from an existing THC formulation, UDC incorporated mechanical and geochemical couplings in order to account for porosity changes caused by swelling phenomena (THCm). In addition, reactive gaseous species, such as O_2, CO_2, and H_2 were incorporated. The improved model was tested with the data from the FEBEX mock-up test. Further tests were performed using different experiments performed at CIEMAT:

- The CG experiments performed on 60 cm long bentonite columns with durations ranging from 0.5 to 7.5 years;
- Corrosion experiments to study the corrosion products generated at the canister-bentonite interface under repository conditions and analyse how the corrosion products affect the properties of the bentonite. These experiments were performed on samples of several lengths (25 mm for SC tests and 100 mm for FB tests) and temperatures (25 ºC, 50 ºC and 100 ºC);
- The HB experiments to study the interactions of concrete and bentonite, including a 30 mm layer of concrete which was in contact with the hydration system and a 71.5 mm thick layer of bentonite;

- The so-called double interface tests which include a 3 mm thick layer of cement mortar which is in contact with the hydration system, a 18 mm thick layer of bentonite and a 2 mm layer of powder magnetite.

Although some uncertainties remain, many aspects of the different experiments were successfully reproduced with the improved model (Deliverable D3.4-1).

With the enhanced model, the cumulative inflow measured in the FEBEX mock-up for the last 14 years could be reproduced. The fit of relative humidity, however, shows some discrepancies possibly caused by some model limitations such as the consideration of a single porosity model.

Regarding the 60 cm long (CG) experiments, the numerical model reproduced the observed temperatures, saturation degrees, porosities and dissolved an exchanged chemical data. Geochemical predictions improved when the changes in porosity caused by swelling were considered and when some parameters such as vapour tortuosity, heat dissipation and cation selectivities were estimated.

With respect to the corrosion experiments, simulations agreed well with experimental data for the most part. Model results indicated that

- The main properties of the bentonite remain unaltered;
- There is a sequence of corrosion products, $Fe(OH)_2(s)$ and magnetite being the end members;
- Fe^{2+} is sorbed by surface complexation;
- Fe^{2+} cation exchange is less relevant than Fe^{2+} sorption;
- Corrosion products penetrate a few mm into the bentonite.

For the most part, the model also reproduced the reactions observed at the concrete-bentonite tests, including calcite and brucite precipitation in the hydration contact and the dissolution of portlandite and precipitation of CSH, calcite and MSH near or at the bentonite-concrete interface. The model predictions for ettringite and gypsum were less accurate. The precipitation of CASH phases was not accounted for in the models due to the lack of thermodynamic data. The nature of low crystal size C-(A)-S-H and M-S-H at the bentonite-concrete interface is still unclear.

5.2 Long-term extrapolation

Task 3.5 – “Extrapolation to repository long-term evolution” had the objective to use the data and improved models from Task 3.1 – Task 3.4 for extrapolation to long-term evolution of the repository and to investigate model uncertainty and its impact on long-term prediction, thus providing input to WP 4 “Analysis of impact on long-term safety and guidance for repository design and construction”. This involved

- Critical assessment of the results of the other WP 3 tasks regarding their implications for different time and space scales including long-term conditions;
- Identification of the significant processes in the resaturation phase and after resaturation;
- Development or modification of the available HM, THM and THMC formulations to incorporate phenomena and processes deemed to be relevant for long-term predictions;
- Performance of coupled numerical analysis for long-term evolution of the engineered barrier system in the repository, with different degrees of abstraction and different focuses according to the different modelling teams;
- Evaluation of the model uncertainty and its implications for long-term prediction and safety analysis.

An additional objective of Task 3.5 was the compilation and evaluation of the usefulness of natural analogues for providing support, testing and validation of long-term predictions of current THMC models. Furthermore, a study of the thermo-mechanical continuum theory of mixtures was included in Task 3.5, in order to approach long-term evolution from a different point of view and to provide a relevant material model applicable for systems consisting of bentonite (montmorillonite), water and air.

One of the major exercises of Task 3.5 “Long-term extrapolation” was to define and numerically model a set of simulation cases relevant for the repository long-term evolution, building on the insights from the other PEBS tasks and providing input to WP 4. In order to have a maximum benefit from this exercise, it was concluded that

- The processes which exhibit uncertainties were the most relevant for the extrapolation consideration;
- Substantial data to improve their description should be provided within PEBS;

- The modelling cases to be considered should be of interest to more than one of the partners.

With these criteria in mind, the following long-term simulation cases were defined:

- Simulation Case 1 – Isothermal buffer evolution;
- Simulation Case 2 – Thermo-hydro-mechanical evolution of the buffer at temperatures up to 100 °C;
- Simulation Case 3: Thermo-hydro-mechanical evolution of the buffer with temperatures temporarily exceeding 100 °C;
- Simulation Case 4: Geochemical evolution at canister-bentonite and bentonite-concrete interfaces, including a long-term simulation of a repository in granite.

The detailed description of the cases and the simulation results are found in Deliverable D3.5-4 /WIE 14/ of the PEBS project.

GRS took part in the Simulation Case 3. Section 5.2.1 presents the GRS results as they can be found in D3.5-4. Section 5.2-2 gives a summary of all results obtained in Task 3.5, which can again be found in the PEBS Final Scientific Report, /SCH 14/, Deliverable D5.16 of the project.

5.2.1 Long-term modelling by GRS

Modelling Case 3 is based on the Swiss reference concept of drift disposal, with waste canisters resting on compacted bentonite blocks and the remaining void backfilled by bentonite pellets. The heat power per canister is 1500 W at emplacement and decreases with time as shown in Fig. 5.13.

Three teams (Nagra, GRS and CIMNE) were involved in the simulation of this case; all of them simulated a disposal cell including a single canister. Nagra and GRS both used a three-dimensional model, giving a realistic geometrical representation of the repository cell, but reduced the complexity of the problem by performing thermal-hydraulic simulations, neglecting mechanical effects. CIMNE used a full THM coupling with the simplification of a two-dimensional axisymmetric geometry which did not consider adjacent emplacement galleries.

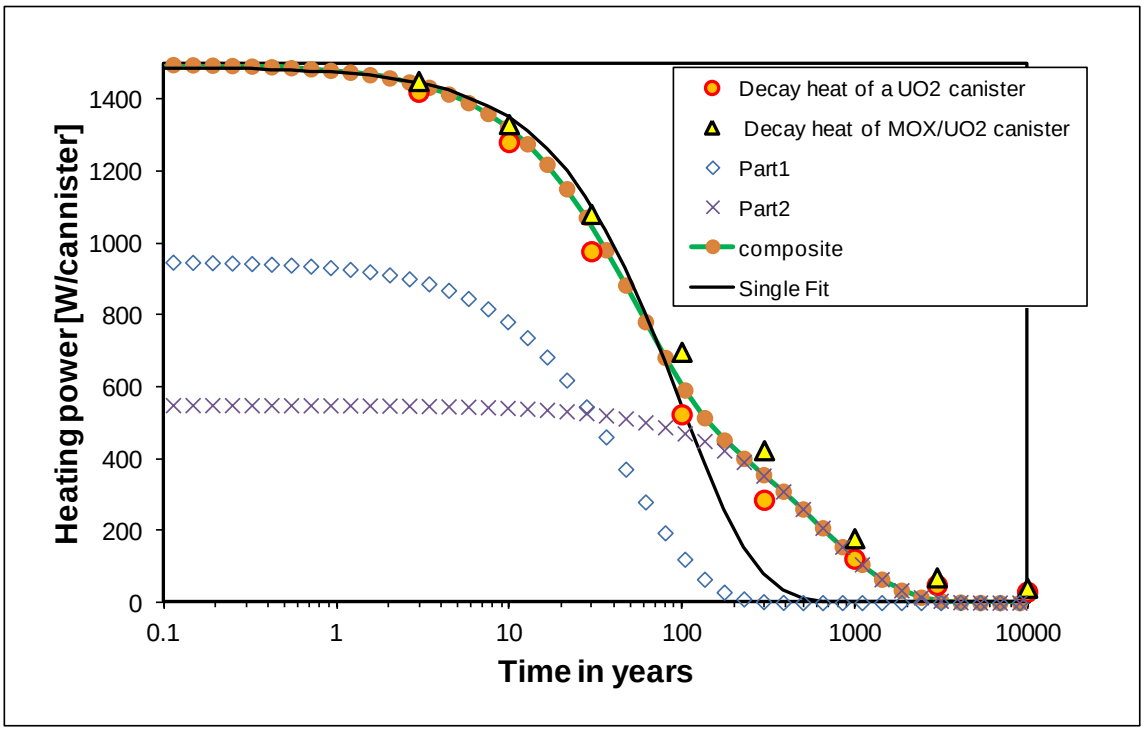

Fig. 5.13 Heat decay curve for UO2 and MOX/UO2 canisters and various curve fits ("composite" is the sum of "part 1" and "part 2")

5.2.1.1 Modelling approach

GRS used CODE_BRIGHT for a coupled TH simulation with a 3D model, neglecting mechanical effects in the same way as Nagra with TOUGH2. Modelling starts with instantaneous construction of the emplacement gallery, which is then left open for one year. Afterwards, canister, bentonite blocks, and granular bentonite are emplaced also instantaneously. Initial saturation of the blocks is 63 %, while the granular bentonite starts at 20 % initial saturation.

The heat output of the canister could not be entered using a composite exponential function. Instead, the heat decay curve given in Fig. 5.1 was approximated by three individual exponential curves each active in a different time window, as shown in Fig. 5.14.

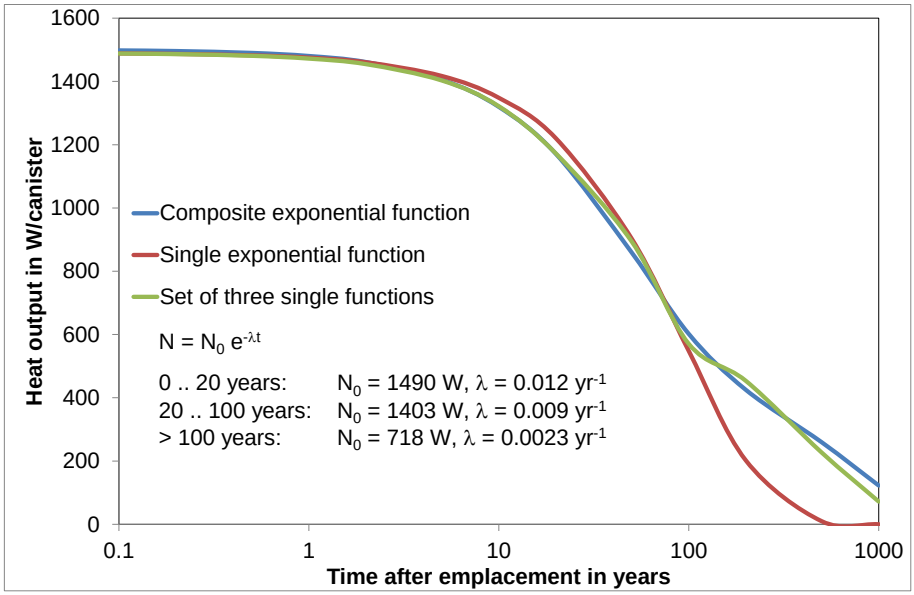

Fig. 5.14 Approximations of canister heat decay curve: The set of three single functions was used for the GRS simulation

5.2.1.2 Geometry, conditions and material parameters

The dimensions of the model are given in Tab. 5.2. The complete geometrical model and a detail near the emplacement gallery are shown in Fig. 5.15.

Tab. 5.2 Model dimension and initial conditions

	Values	Comment
Model Domain		
Height (m)	150	greater than typical OPA thickness of 100 m
Lenght (m)	4	(half canister + bentonite)
Width (m)	20	(half distance between adjacent emplacement tunnels
Emplacement Tunnel		
Tunnel Radius (m)	1.25	
Canister radius (m)	0.525	
Canister lenght (m)	2.5	(half length)
Initial Conditions		
Pressure at z = 75 m (MPa)	5.9	Hydrostatic at 600 m depth
Temperature at z = 75 m (°C)		Temp. gradient: 0.043 °C/m, Surface Temperature: T_0 =1 0°C
Capillary Suction (MPa)	2	Capillary suction for ventilated tunnel at atmospheric pressure (1.0135E+5 Pa)

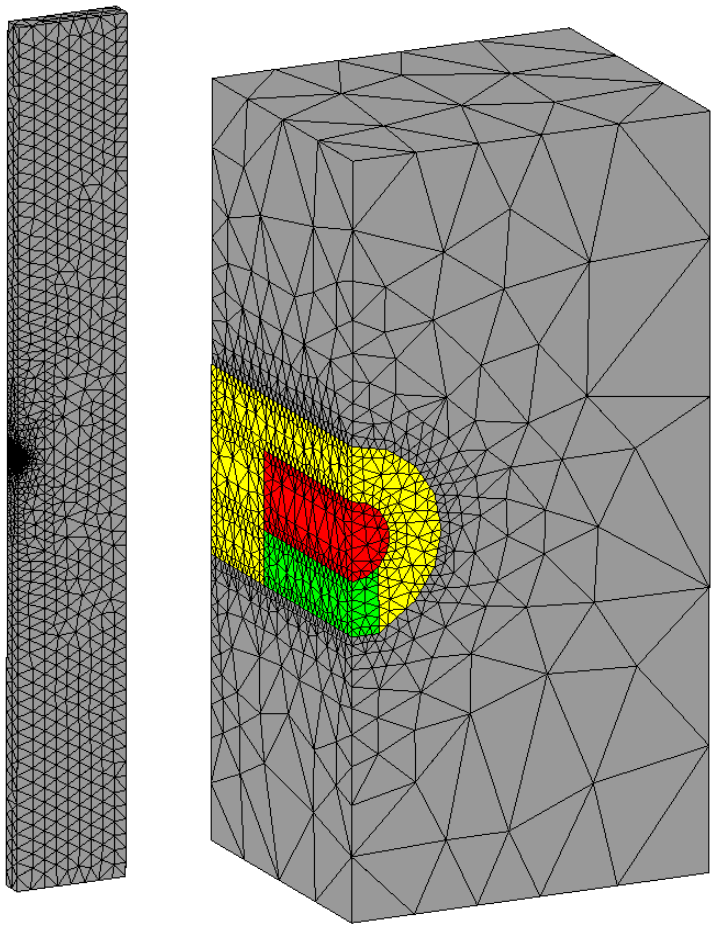

Fig. 5.15 Finite element model used for the simulation (left: detail near the gallery)

Boundary conditions at bottom and top of the model are given by prescribed temperatures and fluid pressures (32.575 °C and 5.15 MPa 75 m above the gallery axis and 39.025 °C and 6.65 MPa 75 m below the gallery axis). Initially, temperature and pressure increase linearly with depth, resulting in an initial temperature of 35.8 °C and a pressure of 5.9 MPa at gallery level. At the four model sides, no-flow boundary conditions are applied in consideration of the model symmetry. An excavation damaged zone with altered hydraulic properties was not considered.

During the gallery ventilation phase, a suction pressure of -29.5 MPa (corresponding to 94 % water saturation) is applied to the gallery wall.

The material parameters are those defined by the HE-E modellers data set, as given in Tab. 5.3.

Tab. 5.3 Relevant input parameters in the model

	OPA	EDZ	Bentonite blocks	Bentonite pellets	Heater
Permeability: k [m^2]	1.0E-20	5.0E-20	2.5E-21	3.5E-20	1.0E-50
Porosity: ϕ [-]	0.12	0.14	0.33	0.45	0.001
Pore compressibility: Cp [1/Pa]	1.7E-09	1.7E-09	3.0E-09	3.7E-09	0
Van Genuchten[1] P_0 [Pa]	1.8E+07	9.0E+06	2.19E+07	1.0E+07	1.0E+06
Van Genuchten[1]; n (k_r)	1.67	1.67	1.42	1.67	2
Van Genuchten[1]; n (P_c)	1.67	1.67	1.42	1.67	2
Residual. Water Saturation: K_r-S_{wr} (Pc-S_{wr})	0.1 (0.01)	0.1 (0.01)	0.1 (0.01)	0.1 (0.01)	0.01 (0.01)
Residual Gas Saturation: S_{gr}	0	0	0	0	0
Therm. Expansion T_x [1/K]	1.7E-05	1.7E-05	2.5E-05	2.5E-05	1.5E-05
Thermal conductivity (linear between T_{cs} and T_{cd})					
Wet: T_{cw} [W/m K]	1.9	1.9	1.3	1.3	52
Dry: T_{cd} [W/m K]	1.3	1.3	0.81	0.3	52
Specific Heat: S_h [J/kg C]	995	995	1058	893	440
Initial saturation (S_w)	1.0	1.0	0.63	0.2	0.01

Two-Phase Parameter Model	[1]van Genuchten		[1]van Genuchten/Mualem
	$P_c = P_o \cdot \left(S_{ec}^{\,n/(1-n)} - 1\right)^{1/n}$	$S_{ec} = \frac{S_l - S_{lr}}{1 - S_{lr}}$ $m = 1 - 1/n$	$k_{r,l} = S_e^{\gamma} \cdot \left[1 - \left(1 - S_e^{\frac{1}{1-n}}\right)^{\frac{n-1}{n}}\right]^2$ $k_{r,g} = (1 - S_e)^{\varepsilon} \left(1 - S_e^{\frac{n}{1-n}}\right)^{2(1-1/n)}$ $S_e = \frac{S_l - S_{lr}}{1 - S_{lr}}$ γ=0.33; ε=0.5

5.2.1.3 Modelling results

The actual simulation proved to be extremely time consuming. After a calculation time of several months only 220 years of repository evolution had been simulated. Therefore, an additional simplified model was used which is identical to the original model except for the fact that water evaporation is suppressed. This model worked much more efficient, so that a simulation time of 1000 years was reached. Of course, this simplification is not adequate for the early evolution when temperatures above 100 °C occur and when the buffer is only partially saturated. At later times sporting moderate temperatures and full buffer saturation, however, the full model and the simplified one yield identical results, as will be shown further down in this section.

The simulation results of the two models are shown for evaluation points on the canister surface, on the tunnel wall and the floor, and at various locations in the granular bentonite buffer and in the bentonite blocks, as shown in Fig. 5.16.

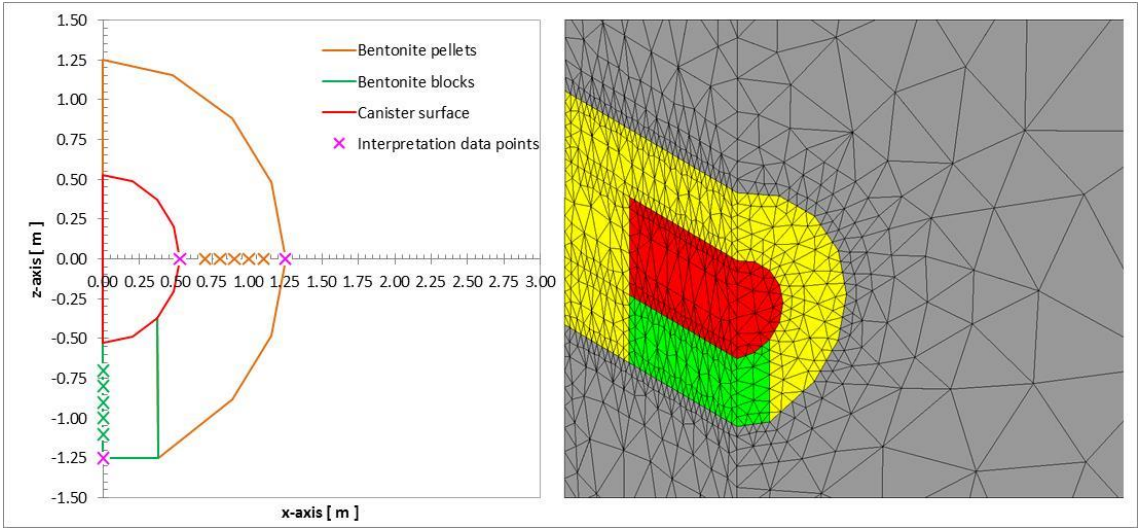

Fig. 5.16 Location of evaluation points on the canister, the tunnel surface, and in the buffer

Temperature

Figures 5.17, 5.18 and 5.19 show the temperature evolution on the canister and tunnel surface, in the granular buffer, and in the bentonite blocks, respectively. At simulation times up to 27 years there is a significant difference between the full (symbols) and the simplified (dashed lines) model, because suppressing of evaporation accelerates saturation of the buffer, leading to higher thermal conductivity of the buffer. After 27 years

simulation time, the curves are identical, so that the simplified model can be considered representative for the long term. The maximum temperature on the canister surface of 145 °C is reached at about five years after emplacement (Fig. 5.17). 1000 years after emplacement, the temperature has reduced to about 45 °C everywhere in the buffer.

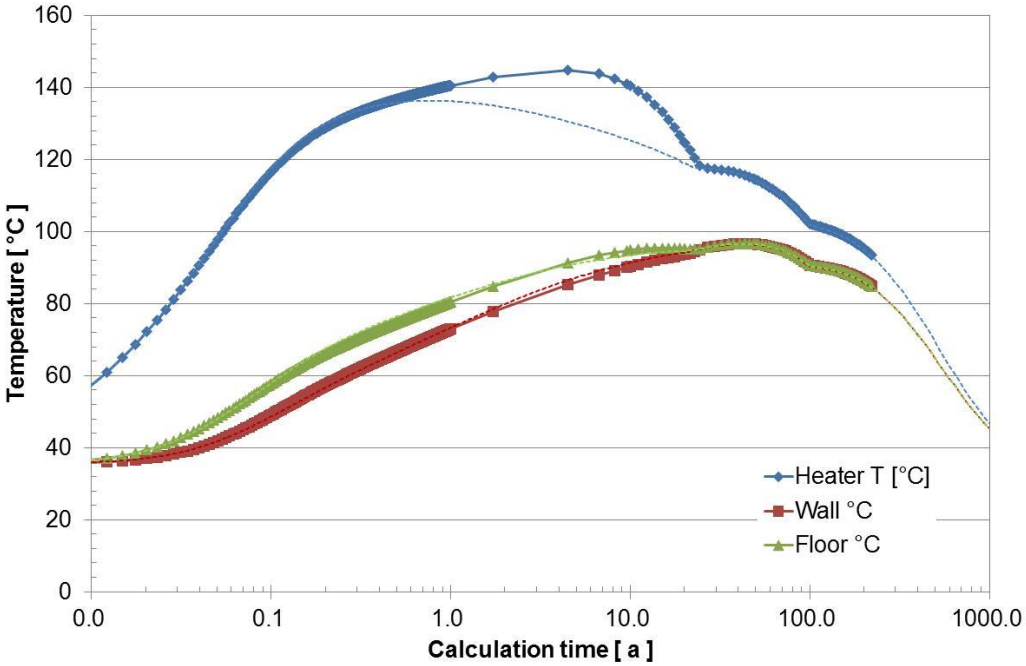

Fig. 5.17 Temperature evolution on the canister and on the tunnel surface

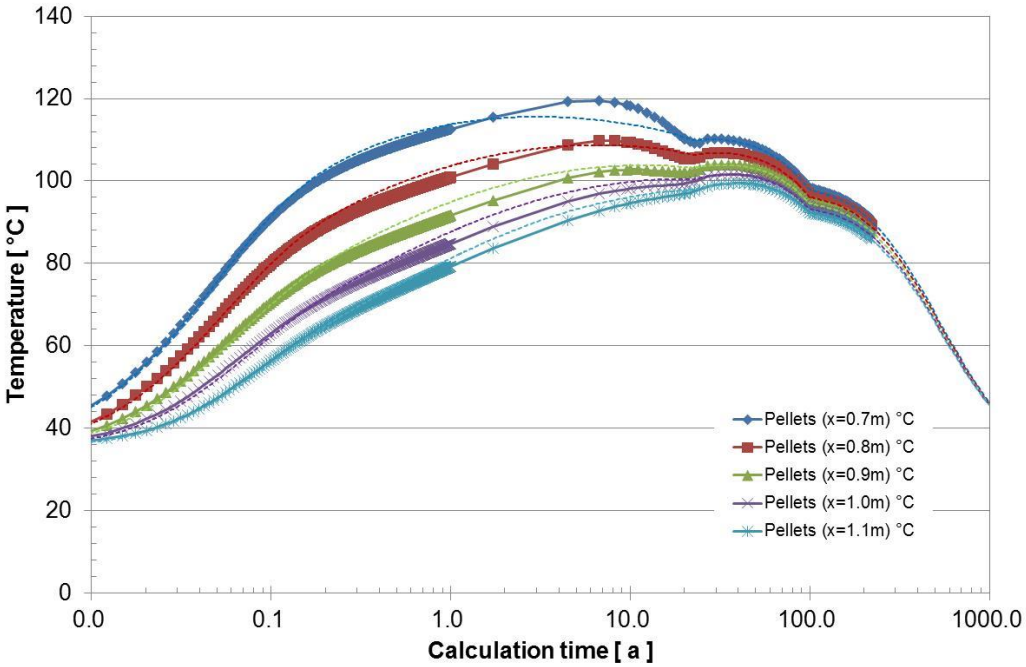

Fig. 5.18 Temperature evolution in the granular buffer

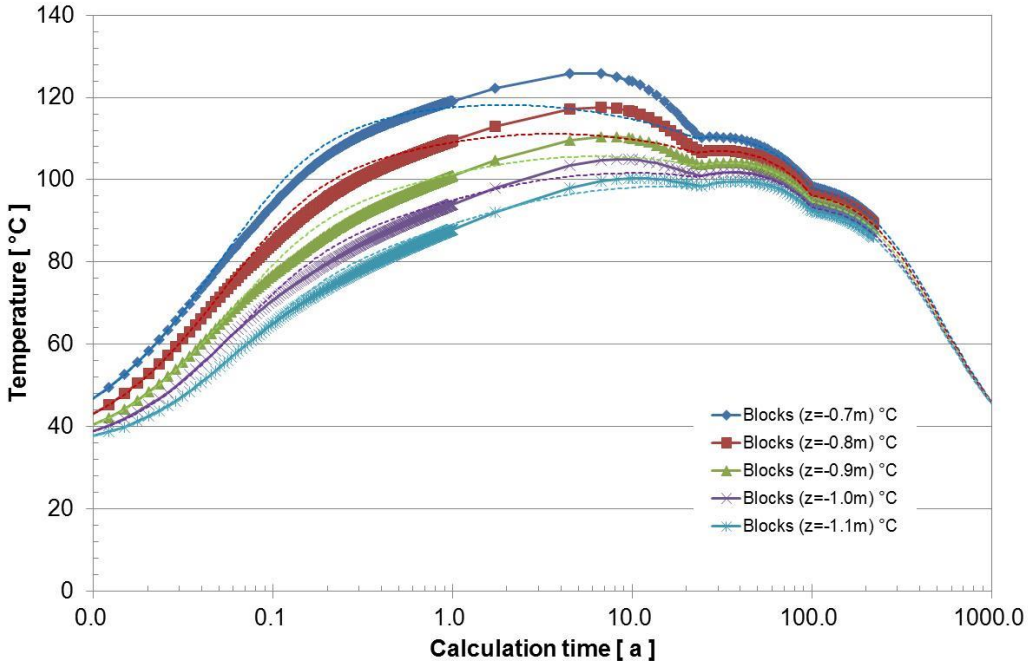

Fig. 5.19 Temperature evolution in the bentonite blocks

The temperature in the host rock is shown as profiles for different times in Fig. 5.20. The rock temperature remains below 100 °C all the time. The maximum temperature of 71 °C at the symmetry plane between two emplacement galleries is reached after 100 years; then, the temperature is decreasing everywhere in the model.

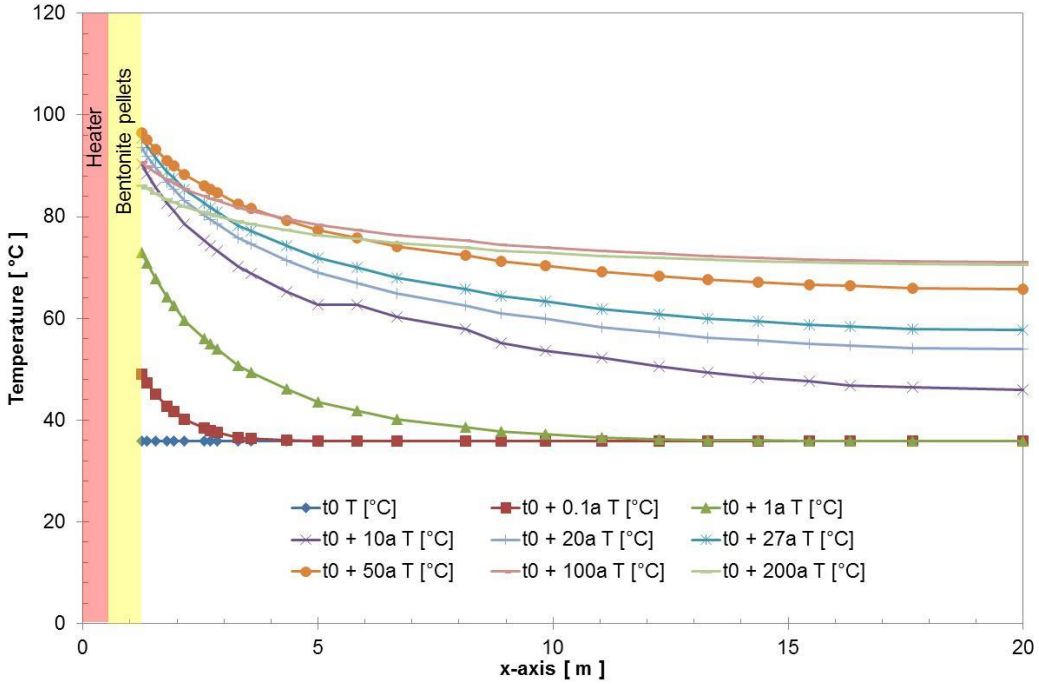

Fig. 5.20 Temperature profile in the rock for different simulation times

Saturation and relative humidity

The saturation evolution of the granular buffer and of the bentonite blocks is shown in Fig. 5.21 and Fig. 5.22, respectively. Naturally, the saturation curves of the simplified model (dashed lines) are not realistic, because evaporation is suppressed, which has a high effect on saturation rates. In particular, desaturation of the blocks at high temperature is nearly not observed in the simplified model. The time to full saturation is, however, not very different in the simplified and the full model.

In the full model (symbols in the figures), there is an early desaturation of the bentonite blocks close to the canister (Fig. 5.22) due to evaporation at high temperature. The pellets are at very low saturation from the beginning, therefore there is no further desaturation, but saturation rates are very low. Five years after emplacement, when the temperature starts to decrease, saturation rates are accelerated due to condensation of water vapour. 27 years after emplacement the buffer is fully saturated.

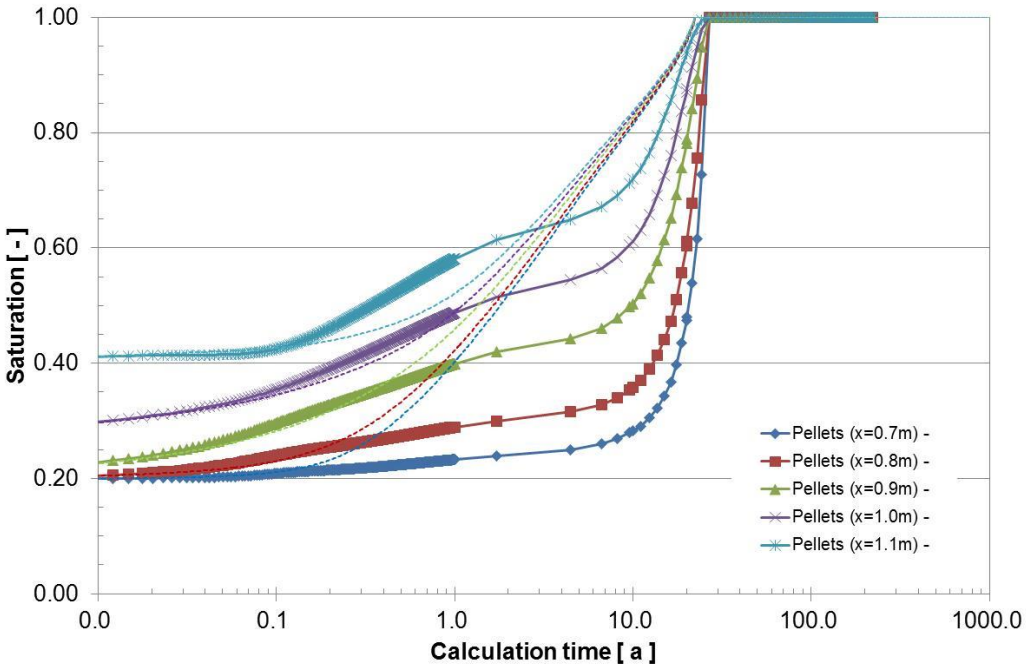

Fig. 5.21 Saturation evolution in the granular buffer

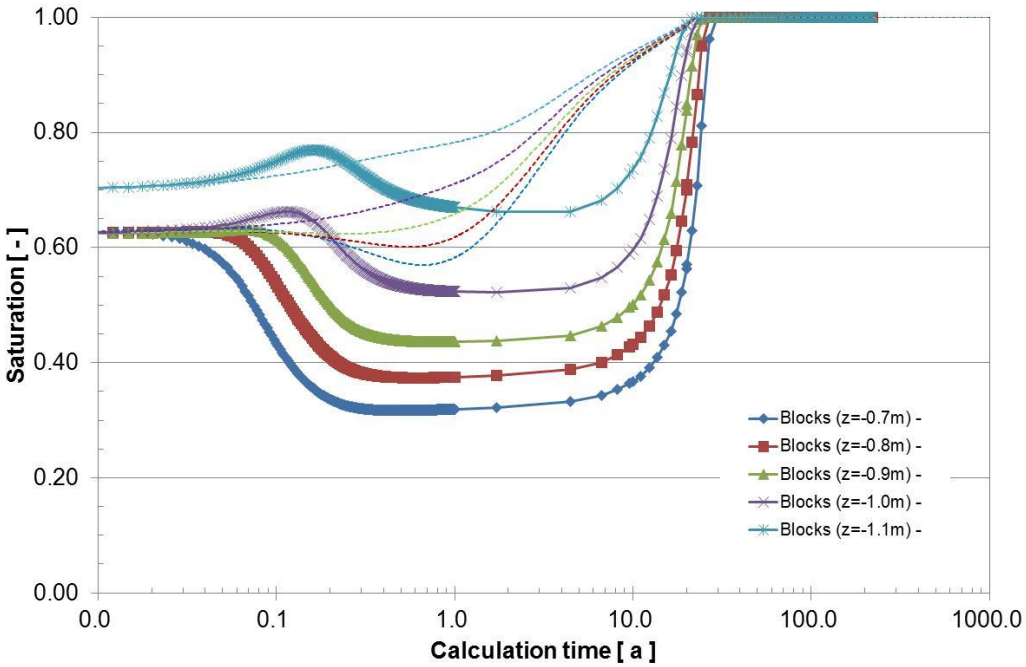

Fig. 5.22 Saturation evolution in the bentonite blocks

The Figures 5.23 and 5.24 show the evolution of relative humidity corresponding to the saturation for the granular pellet buffer and the bentonite blocks.

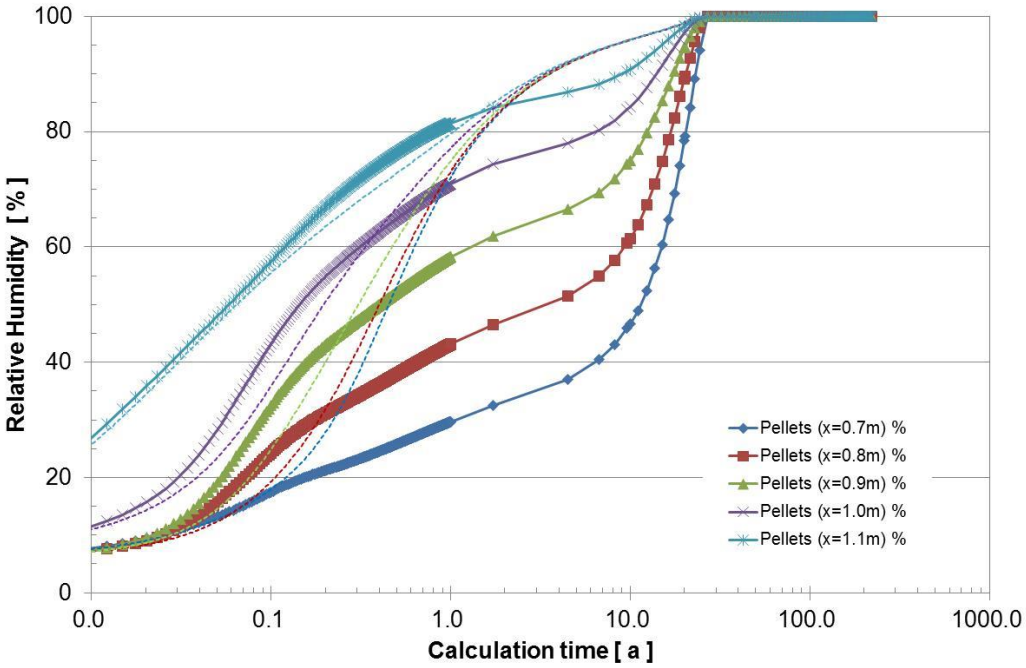

Fig. 5.23 Evolution of relative humidity in the granular buffer

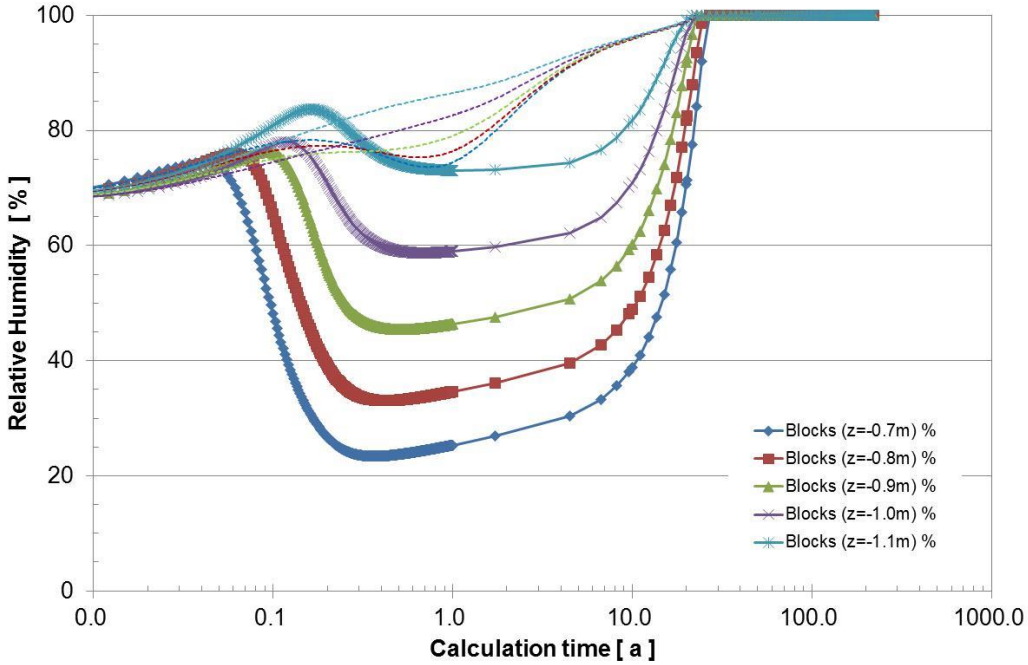

Fig. 5.24 Evolution of relative humidity in the bentonite blocks

Pore pressure in the rock

Pore pressure profiles in the rock for different simulation times are presented in Fig. 5.25. A pore pressure of 10 MPa is already reached after 10 years, later, the pore pressure increases even further. This is not realistic, but stems from the fact that in this calculation a distinction between thermal expansion coefficients for the solid grains, the pore liquid, and the grain skeleton was not possible. This improvement was introduced by CIMNE (see /WIE 14/).

5.2.1.4 Alternative simulation case

Due to the very high simulation times with the full model, consideration of alternative cases was very limited. Only one alternative case with an altered saturation of the tunnel surface at emplacement time was considered, since this is a parameter which is not well defined. It was found, however, that the influence in terms of temperatures and buffer saturation time was negligible.

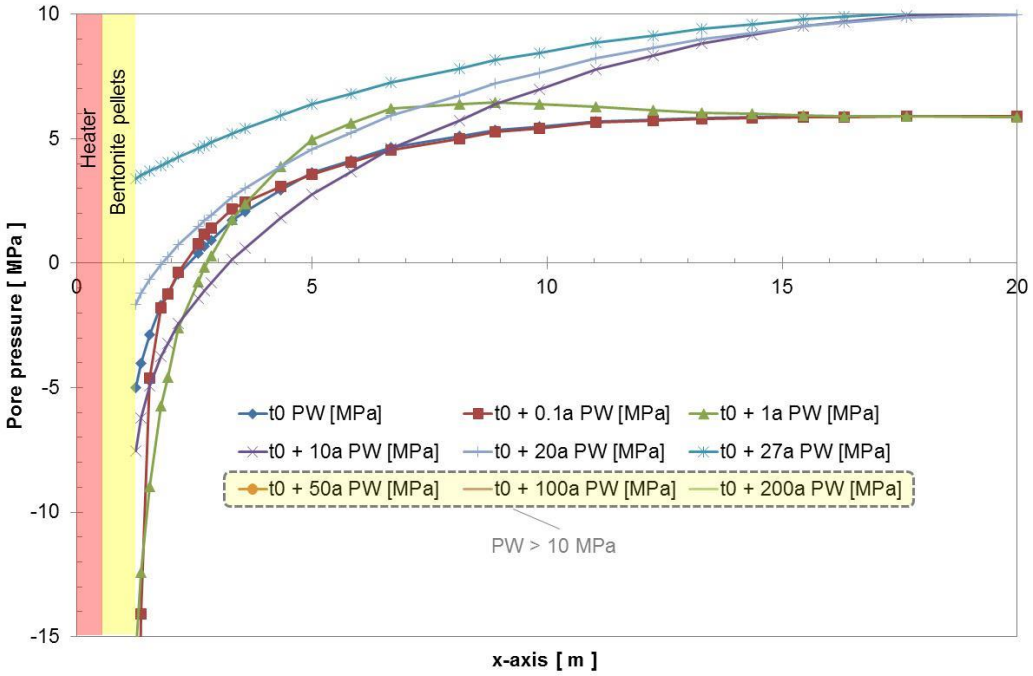

Fig. 5.25 Pore pressure profile in the rock for different simulation times

5.2.1.5 Conclusions

Simulation of a 3D TH model of an emplacement cell representing the Swiss repository concept proved possible with CODE_BRIGHT, although the calculation effort was very high. Compared to the results of Nagra using a similar model with TOUGH2, temperatures are similar, while saturation time is lower and pore pressures are higher. This is likely caused by two differences:

- In the GRS model, no EDZ with altered hydraulic properties was considered.
- Thermal expansion coefficients for the solid grains, the pore liquid, and the grain skeleton were possibly not in an adequate relation in the GRS model.

An improvement of the long-term simulations can be expected if the TH calculation is replaced by a full THM-coupled simulation, especially if a realistic representation of the rock behaviour including time-dependent deformation and damage can be used. With the calculation times of months for the TH simulation, this could not be performed with the 3D model.

5.2.2 Overview of Task 3.5 results

5.2.2.1 Simulation Case 1: Isothermal buffer evolution

For the numerical simulation of the long-term isothermal buffer evolution CIMNE extrapolated the EB experiment over a period of 100 years. In particular, the new double structure model was used for the simulation. In contrast to the other simulation cases, no thermal effects had to be considered, so that a pure hydro-mechanical formulation could be used.

The simulation of the EB experiment was continued until reaching a time of 100 years to examine the long-term behaviour of an engineered barrier under isothermal conditions. Since the barrier was in a state of full saturation or near full saturation at the end of the EB field test, few changes were computed in the extended analysis. Basically, the rock mass returned to the initial state before excavation and buffer emplacement, and the barrier naturally stayed saturated.

The most relevant observation is the fact that the degree of heterogeneity remained unchanged so the distribution of porosity (or dry density) observed at dismantling remained constant. It is likely that this conclusion is quite dependent on the degree of irreversibility implicit in the constitutive model of the barrier material. Although the constitutive model and parameters used have proved very adequate when modelling the observed behaviour of the test, it is conceivable that different constitutive models could lead to potentially different results. This is an issue that probably deserves more attention in the future. It should also be noted that no creep phenomena (i.e. deformation under constant effective stress) have been considered either in the buffer or in the rock. If creep is relevant over the long period considered, it would probably lead to a higher degree of homogenization. Creep is potentially an important phenomenon in long-term predictions and should be the subject of focused research.

5.2.2.2 Simulation Case 2: Buffer THM evolution up to 100 °C

This case is based on the Spanish disposal concept in granitic rock as described by the ENRESA Performance Assessment exercise “ENRESA 2000” (ENRESA, 2001) and the R&D programme on bentonite material, particularly the FEBEX project (ENRESA, 2006). The repository concept in granite considers the disposal of spent fuel in carbon

steel canisters in long horizontal disposal drifts. Canisters are surrounded by high-density bentonite. A canister measures 4.54 m in length and 0.90 m in diameter, and contains 4 PWR or 12 BWR fuel elements in a subcritical configuration. The thermal power at the beginning of the geological storage thermal power amounts to 1220 W per canister. Two case variants were considered, one being a long-term simulation with constant thermal output after reaching a maximum temperature of 100 °C, which is not realistic but included for reference, the other incorporating a realistic thermal output of the emplaced canisters.

CIMNE performed full THM long-term simulations of the two case variants over 1000 years of emplacement using CODE_BRIGHT with an axisymmetric geometry. For the bentonite buffer behaviour, three formulations were compared to each other:

- Reference analyses, using the conventional THM formulation (BBM);
- Analyses incorporating thermo-osmosis;
- Analyses incorporating the evolution of micro-fabric by means of the new double structure constitutive law.

A detailed description of new processes included in long-term simulations is given in Deliverable D3.5-2, “Formulation of a model suitable for long-term predictions”.

TK Consult and Nagra simulated the case variant with realistic thermal output using the code TOUGH2 with a TH formulation over 100 years. The geometric model was again axisymmetric and represented the centre of a disposal drift. An additional model representing the end of the drift was also investigated.

The parameters for the different materials were taken from the inverse modelling of the FEBEX experiment described in Section 4.3.3. With the inverse framework provided by the code iTOUGH2, also confidence intervals for the modelling results could be given. Beside the statistic parameter uncertainty and the geometry effect, two additional conceptual uncertainties were investigated by alternative simulations, namely an increased initial fluid pressure in the rock of 5 MPa corresponding to 500 m depth below surface of the disposal drift and a lower initial saturation of the buffer.

When comparing the two case variants (constant temperature and heat decay), the patterns of the early transient results in the two variants are naturally very similar. However, the long-term predictions are of course quite different.

In CIMNE's simulations, temperatures reach a peak and start to fall after a few centuries in the heat decay variant. Temperatures have practically recovered to the initial values at the end of the analysis (1000 years). It should be stated, however, that long-term temperature predictions are sensitive to the particular geometry (i. e. axisymmetry) adopted that, at those times, may not be quite representative of the actual repository.

In the heat decay reference case (without thermo-osmosis or double structure of the buffer), full saturation of the barrier is achieved after approximately 8.5 years – a significantly shorter time than in the constant temperature analysis. Swelling pressure also fully develops over similar times. Observing the long-term results, it can be noted that, after achieving the maximum values, the stresses reduce somewhat, because of the contraction associated with temperature reduction.

The incorporation of thermo-osmosis changes significantly the hydration times of the barrier. In the constant temperature case it prevents full saturation indefinitely, but even in the heat decay analyses, full saturation is only achieved towards the end of the analysis (1000 years). Development of swelling pressure follows the progress of hydration, so the full final value is only achieved at the end of the analysis. Similarly, consideration of the micro-fabric evolution also delays full hydration (and full swelling pressure development) until the end of the analysis, i. e. 1000 years. As expected, temperature fields are affected very weakly by using the alternative hypotheses of the enhanced models.

The results correspond to a specific geometry and a single set of parameters. The parameters chosen have the only merit of providing a reasonable good representation of the observed short-term transient behaviour but here they are applied to long-term calculations, so a significant uncertainty inevitably remains. Even modest variations of parameters can result in significant changes in predicted THM behaviour. A sensitivity study for the long-term situation would thus be quite valuable to assess the degree of uncertainty and the reliability of the reported results.

TK Consult and Nagra received confidence intervals for their results with respect to parameter uncertainty and also performed some alternative calculations with altered initial conditions. The simplification of disregarding mechanical effects, on the other hand, led to best-fit parameters that are not in all cases reflected by measurements (e. g., bentonite porosity).

In the reference case, full saturation of the buffer was predicted to be achieved after 15 to 20 years. With increased initial pressure this time was reduced to 5 to 8 years, while it was increased to above 20 years with lower initial water content of the buffer. This variant also led to slightly increased temperatures (4 °C maximum). The model considering the end of the emplacement drift showed slightly lower temperature at later times, which can be expected as a consequence of the additional axial heat flow component. The confidence bandwidth of results coming from the confidence intervals of the parameters was rather narrow as a consequence of small standard deviations of the parameters. On the whole, the results confirmed current knowledge regarding evolution of temperature and resaturation and showed the capability of the systematic error analysis to provide additional input to the assessment of modelling results.

5.2.2.3 Simulation Case 3: Buffer THM evolution above 100 °C

Three teams (Nagra, GRS and CIMNE) were involved in the simulation of this case, which is based on the Swiss reference concept of drift disposal, with waste canisters resting on compacted bentonite blocks and the remaining void backfilled by bentonite pellets. The heat power per canister is 1500 W at emplacement. All teams simulated a disposal cell covering a single canister, making use of the obvious symmetry boundaries, and different additional simplifications.

Nagra and GRS both used a three-dimensional model, giving a realistic geometrical representation of the repository cell, but reduced the complexity of the problem by performing thermal-hydraulic simulations, neglecting mechanical effects. Nagra used TOUGH2 and simulated various cases in order to get an insight into modelling uncertainties: A reference case with the material parameters from the HE-E database and variants with reduced thermal conductivity of the buffer, reduced pore expansivity of the clay rock, altered hydraulic parameters of the bentonite blocks, the pellets, or the clay rock. GRS used CODE_BRIGHT and simulated the reference case. Due to very high calculation times (months), only an altered initial saturation profile of the rock was considered beside the reference case. An additional difference between Nagra's and GRS' models was Nagra's consideration of a 0.7 m wide excavation damaged zone (EDZ) with increased permeability in the rock.

CIMNE also used CODE_BRIGHT, but with full THM coupling and the simplification of a two-dimensional axisymmetric geometry. Since the heterogeneous buffer composi-

tion (bentonite blocks and pellets) cannot be represented in such a model, two variants were considered: a pure pellet buffer and a buffer where the canister is completely surrounded by blocks. Adjacent emplacement drifts had to be neglected due to the geometry. A 0.6 m wide EDZ was considered. Due to long calculation times, only the reference case using the database parameters with the conventional THM formulation could be simulated.

With respect to the temperature evolution, all three teams predicted the peak temperature to be reached after 5 to 6 years. The 3D-models of Nagra and GRS came up with values of 141 °C and 145 °C, respectively, using the reference parameter values. After 130 to 185 years, the temperature dropped below 100 °C everywhere in the buffer. Nagra's model variations using reduced thermal conductivities of the buffer resulted in peak temperatures of 152 °C. A change in the hydraulic parameters had no significant influence on the peak temperature. The temperature evolution in the clay rock is not visibly influenced by the buffer thermal conductivity.

CIMNE's 2D models considered the canister completely surrounded by bentonite pellets or by blocks, respectively. Due to the considerably higher initial thermal conductivity of the blocks, the peak temperature amounts to 165 °C for the pellet variant and to 115 °C for the block variant.

In the reference case, full saturation of the buffer was reached after 50 years (Nagra), 27 years (GRS), 85 years (CIMNE pellet variant), or 56 years (CIMNE block variant). The low value for GRS is possibly due to a deficiency in the suction curve match, but may also be due to the disregard of an EDZ. Nagra's model variations showed that changing the buffer hydraulic parameters has only little influence, while decreasing the rock permeability prolonged the saturation time to 100 years.

Nagra calculated a maximum pore pressure in the rock of 10 MPa, reached after about 100 years. In the GRS simulation, 10 MPa pore pressure are reached already after ten years, which is another reason for the lower saturation time of the buffer in this model. In contrast to the TH calculations of Nagra and GRS, CIMNE considered different thermal expansion coefficients for the solid grains, the pore liquid, and the grain skeleton. This improvement has a direct effect on pore pressure evolution and leads to maximum pore pressures slightly below 8 MPa, reached after ten years at 15 m distance from the emplacement tunnel. It has, however, to be mentioned that, while this value is

lower than those of the other simulations, CIMNE's model neglects additional parallel emplacement tunnels which will have an effect on pore pressure.

All in all, the different simulations of Case 3 led to comparable results. Where significant differences occurred, they could be explained by the different model assumptions and simplifications. The different models complemented one another, increasing confidence in the results.

5.2.2.4 Simulation Case 4: Geochemical evolution at interfaces

For the simulation of the geochemical evolution at the canister-bentonite and bentonite-concrete interfaces UDC used the THCm formulation introduced in Section 5.1.2.4.

For the long-term simulation of the canister-bentonite interface, a one-dimensional axisymmetric model of the Spanish disposal concept in granitic rock was used, including the steel canister and the surrounding bentonite blocks. Granitic porewater was supplied from the outer boundary of the model. The model considered canister corrosion, the interactions of corrosion products with bentonite and the pH buffering mechanism, with the reaction types of aqueous complexation, acid/base reactions and redox reactions. The model accounted for dissolution/precipitation of calcite, gypsum, quartz, magnetite, siderite and goethite. The model also accounted for cation exchange of Na^+, Ca^{2+}, Mg^{2+}, K^+ and Fe^+ and surface complexation reactions, which were modelled with a triple sorption site model in the bentonite. All reactions were assumed at equilibrium in the reference model. In the frame of an uncertainty analysis, some simulations were performed accounting for kinetically-controlled precipitation of some minerals or including new minerals such as smectite.

Simulations were performed for a time span of one million years at a constant temperature of 25 °C, neglecting the early post-closure temperature transient. Simulations considering the temperature gradient were, however, also performed to explore the temperature influence on the geochemical evolution. Most of this work is described in Deliverable D3.5-3 of the PEBS project, an update is found in Deliverable 3.5-4 with the other cases.

The bentonite-concrete interface was modelled with a one-dimensional axisymmetric model representing the Spanish disposal concept in clay rock, including in the base variant three material zones: The bentonite buffer, concrete, and clay formation. Initial-

ly, the buffer is unsaturated with a water content of 14 vol.%. Clay pore water infiltrates into the concrete, interacting with the cementitious materials and producing hyper alkaline pore water, which then diffuses into the bentonite. The bentonite is saturated, but the high pH fluid interacts with the bentonite minerals as it diffuses, inducing the dissolution of the primary minerals and the precipitation of secondary minerals in the bentonite and the concrete. Until full saturation, mechanical effects (porosity reduction from swelling) are considered. Water flow is negligible once the bentonite buffer is saturated. Then, solute transport occurs entirely by molecular diffusion.

The minerals considered in the base variant were calcite, gypsum, quartz, portlandite, brucite, sepiolite, tobermorite, and gyrolite. In an enhanced model, canister corrosion was considered additionally. This resulted in adding dissolved iron and oxygen to the chemical components and solid iron, magnetite, siderite and goethite to the minerals. A further enhancement also considered smectite dissolution, which extended the list of minerals by smectite, analcime, saponite and cronstedite. Temperature evolution was considered in the simulations; for the variants with corrosion a constant corrosion rate of 2 µm/y was assumed.

Besides the four long-term simulation cases, additional effort was made in different directions. The usefulness of natural analogues for providing support, testing and validation of long-term predictions of current models was investigated. The possibility of deriving scaling laws by integrating available data for bentonites from different scales and using them for extrapolation was explored. A long-term simulation of a repository in granite (Spanish concept) was performed. The thermo-mechanical continuum theory of mixtures was studied in order to approach long-term evolution from a different point of view.

The canister corrosion, the interactions of corrosion products with bentonite and the pH buffering mechanisms were simulated over one million years at a constant temperature of 25 ºC for a spent-fuel carbon-steel canister repository in granite. The canister was fully corroded after 5104 years for a constant corrosion rate of 2 µm/y. Canister corrosion caused an increase in the concentration of dissolved Fe^{2+} and pH, and a decrease in Eh. Most of the released Fe^{2+} diffused from the canister into the bentonite where it precipitated or sorbed. The largest pH in the bentonite was almost 9.5 at 2105 years. The evolution of the concentration of dissolved Fe^{2+}, pH and Eh are determined by the generation of corrosion products, the precipitation of magnetite and Fe sorption on weak sites.

Magnetite was the main corrosion product in the bentonite. Approximately 70 mol/L of magnetite precipitated in the canister-bentonite interface before the canister was fully corroded and the precipitation stopped. Its precipitation progressed as Fe^{2+} diffused into the bentonite. The thickness of the bentonite zone where magnetite precipitated was about 7 cm. Siderite precipitation was much smaller due to the limited availability of dissolved bicarbonate. The thickness of the bentonite zone where siderite precipitated was similar to that of the magnetite. Calcite dissolved in most of the bentonite except near the canister where it precipitated due to the increase in pH induced by canister corrosion. Dissolution/precipitation of quartz and gypsum were not significant.

The precipitation of the corrosion products close to the canister led to a very relevant decrease of bentonite porosity near the canister-bentonite interface. The bentonite thickness significantly affected by porosity reduction increased with time to about 7 cm after one million years. A negligible increase of the porosity was observed in the rest of the buffer.

The interaction of the bentonite with the concrete liner was evaluated with a two-dimensional axisymmetric THCm model. Mineral dissolution/precipitation is especially marked in the concrete. Kinetically-controlled smectite dissolution leads to analcime precipitation. Model results indicate that smectite dissolution in the presence of an OPC concrete liner in a repository in clay is about 4 times more relevant than in the case of the repository in granite. Magnetite precipitates near the canister. The thickness of the altered zone at the canister-bentonite interface in the presence of the high pH plume is 4 cm. This is half of the thickness of the altered zone for a repository in granite.

The pH in the concrete increases due to portlandite dissolution. It also increases in the bentonite due to the penetration of the hyperalkaline plume from concrete. The precipitation of calcite, brucite and sepiolite buffers the hyperalkaline plume. The high pH plume extends throughout the bentonite and causes mineral precipitation, changes in the composition of the exchanged cations and a reduction of the porosity of the bentonite. The pH is about 11 after 105 years and later decreases to 9.5. The hyperalkaline plume from the concrete penetrates 1 m into the clay host rock after one million years.

Numerical models predict pore clogging in a 4 cm thick zone near the canister, 5 cm in the concrete-bentonite interface and 5 cm in the clay-concrete interface. Changes in porosity caused by mineral dissolution precipitation are significant throughout the bentonite and in a narrow band (25 cm) of the host rock.

5.2.2.5 Natural analogues

One of the activities carried out by UDC in Task 3.5 was the compilation and evaluation of the usefulness of natural analogues (NA) for providing support, testing and validation of long-term predictions of current THMC models. Several NA projects were studied in this regard. The results are summarized in the PEBS Milestone 3.5-3 document.

Natural analogues were used initially to improve the understanding of key processes and model/database testing. This is still a major justification for some analogue projects. More recently NA have been used to provide general support for the safety case by studying the evolution of relevant systems over geological timescales and to increase confidence in extrapolating results from lab and field experiments to the repository. Natural analogues are, however, not well defined in terms of boundary and initial conditions and model parameters. Therefore, their use as a tool for validating long-term predictions is limited.

5.2.2.6 Scaling laws

A large number of hydrodynamic, geochemical and thermal data has been collected for compacted bentonites during the last 30 years to characterize their properties and evaluate the suitability of compacted bentonite for EBS in a HLW repository. Past and on-going experiments cover a wide range of time and spatial scales. Their durations range from a few months in the case of the CT cells to more than 14 years in the case of the FEBEX mock-up and in-situ tests. The size of the experiments ranges from 10 cm in CT cells to more than 10 m in the in-situ test. An integrated analysis of the hydrodynamic, thermal and chemical data from several space and time scales was performed by UDC in terms of dimensionless variables. This work is documented in Deliverable D3.5-1.

The main conclusions of the integrated analysis of water uptake data were that there is a clear difference for one-dimensional and axisymmetries, and that an upscaling of small tests was not possible. With regard to water content, initial conditions and boundary conditions were too different in the various tests. The chemical composition of the bentonite is most often derived from aqueous extract tests which must be interpreted numerically with inverse geochemical models, which adds a difficulty to the integrated analysis of chemical data. The overall conclusion was that data from different space-time scales cannot be integrated, so there is no possibility for extrapolation in

time from available data using the scaling law approach. Therefore, this approach was not pursued further.

5.2.2.7 Mixture theory

Clay Technology performed a review of thermomechanical continuum mixture theories potentially applicable for EBS materials. It was motivated by several limitations or inadequacies of common material representations, such as the lack of coupling retention to mechanics, the uncertainty in the actual mechanism of water transport or the limited validity of mechanical representations which were developed for typical geomaterials instead of clayey swelling materials.

Following the study, a concept of non-associative immiscibility which gives a mixture with immiscibility on different levels was developed. An attempt to schematically formulate a material model using this concept was described. Deliverable D3.5-4a summarizes the related work.

Continuum mixture theory is a macroscopic representation of the thermo-mechanical behaviour of a material body consisting of a mixture of several constituents, i. e. a multi-component formulation. The framework is capable of incorporating diffusion, phase transition, and chemical reactions in the broadest sense. Miscible and immiscible formulations are possible. Immiscibility leads to adopting a material structure represented by volume fractions. Porosity and degree of saturation may be defined in terms of volume fractions. In mixture theory, the fundamental variable is the chemical potential. Pore pressures for fluid phases are generally not “physical” pressures, but scaled chemical potentials. As a consequence, capillary pressure, or suction, is the difference between scaled chemical potentials. Darcy’s law and Fick’s law are obtained as simplifications. Chemical potential and temperature are the basic driving forces. A concept of non-associative immiscibility developed by Clay Technology gives a mixture with immiscibility on different levels. A schematic formulation of a respective material model led to porosities belonging to the different levels. Chemical reactions were not addressed, but their incorporation seems unproblematic.

5.2.3 Summary and future perspective

In the framework of PEBS comprehensive numerical simulations were performed in order to interpret the experimental results, improve the basis for long-term extrapolation, predict long-term repository evolution, and quantify and reduce uncertainties in the predictions. The performed simulations covered:

- HM modelling for the interpretation of the EB experiment;
- THM modelling for design, interpretation and of the HE-E experiment;
- Investigations of various aspects of buffer THM behaviour, involving modelling of various laboratory tests, the FEBEX mock-up and the FEBEX in-situ test;
- THMC modelling of several experiments investigating the processes at the interfaces canister-bentonite and bentonite-concrete;
- Long-term extrapolation modelling of repository configurations representing the Swiss and the Spanish concepts.

Some of the simulations were performed using conventional models, but there was also considerable progress in enhancement of existing and development of alternative models.

Regarding the THM behaviour of the buffer, additional processes, like non-Darcy flow and thermo-osmosis were considered, and a double porosity model was implemented. The double porosity model proved suitable for characterizing the buffer evolution in the EB experiment. All the enhanced models were able to simulate the previously unexplained slowdown of buffer resaturation; a decision on the most likely process (or combination of processes) is, however, not yet possible. Further monitoring of the running long-term experiments will aid in the discrimination.

For reducing uncertainties in TH material data, an inverse framework was implemented for detecting best estimates of parameter combinations. This provided also uncertainty estimates of the resulting parameters in the form of standard deviations.

A new approach was taken by considering the buffer from the viewpoint of thermo-mechanical continuum mixture theory. A non-associative immiscibility concept was presented which, in the future, may provide an alternative description of buffer behaviour with the chemical potential as fundamental variable.

THMC models were developed further, taking into account porosity change by swelling and incorporating reactive gaseous species. For the most part, simulations agreed well with experimental data from corrosion experiments. This holds also for the bentonite-concrete interface, although some phases (e. g., precipitated CASH) could not be accounted for.

An approach to an integrated analysis of THMC data from different test scales proved less successful – the differences in the various geometries and test conditions was too large.

For the long-term extrapolation exercise, four simulation cases were defined.

- Case 1: Isothermal buffer evolution, an extrapolation of the EB experiment to long-term
- Case 2: Thermo-hydro-mechanical evolution of the buffer at temperatures up to 100 °C, a simulation of the Spanish reference repository concept in granite
- Case 3: Thermo-hydro-mechanical evolution of the buffer with temperatures temporarily exceeding 100 °C, a simulation of the Swiss reference repository concept in clay rock
- Case 4: Geochemical evolution at canister-bentonite and bentonite-concrete interfaces, including a long-term simulation of a repository in granite

The most important results of these simulations were the following:

- Case 1: Little change in the buffer was found during long-term extrapolation of the EB experiment, since the buffer was already close to saturation at the end of the field test. Heterogeneities in density remained as a consequence of the constitutive model – no creep had been considered. Creep is potentially an important phenomenon in long-term predictions and should be the subject of future research.
- Case 2: Including model enhancements like thermo-osmosis or double porosity in the simulation led to considerable extension of saturation time. Instead of values in the range of 10 years, buffer resaturation went on over 1000 years. The results are strongly dependent on the parameter set, even modest variations in parameters can have significant effects. A sensitivity study for the long-term situation will be useful to reduce uncertainty. In addition, further monitoring of the ongoing long-term experiments will provide more reliable data.

- Case 3: Due to problems with high calculation times, the simulation of this case could only be performed with standard models. Different simplifications were introduced by different modelling teams; taking these differences into account, the results are quite comparable.
- Case 4: THMC modelling of the canister-bentonite interface in a repository in granite led to an altered zone with a thickness of about 7 cm, where porosity is reduced due to precipitation of magnetite and siderite. In a clay repository, the thickness of the altered zone is only 4 cm, due to the different pore water chemistry. Near the concrete, pore clogging is predicted 5 cm in the concrete-bentonite interface and 5 cm in the clay-concrete interface. Changes in porosity caused by mineral dissolution/precipitation are significant throughout the bentonite and in a narrow band (25 cm) of the host rock.

The modelling exercises performed within PEBS have identified several directions most relevant for performing future studies:

- Continuation of existing long-term experiments in order to distinguish between processes potentially relevant for the long-term THM behaviour (e.g. thermo-osmosis, double porosity, creep) and to reduce uncertainty in parameter estimates;
- Calibration of enhanced models with the additional data and use of these models for long-term simulations;
- Further investigation of promising alternative models;
- Further improvement and validation of THMC models and parameters.

6 Impact on long-term safety considerations

6.1 Description of approach

The main aim of the PEBS project is to evaluate the sealing and barrier performance of the EBS with time, through development of a comprehensive approach involving experiments, model development and consideration of the potential impacts on long-term safety functions. WP4 focuses in particular on the importance of uncertainties arising from potential disagreement between the process models for THMC evolution and the relevant laboratory and in-situ experiments performed both within and outside PEBS. The implications for extrapolation of results are treated, with particular emphasis on extrapolation of long-term performance.

In order to permit integration of a broad range of information and to put information in context, four “cases” were identified and the performance of the bentonite barrier in the context of these cases was assessed. The cases (which are not to be confused with the cases for long-term extrapolation of WP3) represent a method of examining the various THMC processes that occur during the evolution of the EBS, along with their impacts on long-term performance, in a manner that provides for each case a specifically different focus. An overview of the cases is given in Tab. 6.1. For each case, the available information gained both from PEBS as well as from earlier projects was collected and evaluated in a formal way. The results of the evaluation are documented in detail in Deliverable D4.1 /JOH 14/ of the project. A summary taken from this deliverable is given below.

Tab. 6.1 Cases related to early evolution of the EBS to be used as a basis for integration of project findings /JOH 14/

Case number	Case description (principal focus)	Origin of the case (from WP1)	PEBS activities feeding into case assessment
Case 1	Uncertainty in water uptake in buffer (T<100 °C)	Discrepancies between standard THM model and FEBEX observations	1. FEBEX mock-up data and modelling 2. THM Column Tests at CIEMAT 3. EB experiment 4. Extension modelling of FEBEX in situ test
Case 2	Uncertainty in temperature evolution in buffer (T>100 °C) and impact on buffer properties	Lack of validation of TH model for high temperature and low saturation rate	1. HE-E experiment, column experiments and modelling
Case 3	Uncertainty in HM evolution of buffer	Limited large-scale experiments	1. EB experiment and modelling 2. HE-E experiment, column experiments and modelling 3. Febex mock-up and in situ 4. Stress-strain behaviour studies 5. Analytical model of homogenisation
Case 4	Uncertainties in geochemical evolution	Experiments versus models of corrosion product/bentonite and cement/bentonite interactions	1. GAME experiments and modelling 2. Interface studies (WP2.3) 3. Modelling in WP3.4

6.2 Summary of results

Case 1: Uncertainty in water uptake in the buffer below 100 °C

- There was good agreement in THM modelling between models and data for large-scale heater experiments (with high resaturation rate/water supply), but late stage resaturation is slower than predicted with models.
- Various model variants (double porosity, thermo-osmosis, Darcy threshold) were tested but results do not clearly permit discrimination.

- Despite this, the context from long-term safety is clearly improved – it can be stated that even though saturation is not yet fully achieved (e. g., after 15 years of FEBEX), the safety function is achieved because sufficient swelling pressure is reached throughout the barrier at 85-90 % average saturation. The model uncertainty is thus not important from a long-term safety perspective.

Case 2: Uncertainty in the thermal evolution of the buffer above 100 °C

- A new 1:2 scale URL experiment (HE-E) shows that there is reasonable agreement between models and measured TH parameters in early resaturation; temperature field in EBS and host rock (up to 140 °C) is modelled accurately.
- Resaturation is slow (as expected; driven by host rock water supply) and so it will require some years of monitoring to adequately test models for resaturation.
- Further studies of the effects of heating bentonite above 100 °C in a partially saturated state suggest that the swelling pressure may be somewhat reduced (~25 %), but will still meet requirements.
- Review of process understanding and data support do not suggest important changes in performance in this high temperature range.

Case 3: Uncertainty in HM evolution of the buffer

- Cementation during heating-cooling cycle can increase strength of dense bentonite; more data has been obtained, which has shown that the effects are small below 100 °C.
- The observed cementation process is not kinetic – i. e., results are basically the same for a one day or long duration cycle.
- Safety relevance is related to mechanical impacts on canister (e. g., shear across a borehole); cementation also reduces swelling pressure, but has little effect on hydraulic conductivity.
- Various laboratory and field (EB) experiments show that dense bentonite pellets evolve to a swelled material indistinguishable from swelled block material from a hydro-mechanical perspective.

- The EB experiment shows that even under non-optimum emplacement conditions swelling of mixtures of blocks and pellets with large initial density differences can achieve effective sealing.

Case 4: Uncertainty in geochemical evolution of the buffer and its interfaces with the canister and rock or liner/tunnel support

- The main effects of geochemical evolution are clearly at interfaces.
- Based on review of published data, below about 130 °C, limited alteration of smectite will occur within the main part of the barrier based on alteration models and natural analogues – an important factor is that the thermal phase is short.
- At a steel canister interface, the bentonite alteration is very limited over periods of several years, but is difficult to estimate over long periods.
- Impacts on system interfaces can be bounded (a few cm reaction zone over the very long term), although porosity evolution clearly requires work (both for steel-bentonite and cement-bentonite).
- It should be kept in mind that geochemical modelling provides valuable insights but is not fully predictive (especially over the long term) – a lot of model testing and supporting information is needed.

6.3 Future perspectives and lessons learned

Over the next years there are good prospects for resolving residual uncertainties in the performance of bentonite barriers that relate to how the thermal and resaturation period may affect the long-term performance. Some important experiments that will contribute to this improvement in understanding include:

- The excavation of the in-situ FEBEX experiment, which will obtain valuable information on the properties of a bentonite barrier that has been exposed to partial saturation at temperatures of up to 100 °C for 15 years.
- Continuing observations in the FEBEX mock-up test over a longer period should provide relevant information on the likely mechanisms operating at the later stages of saturation.

- The HE-E experiment, which permits models for TH evolution of bentonite barriers and near-field clay rock to be compared – the slow resaturation of the bentonite should permit further testing of models and eventual decommissioning will permit the properties of bentonite exposed to temperatures of up to 140 °C to be assessed.
- The first two heaters in the Prototype Repository at the Äspö HRL have been excavated and the results from the investigations are about to be published. The ABM test at Äspö, where a number of different bentonites are/have been exposed to temperatures up to 130 °C for different time periods and the mineralogical effects are being investigated.
- Work on cement-bentonite and cement-host rock interfaces, in particular determination of porosity and nature of alteration is ongoing at a number of institutes and has been proposed for a European project.

In relation to lessons learned from the PEBS studies that provide relevant feedback to design, the following points are noted:

- Laboratory and field studies have shown similar performance of blocks and pellets after resaturation, which provides some confirmation that suitable design concepts are being used.
- In terms of cement/bentonite interactions, while there are improvements in the overall chemical modelling of the associated processes, it remains difficult to constrain the long-term impacts without use of low pH cement as a design measure.
- The studies performed help to define buffer design parameters such that early resaturation phase-induced heterogeneities in density are occurring within a range that will not violate the safety function indicators related to sufficiently high swelling pressure and low hydraulic conductivity even if it is assumed that the heterogeneities do not disappear over time.

References

/CZA 11/ Czaikowski, O., Garitte, B., Gaus, I., Gens, A., Kuhlmann, U., Wieczorek, K. (2011): Design and predictive modelling of the HE-E test, Deliverable D3.2-1 of the PEBS project.

/DOW 10/ Seventh Framework Programme, Theme: Fission-2009-1.1.1, Theme Title: Long-term performance of Engineered Barrier Systems (EBS), Description of Work, 2010.

/FRE 93/ Fredlund, D.G., Rahardjo, H. (1993): Soil Mechanics for Unsaturated Soils, John Wiley&Sons, Inc.

/GAU 14/ Gaus, I., Garitte, B., Senger, R., Gens, A., Vasconcelos, R., Garcia-Siñeriz, J.-L., Trick, T., Wieczorek, K., Czaikowski, O., Schuster, K., Mayor, J.C., Velasco, M., Kuhlmann, U., Villar, M.V. (2014): The HE-E Experiment: Lay-out, Interpretation and THM Modelling, Combining D2.2-11: Final Report on the HE-E Experiment and D3.2-2: Modelling and Interpretation of the HE-E Experiment of the PEBS Project.

/HDT 07/ Instruction Manual, Hot Disk Thermal Constants Analyser, Hot Disk AB, 2007.

/JOH 14/ Johnson, L., Gaus, I., Wieczorek, K., Mayor, J.C., Sellin, P., Villar, M.-V., Samper, J., Cuevas, J.A., Gens, M., Velasco, M., Turrero, M.J., Montenegro, L., Martin P.-L., Armand G. (2014): Integration of the Short-term Evolution of the Engineered Barrier System (EBS) with the Long-term Safety Perspective, Deliverable D4.1 of the PEBS project.

/MAY 07/ Mayor, J. C., García-Siñeriz, J. L., Velasco, M., Gómez- Hernández, J., Lloret, A., Matray, J.-M., Coste, F., Giraud, A., Rothfuchs, T., Marshall, P., Roesli, U. & Mayer, G. (2007): Ventilation Experiment in Opalinus Clay for the disposal of radioactive waste in underground repositories. - In: Bossart, P. & Nussbaum, C. (Eds.): Mont Terri Project - Heater Experiment, Engineered Barrier Emplacement and Ventilation Experiment (p.182 - 240). - Rep. Swiss Geol. Surv. 1.

/OLI 96/ Olivella, S., Gens, A., Carrera, J., Alonso, E.E. (1996): Numerical Formulation for a Simulator (CODE_BRIGHT) for the Coupled Analysis of Saline Media. Engineering Computations, 1996, Vol. 13, No 7, pp 87-112.

/ROT 14/ Rothfuchs, T., Czaikowski, O., Hartwig, L., Hellwald, K., Komischke, M., Miehe, R., Zhang, C.-L. (2012): Self-sealing Barriers of sand/bentonite-mixtures in a clay repository - SB-Experimentin the Mont Terri Rock Laboratory, Final Report, GRS-302, Gesellschaft für Anlagen- und Reaktorsicherheit (GRS) mbH.

/SCH 14/ Schäfers, A. (Ed.), Gaus, I., Johnson, L., Liu, Y., Mayor, J.C., Sellin, P. Wieczorek, K. (2014): PEBS Final Scientific Report, Deliverable D5.16 of the PEBS project.

/WIE 11/ Wieczorek, K., Miehe, R. (2011): Measurement of Thermal Parameters of the HE-E Buffer Materials, Deliverable D2.2-5 of the PEBS project.

/WIE 13/ Wieczorek, K., Miehe, R. (2013): Thermal Characterisation of HE-E Buffer, Deliverable D2.2-9 of the PEBS project.

/WIE 14/ Wieczorek, K. (Ed.), Czaikowski, O., Gaus, I., Gens, A., Kuhlmann, U., Mon, A., Montenegro, L., Naves, A., Samper, J., Sanchez, M., Senger, R., Vasconcelos, R. (2014): Extrapolation of the models developed to the repository long- term evolution and evaluation of uncertainties, Deliverable D3.5-4 of the PEBS project.

/TEO 12/ Teodori, S.-P., Gaus, I. (Ed.) (2012): Report of the construction of the HE-E experiment, Deliverable D2.2-3 of the PEBS project.

/UPC 02/ UPC (2002): A 3-D program for thermo-hydro-mechanical analysis in geological media.

List of figures

List of tables

A List of scientific PEBS deliverables

Deliv. No.	Title	Publ./Restr.
D1.1/D1.2	The Early Evolution of the EBS in Safety Assessments	Public
D2.1-1	Horizontal borehole results (geophysics, hydro test, laboratory test)	Public
D2.1-2/D2.1-3	Engineered Barrier Emplacement Experiment in Opalinus Clay: “EB” Experiment, Test Plan and Sampling Book	Restricted
D2.1-4	Engineered Barrier Emplacement Experiment in Opalinus Clay: “EB” Experiment, As-Built of Dismantling Operation	Restricted
D2.1-5	EB Experiment, Laboratory Infiltration Tests Report	Public
D2.1-6	Engineered Barrier Emplacement Experiment in Opalinus Clay: “EB” Experiment, EDZ seismic results – seismic transmission measurements	Public
D2.1-7	EB Experiment, Laboratory post-mortem analyses report	Public
D2.1-8	EB dismantling synthesis report	Public
D2.1-9	Engineered Barrier Emplacement Experiment in Opalinus Clay: “EB” Experiment, Geoelectrical monitoring of dismantling operation	Public
D2.2-1	FEBEX mock-up Sampling Book	Restricted
D2.2-2	Mont Terri HE-E experiment: detailed design report	Restricted
D2.2-3	Report of the construction of the HE-E experiment	Public
D2.2-4	FEBEX mock-up: Instrument Annual Report	Restricted
D2.2-5	Measurement of Thermal Parameters of the HE-E Buffer Materials	Public
D2.2-6	FEBEX mock-up database on THM processes	Restricted
D2.2-7.1	Long-term THM tests report: THM cells for the HE-E test: setup and first results	Public
D2.2-7.2	Long-term THM tests report: Isothermal infiltration tests with materials from the HE-E	Public
D2.2-7.3	Long-term THM tests report: THM cells for the HE-E test: update of results until February 2014	Public
D2.2-8	HE-E annual monitoring report	Public
D2.2-9	Thermal Characterisation of HE-E Buffer	Public

Deliv. No.	Title	Publ./Restr.
D2.2-10	Seismic data report on EDZ and EBS evolution (HE-E)	Public
D2.2-11/D3.2-2	The HE-E Experiment: Lay-out, Interpretation and THM Modelling	Public
D2.2-12	Laboratory studies on stress-strain behavior	Public
D2.3-1/D2.3-2.1	Feasibility on GAME mock-ups / Report on GAME status, 1st period	Public
D2.3-2.2/D2.3-5	Report on GAME status, 2nd period / GAME data analysis report before dismantling	Public
D2.3-3.1	Laboratory tests at the interfaces – First results on the dismantling of tests FB3 and HB4	Public
D2.3-3.2	Laboratory tests at the interfaces – Results of Small Cells with mortar-bentonite-magnetite	Public
D2.3-4	Test Plan of the GAME Dismantling Operation	Restricted
D2.3-6.1	Geochemical interactions at the concrete-bentonite interface of column experiments	Public
D2.3-6.2	Formation of iron oxide and oxyhydroxides under different environmental conditions	Public
D3.1.1/D3.1-2	Modelling and interpretation of the EB experiment hydration/Interpretation of the final state of the EB experiment barrier	Public
D3.2-1	Design and predictive modelling of the HE-E tests	Public
D3.3-1	Inverse Modelling of the FEBEX in situ test using iTOUGH2	Public
D3.3-2	Report on the modelling with initially available data	Public
D3.3-3	Modelling and interpretation of the FEBEX mock up test and of the long-term THM tests	Public
D3.4-1	Report on testing multiple-continua THC(m) models with lab and large-scale tests	Public
D3.5-1	Report on integration of available data for bentonites from different scales and scaling laws and extrapolation for long-term analyses for clay barriers	Public
D3.5-2	Formulation of a model suitable for long-term predictions	Public
D3.5-3	Report on long-term THC(m) predictions of a HLW repository in granite	Public
D3.5-4	Extrapolation of the models developed to the repository long- term evolution and evaluation of uncertainties	Public

Deliv. No.	Title	Publ./Restr.
D3.5-4a	Extrapolation of the models developed to the repository long- term evolution and evaluation of uncertainties - Review of thermomechanical continuum mixture theories applicable for EBS materials	Public
D4.1	Integration of the Short-term Evolution of the Engineered Barrier System (EBS) with the Long-term Safety Perspective	Public
DB-1	Report on the Detailed Design of China-Mock- up Experiment	Public
DB-2	China-Mock-up status Annual Report	Restricted
DB-3	China-Mock-up data analysis report	Restricted
DB-4	Test plan of the China-Mock-up dismantling operation	Restricted
DB-5	Plan of China-Mock-up post-mortem analysis	Restricted

Gesellschaft für Anlagen- und Reaktorsicherheit (GRS) gGmbH

Schwertnergasse 1
50667 Köln
Telefon +49 221 2068-0
Telefax +49 221 2068-888

Forschungszentrum
85748 Garching b. München
Telefon +49 89 32004-0
Telefax +49 89 32004-300

Kurfürstendamm 200
10719 Berlin
Telefon +49 30 88589-0
Telefax +49 30 88589-111

Theodor-Heuss-Straße 4
38122 Braunschweig
Telefon +49 531 8012-0
Telefax +49 531 8012-200

www.grs.de

ISBN 978-3-944161-33-4